Hyaluronic acid-coated nanoparticles as biofunctional pharmaceutical carriers

A thesis submitted to the University of Manchester for the degree of

Doctor of Philosophy

in the Faculty of Medical and Human Sciences

2013

Abdulaziz Almalik

School of Pharmacy and Pharmaceutical Sciences

Table of Contents

Table of Contents

Word count: 37,236 words

List of Figures

List of Figures

List of Figures

List of Schemes

List of Tables

Abstract

The University of Manchester
Abdulaziz Almalik
Doctor of Philosophy
Hyaluronic acid-coated nanoparticles as biofunctional pharmaceutical carriers
2013

In recent years, the use of nanotechnology for drug delivery purposes has witnessed a very significant growth aiming to improve the efficacy and/or reduce toxicity of existing drugs. This project aimed to design hyaluronic acid (HA)-coated chitosan-triphosphate (TPP) nanoparticles applicable for the delivery of genetic payload, and predominantly focused on the study of chitosan molecular weight-dependent effects. Firstly, we explored the effect of chitosan molecular weight (MW) on the physico-chemical characteristics and morphology/structure of chitosan-TPP nanoparticles and their functional behaviour. Combining dynamic light scattering and atomic force microscopy analysis allowed to highlight the influence of chitosan MW on the porosity, environmental response and HA adsorption of the resulting particles. For example, increasing chitosan MW provided increasingly porous nanoparticles. Upon coating with HA, HA showed a different adsorption mode depending on the nanoparticle porosity (and therefore on chitosan MW), with deeper penetration in more porous nanoparticles and the formation of an HA corona for less porous ones. This different mode of HA adsorption on nanoparticles appears to largely influence the enzymatically triggered payload release from the nanoparticles, the protein adsorption on the surface of the nanoparticles and also to affect the overall stability of the nanoparticles.

As a spin-off of this study, we became interested in the effect of the different mode of HA adsorption described earlier on the way HA is presented to phagocytic cells (264.7 RAW macrophages), and therefore on the kinetics and possibly also on the mechanism of nanoparticles uptake. Here, we provide conclusive evidence that HA-coated nanoparticle internalisation is a CD44-mediated phenomenon. Interestingly, our data suggest that a better presentation of HA, i.e. hyaluronic acid less tightly complexed on the nanoparticle surface, is linked to both higher affinity and lower capacity/uptake rate. Paradoxically, particles with a lower affinity for CD44 may allow a more efficient HA-mediated delivery of payloads.

Finally, we investigated the feasibility of CD44-dependent therapeutic approaches using HA-coated nanoparticles made from different chitosan MWs with or without a nucleic acid payload. The physico-chemical characteristics and nucleic acid encapsulation efficiency were compared. Transfection efficiency in cells characterised by a significantly different expression of CD44 and the possibility for the HA-coated nanoparticles to exert a direct anti-inflammatory effect were also analysed. HA-coated nanoparticles allowed successful entrapment and delivery of both siRNA and pDNA, with significant effects of the nanoparticle bulk structure (i.e. chitosan MW). We also showed an unprecedented anti-inflammatory effect of HA-coated nanoparticles devoid of any payload, which was more potent than the effect resulting from soluble HA. We speculate that the different organisation and possibly different crowding and mobility of HA chains may give rise to significant effects on macrophage inflammatory activation possibly arising from clustered binding to HA receptors such as CD44. These results indicate the potentiality of CD44-mediated therapies using HA-coated nanoparticles.

Declaration

No portion of the work referred to in the thesis has been submitted in support of an application for another degree or qualification of this or any other university or other institute of learning.

Copyright Statement

i. The author of this thesis (including any appendices and/or schedules to this thesis) owns certain copyright or related rights in it (the "Copyright") and s/he has given The University of Manchester certain rights to use such Copyright, including for administrative purposes.

ii. Copies of this thesis, either in full or in extracts and whether in hard or electronic copy, may be made only in accordance with the Copyright, Designs and Patents Act 1988 (as amended) and regulations issued under it or, where appropriate, in accordance with licensing agreements which the University has from time to time. This page must form part of any such copies made.

iii. The ownership of certain Copyright, patents, designs, trade marks and other intellectual property (the "Intellectual Property") and any reproductions of copyright works in the thesis, for example graphs and tables ("Reproductions"), which may be described in this thesis, may not be owned by the author and may be owned by third parties. Such Intellectual Property and Reproductions cannot and must not be made available for use without the prior written permission of the owner(s) of the relevant Intellectual Property and/or Reproductions.

iv. Further information on the conditions under which disclosure, publication and commercialisation of this thesis, the Copyright and any Intellectual Property and/or Reproductions described in it may take place is available in the University IP Policy (see http://www.campus.manchester.ac.uk/medialibrary/policies/intellectual-property.pdf), in any relevant Thesis restriction declarations deposited in the University Library, The University Library's regulations (see http://www.manchester.ac.uk/library/aboutus/regulations) and in The University's policy on presentation of Theses.

Dedication

I dedicate this thesis to the following people

1) The most important and inspirational person in my life, my mother Hessa Alabbad; without her prayers and support none of this would have been possible. I cannot thank her enough and I will be eternally grateful to her for everything that she has done for me.

2) My father Malik Almalik, sisters and brothers; specifically, my big brother Amer and my cute little sister Hala for their unconditional love, encouragement and support.

3) The soul of a great man, a great fighter and a great survivor, my grandfather Nasser Almalik (1850-1930 AC), whose pride, success and achievements were a great source of inspiration to me.

Acknowledgements

I would like to express my thanks and gratitude to Almighty God for everything.

I am also thankful to King Abdulaziz City of Science and Technology (KACST) for funding this project.

I also would like to thank my main supervisor, Professor Nicola Tirelli, whose expertise and knowledge added considerably to my graduate experience. I doubt that I will ever be able to convey my appreciation fully, but I dedicate to him all the success I had or will have in my future career life.

I am grateful to my supervisor Dr. Philip Day for his kindness, guidance, advice, and endless support during my project.

I would like to express my sincere appreciation and thanks to my colleagues, Dr. Sihem Ouasti, Roberto Donno and Shima Karimi for their help in my experiments. Beside Sihem's experimental advice and help, her continuous encouragement was a source of confidence that I cannot deny.

My gratitude is also extended to my colleagues, Chirag, Enrique, Ghislaine, Richard, Christopher, Alessandro, Damien, Jila Ariana Wadea and Jennifer for their help, solid support and comfort during my project.

My sincere thanks to my best friend, Haitham Alrabiah, for his prayers, encouragement, support and patience.

Abbreviations

cm	10^{-2} metre
^{o}C	Degree Celsius
CS	Chitosan
DD	Degree of deacetylation
g	Gram
h	Hour
^{1}HNMR	Proton Nuclear magnetic resonance spectroscopy
kDa	10^{3} Dalton
L	Litre
M	Molar
MDa	10^{6} Dalton
mm	10^{-3} Metre
mM	10^{-3} Molar
mV	10^{-3} Volt
mg	10^{-3} Gram
min	Minute
mL	10^{-3} Litre
μm	10^{-6} Metre
mg	10^{-6} Gram
μL	10^{-6} Litre
nm	10^{-9} Metre
nM	10^{-9} Molar
η_{in}	Intrinsic viscosity
η_{rel}	Relative viscosity
η_{sp}	Specific viscosity
η_{inh}	Inherent viscosity
3D	Three-dimensional
AFM	Atomic Force Microscopy
BCA	Bicinchoninic acid
BSA	Bovine Serum Albumin
CD	Cluster of differentiation
DAPI	4',6-diamidino-2-phenylindole
DLS	Dynamic light scattering
DMEM	Dulbecco's Modified Eagle Medium
DMSO	Dimethylsulfoxide
DNA	Deoxyribonucleic acid
ECACC	European Collection of Animal Cell Culture

EDC	N-(3-Dimethylaminopropyl)-N-ethylcarbodiimide
EDTA	Ethylenediaminetetraacetic acid
EIPA	Ethylisopropylamiloride
ELISA	Enzyme-linked immunosorbent assay
FBS	Foetal Bovine Serum
GAGs	Glycosaminoglycans
GPI-AP	Glycosylphosphatidylinositol anchor proteins
HA	Hyaluronic acid
Hz	Hertz
Ig	Immunoglobulins
IL	Interleukin
LPS	Lipopolysaccharides
MTS	3-(4,5-dimethylthiazol-2-yl)-5-(3-carboxymethoxyphenyl)-2-(4-sulfophenyl)-2H-tetrazolium
MW	Molecular weight
MWCO	Molecular weight cutoff
$\overline{M_v}$	average viscosimetric molecular weight
PBS	Phosphate buffer saline
PEG	Poly(ethylene glycol)
pKa	acid dissociation constant
pm	Picometre
RHAMM	Receptor for hyaluronan-mediated motility
RMS	Root mean square
rpm	Round per minute
RITC	Rhodamine isothiocyanate
ROS	Reactive oxygen species
siRNA	Small interfering RNA
TEM	Transmission electron microscopy
TNF	Tumour necrosis factor
TPP	Triphosphate
v/v	Volume by volume
wt.	Weight

Chapter One

Introduction

1.1 Nanotechnology

Nanotechnology is defined as the design, characterisation and production of organic or inorganic materials, structures, devices, and systems by controlling their shape and size within the scale of sub-micron dimensions [1, 2].

The origin of this discipline can be traced to the famous talk delivered by Nobel Prize winner physicist Richard Feynman to the American Physical Society in Pasadena on December 1959 "There's plenty of room at the bottom". The talk was the spark that inspired scientists to explore the possibilities offered by engineering matter at an atomic/nano scale; since then, interest and research on nanotechnology and nanoscience has witnessed an unparalleled growth, often beyond the original expectations. For example, Feynman concluded his talk with a challenge of writing the entire Encyclopaedia Britannica on the head of a pin, which was achieved 25 years later by Stanford graduate student Tom Newman [3, 4].

The last thirty years have also seen the birth of a number of analytical methods, e.g. scanning probe techniques such as scanning tunnelling microscopy (STM) and atomic force microscopy (AFM), which enable scientists to image and manipulate materials at a molecular and atomic level [5, 6]. Further, a number of techniques now allow the fabrication of nano-size materials also controlling their shape [7]. Through the development of these tools, nanotechnology has now applications in a variety of fields such as catalysis, coating, sensors; in this work, we will specifically focus on the emerging field of nanomedicine, where nano materials are used either as imaging or therapeutic agents, respectively for diagnostic and therapeutic purposes [2, 7]. Under this umbrella, the term "nanoparticle" refers to any object with a dimension where Brownian motion overwhelms gravity (1-1000 nm), and additionally has a prevalently elastic behaviour [2].

1.2 Nanomedicine

Nanotechnology has the potential to significantly improve medical sciences both in the aspects related to *in vitro* and *in vivo* diagnosis and in those related to the ability to treat diseases. Additionally, the applications of nanotechnology in medicine are not limited to the above and extend to the manufacture of advanced biocompatible and bioresponsive materials as well as those related to human general well-being, e.g. with the development of nutraceuticals [8].

The application of nanotechnology to drug delivery aims to improve the cell or tissue specificity of any targeting action, widening the therapeutic window of a drug (reducing its toxicity while maintaining its therapeutic effects), enhancing the physico-chemical properties of drugs (such as solubility/dispersability in biological environment), controlling the release of the entrapped drug, intracellular delivery of macromolecules to the site of action, co-delivering of two or more drugs for combination therapy, and the combination of therapeutic agents with imaging agents to visualise sites of drug delivery [8, 9]. These aims could be achieved with the aid of drug carriers of submicron dimensions (nanocarriers).

1.3 Nanocarriers

A variety of nanocarriers (bearing dissolved, encapsulated and linked drugs) have been developed for drug delivery purposes (Figure 1- 1): for example, self-assembled carriers with vesicular (liposomes, niosomes or polymeric vesicles) or micellar morphology (polymeric micelles), nanoparticular aggregates (made of lipids, hydrophobic polymers, hydrogels), single molecules (dendrimers, carbon nanotubes, linear polymers), viruses and inorganic core-shell nanoparticles [10].
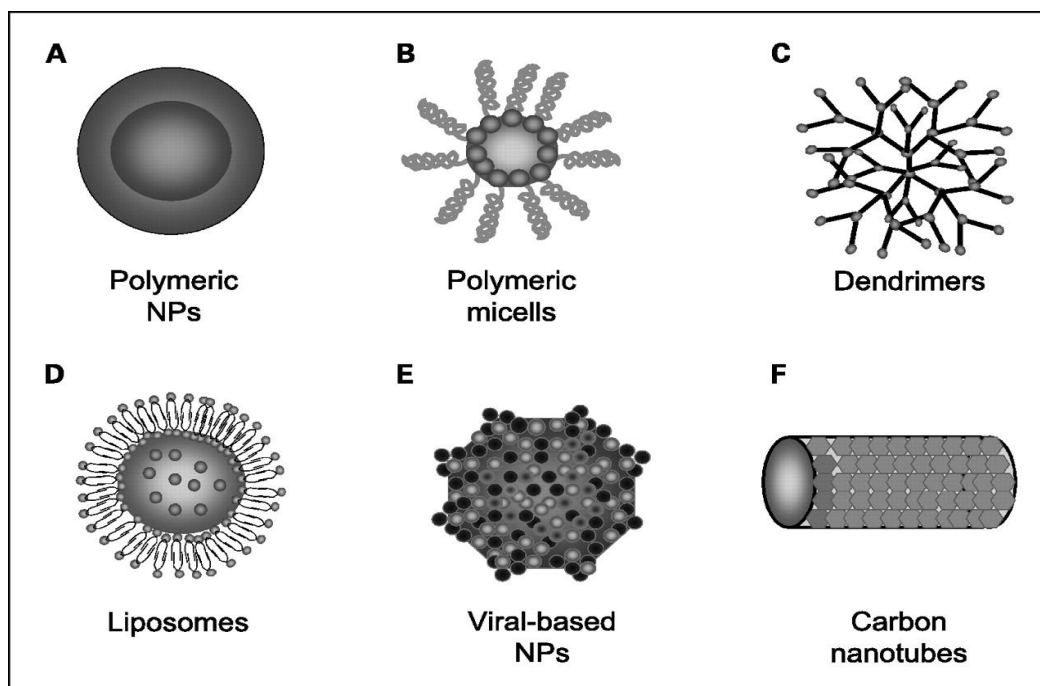
Figure 1- 1 Fundamental types of nanocarriers for drug delivery. Taken from [10]. Polymeric nanoparticles carry active principles dispersed throughout the polymeric matrix (A) Polymeric micelles are assembled from amphiphilic polymers (B). Dendrimers are branched polymers typically symmetric around a central core (C). Liposomes consist of one or several phospholipid bilayers surrounding an aqueous core (D). Viral nanoparticles are symmetric protein cages surrounding an active principle (E). Carbon nanotubes are aromatic rings spatially arranged to form carbon cylinders (F).

Nanoparticles. Nanoparticles are often based on polymers of either natural or synthetic origin. Natural biopolymers include albumin, chitosan, hyaluronic acid and alginic acid; the most common example of synthetic polymers is offered by biodegradable polyesters, such as PLA (poly(lactic acid)) or PLGA (poly(lactic-co-glycolic acid)) [10]. Structurally, polymeric nanoparticles can be divided into two subclasses, (1) **nanospheres** where a drug is more or less homogeneously dispersed all the way through the particles [10, 11], (2) **nanocapsules** which are a type of vesicular system where the drug is in a cavity bordered by a polymeric membrane [11].

Nanoparticles can also be made from lipids characterised by a melting point above room temperature, that yield solid lipid nanoparticles (SLNs). Examples of such lipids are triglycerides (e.g. tricaprin) and fatty acids (e.g. stearic acid). A SLN is generally composed of a solid hydrophobic core stabilised by a surfactant (e.g. Poloxamer 188). The most important advantage of SLN over polymeric

nanoparticles is the lower toxicity emerged from the use of physiological lipids [12, 13].

Polymer micelles for drug delivery are self-assembled from amphiphilic block copolymers in which the hydrophilic shell region stabilizes a hydrophobic core that serves as a reservoir for hydrophobic drugs, which are normally difficult to formulate due to poor solubility in water. The amphiphilic nature of these nanocarriers renders them water-dispersable and appropriate candidates for IV administration [14, 15]. Polymer micelles are specifically interesting due to their low values of Critical Micellar Concentration, which allows for a higher stability against dilution. Therefore, polymer micelles have been used to encapsulate a large variety of highly potent but hydrophobic drugs [10].

Dendrimers. Dendrimers are synthetic polymers that exhibit a three dimensional structure composed of highly branched monomers which spring from a central core. In general, dendrimers are symmetrical and the degree of branching can be modified which offers the possibility to create an active site core via chemical modification of the end groups. For example, water soluble dendrimers with hydrophobic cores can be synthesised by functionalisation of their end groups with carboxylic acids. This easily modifiable surface enables dendrimers to be conjugated with several molecules simultaneously such as therapeutic agents or targeting ligands. Multivalency and monodispersity are additional advantages of dendrimers [10, 16].

Liposomes. Liposomes are lipidic vesicles, formed by one or several phospholipid bilayers surrounding an aqueous core. They are biocompatible, biodegradable and suitable for the delivery of hydrophilic and hydrophobic compounds [17]. Hydrophilic compounds can be encapsulated in the aqueous core while hydrophobic compounds may be contained in the phospholipid bilayers. Currently, several liposomal drug formulations have been approved for the treatment of a variety of diseases [18]. Among these, Doxil, a liposomal formulation of doxorubicin for the treatment of metastasised breast cancer and Daunoxome, a liposomal formulation of daunorubicin for the treatment of AIDS related Kaposi's sarcoma [10, 11, 16].

Viral nanoparticles. Viruses such as the Cowpea mosaic virus, Cowpea chlorotic mottle virus and bacteriophages have been utilised for targeted drug and gene delivery. Viral nanoparticles are well-characterised, monodisperse structures which can be produced in large scale. Their structures are highly symmetrical and therefore

they can be regarded as one of the most versatile and advanced naturally occurring nanomaterials. Viruses consist of a protein coat (capsid) that surrounds their genetic material. Capsid aids binding, internalisation and delivery of the encapsulated material into the target cell by interacting with specific cell surface receptors enable an efficient and organized delivery. Using genetic or chemical means, a number of peptides and molecules can be displayed on their surfaces such as transferrin, folic acid and antibodies for active targeting *in vivo* [10, 19, 20].

Carbon nanotubes. Carbon nanotubes are basically carbon cylinders composed of aromatic rings that have been considered broadly, including vaccine and protein delivery. Structurally, they can be classified into two main categories: single and multi-walled carbon nanotubes where they consist of one or several concentric graphene sheets respectively. The main limitation to their use in nanomedicine is their hydrophobicity and consequently their lack of solubility in solvents compatible with the biological milieu. However, they have large surface area and therefore they can be easily functionalised to tune solubility and to be linked to a variety of active principles. In general, biocompatibility of carbon nanotubes has been improved reducing their size and by functionalisation. Furthermore, carbon nanotubes can be modified to carry multiple molecules at once which is beneficial to drug delivery [10, 16].

1.4 Overcoming physiological barriers for effective delivery

For safe and effective drug delivery, nanocarriers have to overcome many physiological barriers especially for those intended for systemic administration [21, 22]. Although localized drug delivery offers several advantages, including higher bioavailability and fewer side effects, many tissues in the body can only be reached through systemic administration of delivery agents into the bloodstream. Post administration, nanocarriers have to cross biological membranes (e.g. mucosae, blood vessel walls) and navigate the circulatory system of the body, while avoiding aggregation caused by serum proteins, uptake by phagocytes, kidney filtration and degradation of the payload by endogenous enzymes. At the target site, nanocarriers must be able to cross the vascular endothelial barrier, diffuse through the

extracellular matrix, enter the target cell and eventually deliver the payload to the targeted intracellular site [21, 22]. Typically, no nanocarrier can passively permeate through cell membranes in an intact form; on the contrary they are internalised (and sometimes expelled) through energy-dependent mechanisms. In particular, we focus our attention on internalisation mechanisms, which go under the general name of endocytic phenomena.

1.4.1 Endocytic mechanisms

Endocytic mechanisms are generally divided into two main groups: phagocytosis or pinocytosis (Figure 1- 2).
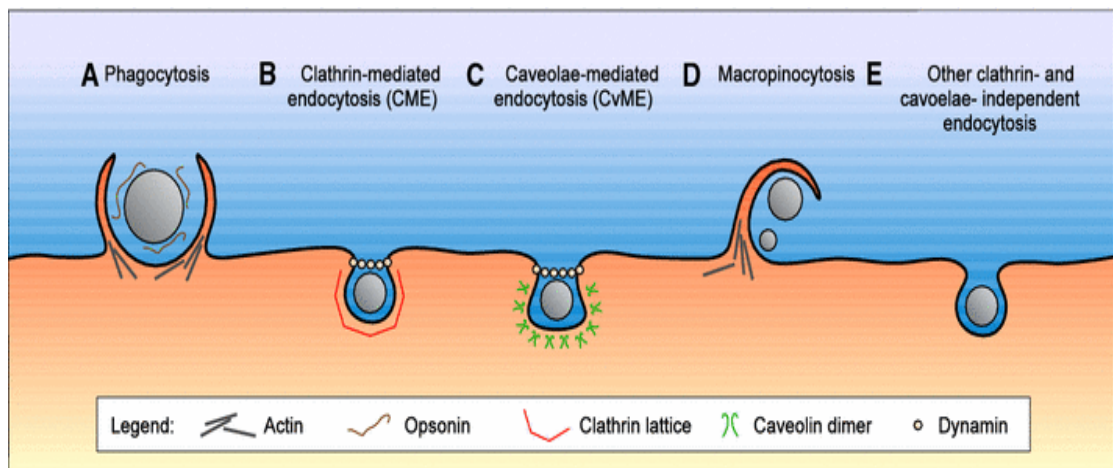
Figure 1- 2 nanocarriers endocytosis pathways in mammalian cells. Taken from [11]. Phagocytosis is an actin-dependent mechanism occurring mainly in professional phagocytes (e.g. macrophages) (A). Clathrin mediated pathway depends on the GTPase dynamin and the formation of clathrin lattice (B). Caveolae-mediated pathway depends on the formation of flask-shaped and caveolin-coated invaginations of the plasma membrane and it is also dependent on dynamin (C). Macropinocytosis is a poorly selective, actin dependent pathway for nanocarriers uptake (D). Other endocytic pathways independent of both clathrin and Caveolae may be involved in nanocarriers internalisation (E).

Phagocytosis is restricted to specialised mammalian cells, including macrophages, neutrophils and monocytes [23]. Other cell types also display some phagocytic activity such as endothelial, epithelial and fibroblast cells [24]. It serves as a significant immunological barrier as it is responsible for the defence against infectious agents or materials recognised as foreign bodies [11, 21]. In general, nanocarriers must avoid phagocytosis, since this allows for prolonged circulation in

body fluids, which is a prerequisite for any targeted action. This endocytic pathway can be described in four distinct steps, which are shown in Figure 1- 3.
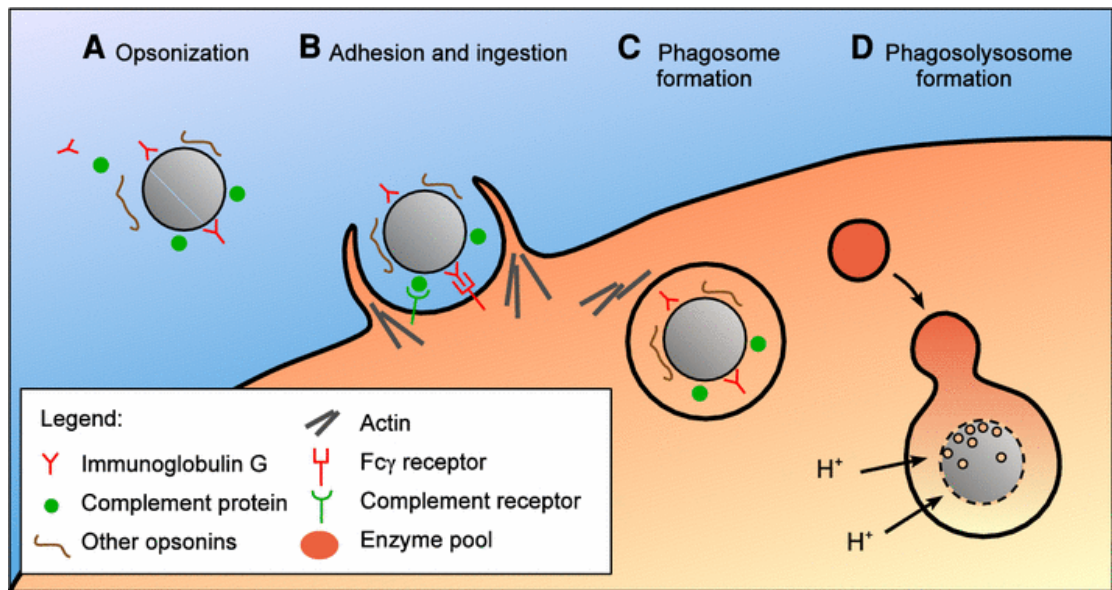
Figure 1- 3 Phagocytosis of nanocarriers. Taken from [11].
In the blood stream, nanocarriers undergo opsonisation by opsonins such as immunoglobulins and complement proteins (A). Opsonised nanocarriers attach to the cell surface receptors through specific receptor-ligand interactions initialising actin assembly and carrier engulfment (B). The nanocarrier is internalised into phagosomes (C) that mature, fuse with existing lysosomes and become acidified and form enzyme rich phagolysosomes where carrier degradation occurs (D).

The first step is termed opsonisation; this is a process where nanocarriers dispersed in a body fluid adsorb proteins called opsonins such as immunoglubulins IgG and IgM, complement components (C3, C4, C5) and other serum proteins (fibronectin, C-reactive protein, laminin, type-I collagen) [11, 25]. Opsonisation kinetics can be very variable, as the protein adsorption can occur in a matter of seconds as well as in many days [26].

The major receptors involved in this process are Fc receptors (FcR) and the complement receptors (CR) [23, 27]. Other receptors can also be involved in phagocytosis, and these include mannose/fructose, scavenger receptors and CD44 [28]. Upon binding of an opsonised nanocarrier to macrophage surface receptors, a signalling cascade regulated by Rho-family GTPase is triggered, leading to actin assembly which forms extensions on the cell surface that wrap around and internalise the particle into a phagocytic vacuole (phagosome) [11, 29].

The phagosome will carry the particle throughout the cytoplasm. Actin is then depolymerised from phagosomes, which undergo a series of fusion and fission events with late endosomes and lysosomes ending up as phagolysosomes [30]. Phagolysosomes have an acidic environment due to the presence of vacuolar proton pump ATPase located in the membrane and acquire many enzymes that enhance particle degradation. This enzymatic content is a key issue for the biodegradability of synthetic polymeric nanoparticles. It can be exploited to ensure degradability which aids to avoid toxicity accompanied by the accumulation of the internalised polymers. Moreover the enzymatic content can be also exploited to produce an enzymatically triggered release of the payload [11].

Since opsonisation makes the particles visible to macrophages and enables their attachment to macrophage surface receptors, its avoidance lowers the chance of immune recognition and enhances the blood residence time of nanocarriers. A common way to reduce the extent of opsonisation is the chemical attachment of poly(ethylene glycol) (PEG) to the circulating object (nanocarriers, but also proteins). PEG chains present have negligible self-attractive forces while they are much hydrated in aqueous environments. Therefore, they can act as a ''shield'' preventing intimate contact of a nanocarrier surface with blood proteins including opsonins [11, 31].

Pinocytosis is a non-phagocytic pathway that occurs in virtually all cells [11]. There can be at least four morphologically distinct mechanisms, which differ in the size of the vesicular compartments, the composition of the coat (if any) and the intracellular fate of any internalised particles [11, 32].

A) Clathrin-mediated endocytosis (CME). occurs in all mammalian cells and plays crucial physiological roles including the uptake of nutrients and intracellular communication. CME is either receptor-dependent or independent. In both mechanisms, endocytosed materials end up in degradative lysosomes. Lysosomal biodegradation of drug-loaded nanocarriers may be tailored to ensure the release of the drug intracellularly.

Receptor-dependent CME is important for drug-loaded nanocarriers bearing targeting ligands on their surface considering that this mode of internalisation is shared by a variety of ligand-receptor endocytosis mechanisms (e.g. transferrin and

epidermal growth factor) [33, 34]. During internalisation, the ligand is strongly bound to specific receptors on the cell surface in regions enriched with clathrin, a key cytosolic coat protein that has a three-leg structure called triskelion (Figure 1- 4). Triskelion can assemble in a polygonal lattice on the membrane forming clathrin-coated pits (CCPs), which are clusters of ligand-receptor complexes of ~150 nm in size. The CCPs then invaginate and pinch off from the plasma membrane by GTPase dynamin to form clathrin-coated vesicles (CCVs), which carry the ligand-receptor complexes into the cells. Depolymerisation of the clathrin coat results in (early or sorting) endosome (pH ~ 6), where dissociation of the ligand-receptor complexes occurs and receptor molecules are recycled for another round of delivery. Then the early endosomes mature to late endosomes (pH ~ 5), which fuse with prelysosomal vesicles containing acid hydrolases, generating an aggressive environment rendering the internalised cargo prone to degradation [11, 33, 34].

In **receptor-independent CME**, internalisation occurs in a similar way to the described above; however, the mode of interaction with the cell membrane differs. Compounds internalised by this pathway usually display hydrophobic or non-specific charge interactions with the membrane. Moreover, the internalisation rate is slower than that of receptor-dependent CME [35].

B) Caveolae-Mediated Endocytosis (CvME). Caveolae are small (50–100 nm) flask-shaped invaginations of the plasma membrane [36]. They are rich in cholesterol and glycosphingolipids. Although caveolae are present in many cell types, they are abundant in endothelial cells and play a key role in cholesterol haemostasis and glycosphingolipids transport [37, 38]. Caveolins, a family of cholesterol-binding proteins, are necessary for the biogenesis of caveolae [39]. In a CvME, particles associate initially with the cell membrane and become trapped in caveolae. Then these are taken up into intracellular organelles called caveosomes (Figure 1- 4). In contrast to the acidic and digestive nature of endolysosomal compartments in CME, molecules internalised by caveolae are mostly transported to the endoplasmic reticulum or Golgi apparatus without suffering a drop in pH or lysosomal degradation [40]. Therefore, caveolae-mediated endocytosis is advantageous for nanocarriers carrying drugs that are highly sensitive to enzymes (e.g. peptides and nucleic acids). In general, caveolae are small in size, slowly internalised and highly stable compared to clathrin–mediated endosomes [11].

C) Macropinocytosis. Upon stimulation by any mitogenic factor, Rho-family GTPases trigger the actin driven formation of membrane extensions (ruffles). These then collapse onto and fuse with the plasma membrane to form macropinosomes that sample large volumes of extracellular milieu [11, 37]. Macropinosomes lose their actin, and the intracellular fate of these vesicles is diverse depending on the cell type. In macrophages, they become acidified and fuse with lysosomes, while in A431 human cells, they recycle most of their contents back to the cell surface without fusing with lysosomes (Figure 1- 4) [33]. Being as large as 5 μm in diameter, macropinosomes are an efficient pathway for the non-selective endocytosis of macromolecules [33].
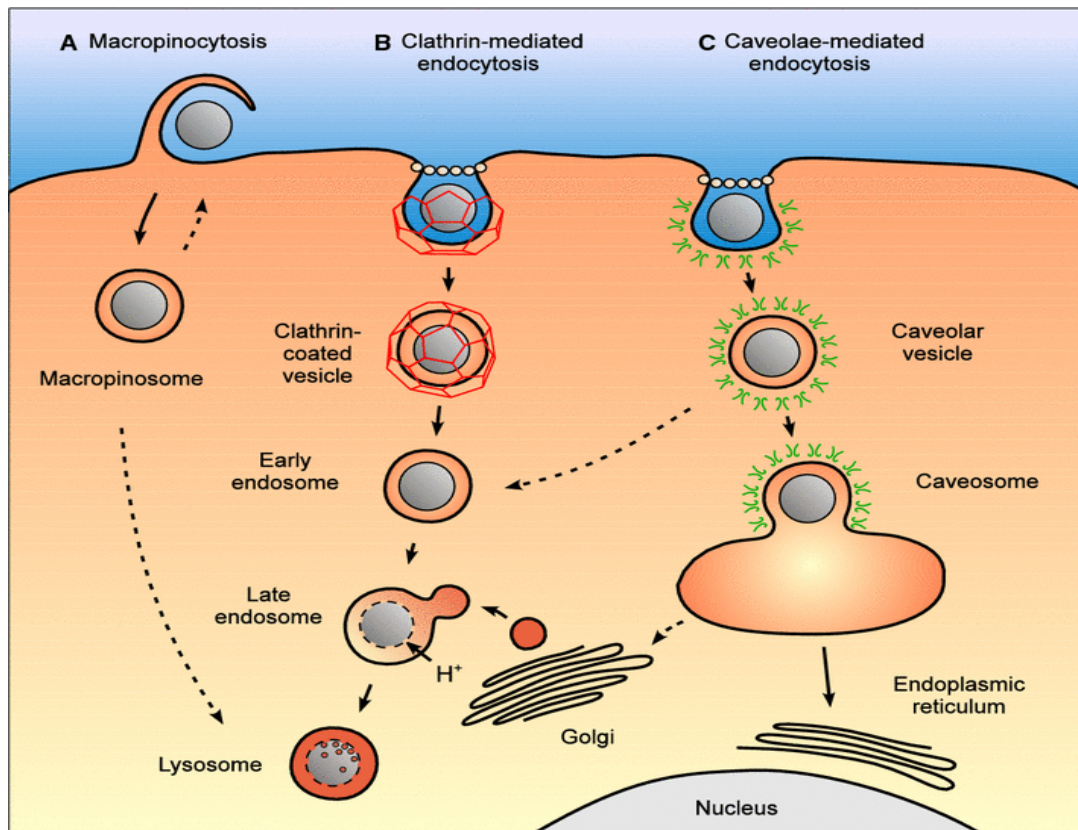
Figure 1- 4 Nanocarrier subcellular trafficking mechanisms following macropinocytosis, clathrin-mediated endocytosis and caveolae-mediated endocytosis. Taken from [11].
Following macropinocytosis, macropinosomes are formed which either fuse with existing lysosomes or recycle their content back to the cell surface (A). Internalisation through CME leads to the formation of early endosomes which mature and become acidified to form late endosomes. Eventually, late endosomes fuse with pre-existing lysosomes leading to the degradation of the entrapped carrier (B). Caveolar vesicles are formed following CvME that can fuse with caveosomes which are mostly transported to the endoplasmic reticulum or the Golgi apparatus (C).

Although this is yet a poorly understood field, some compounds have been shown to be endocytosed by pathways distinct from clathrin and caveolae-dependent endocytosis [11, 37]. Among these mechanisms, the most common appears to be the clathrin-independent carriers and glycosylphosphatidylinositol anchor proteins (GPI-AP)-enriched early endosomal compartments (CLIC/GEEC) pathway, which is responsible for the endocytosis of carriers that are delivered to GPI-AP-enriched early endosomal compartments (GEECs). This internalisation is thought to be regulated by the small G protein cdc42, and the destination of the endocytosed material appears to differ according to the cell type. In baby hamster kidney cells, GPI-AP are transported to reducing late endosomes, while in Chinese hamster ovary cells, they reach recycling endosomes [41].

1.5 Factors affecting nanocarriers fate *in vitro* and *in vivo*

Generally, successful drug delivery correlates well with the toxicological and pharmacological parameters of the nanocarriers such as the maximal tolerated dose, selectivity and residence time in the blood circulation. All these parameters depend on the physicochemical characteristics of the nanocarriers [11, 21, 42]; hereafter, factors affecting nanocarriers fate at the systemic as well as the cellular level will be discussed.

Size. The size of a nanoparticle can modulate kinetics, sensitivity and in some cases intensity of its interactions with the surrounding environment [2, 11, 21].

A) Diffusion coefficient and surface to volume ratio are inversely related to the nanocarrier size. This means the smaller a nanoparticle is, the quicker it can travel, the less it is likely to sediment and the more sensitive to the surrounding environment [2].

B) Particle size, along with surface composition, plays a major role in biodistribution [21]. For example, nanocarriers must be larger than the dimension of the tight junction between endothelial cells (a few nanometres) to avoid extravasation, while they must be smaller than the minimal lumen of capillaries (4-8 μm) to avoid embolisation [2]. In the presence of serum, there is a significant correlation between particle size and protein adsorption: blood clearance and hepatic uptake of smaller nanoparticles are generally lower than those of larger ones [43, 44]. Further, when

the total surface exhibited by distinctly sized particles was adjusted to be constant, proportionately higher levels of opsonin adsorption onto the surface of larger nanoparticles was observed. This was explained by the surface of large nanoparticles being less curved than small particles, providing geometric configuration to achieve efficient adsorption [25]. Kidney clearance occurs typically for molecules of a size less than 50 kDa (e.g. siRNA) [45]. Therefore, loading such payload into nanocarriers with a hydrodynamic size $\geq$ 10 nm can help avoiding glomerular filtration and excretion in urine, thereby improving the payload circulation time.

C) Certain biological environments can be accessed via passive targeting, which is usually a size-dependent phenomenon. Long-circulating nanocarriers are generally supposed to be able to extravasate and accumulate in tumoural tissues, where they could release their payload extra- or intracellularly. This effect of Enhanced Permeation and Retention (EPR) stems from the rapid angiogenetic processes of solid tumours, where hypervascularity is accompanied by the leaky character of newly formed blood vessel: the resulting more porous walls allow the extravasation of colloidal objects sized also hundreds of nanometers; on the other hand, the reduced or absent lymphatic drainage typical of cancers decreases the likelihood of their removal from the interstitial fluids, therefore increasing the permanence in the tumour. This is a unique feature that allows drug nanocarriers to accumulate and diffuse into tumoural tissues in a size selective manner [46].

D) The expression "macrophages can eat bigger than their head" is generally used to highlight the phagocytosis tolerance for a wide range of sizes [47]. In general, polymeric particles (e.g. polystyrene (PSt), poly(methylmetacrylate) and modified cellulose) and liposomes follow the same pattern in phagocytosis regarding size dependency [48-51], phagocytosis increases when particle size increases. However, the surface properties in the case of liposomes seem to have the upper hand in determining the extent and the rate of phagocytosis [52, 53].

Unlike phagocytosis, which occurs primarily in professional phagocytes, non-phagocytic mechanisms may take place simultaneously in virtually all types of cells and can vary accordingly. Therefore, it is difficult to sort the non-phagocytic pathways in accordance with nanoparticles properties [11]. Although its impact may vary upon the cell type [54], the size of nanoparticles may directly affect the mode of

pinocytosis. For example, some studies have shown that CME is the major pathway for nanoparticles with a size limit of around 200 nm. Surprisingly, as the size increased, a shift to CvME uptake pathway became apparent [57]. This trend of size dependency contrasts with the size of early endosomes, which have been reported to be 100 nm for CME and 50-80 nm for CvME, formed as a result of fluid or ligand/receptor complex internalisation [34, 37, 55, 56]. One suggested explanation is that solid nanoparticles may impose more mechanical influence on vesicle formation [11]. Finally, macropinocytosis usually occurs associated with CME or CvME with such size-selectivity [58].

Shape. There is significant evidence that particles shape can modulate their *in vivo* distribution and circulation time after intravenous injection. For example, a study showed that discoidal particles tend to accumulate less in the liver compared to their spherical counterparts [59]. In addition, cylindrically shaped particles showed ten times longer circulation time compared to spherically shaped particles [60]. These findings suggest that modulating the shape could be used to improve *in vivo* targeting of particles. Shallow curvature at the site of particle-cell contact triggers phagocytosis most effectively. A study conducted on alveolar macrophages suggested that initiation of phagocytosis is affected by local particle shape at the site of initial contact. In this study, spherical particles which have shallow curvature throughout their surface were efficiently taken up whereas ellipsoid-shaped particles, which have such curvature only at a certain parts of their surface, were not [61].

The effect of particle shape on endocytosis has only been recently investigated. However, the results were contradictory and any general dependency is still to be determined. For example, spherical gold nanoparticles were found to be internalised faster and more efficiently compared to rod or disk shaped particles [62]. On the contrary, another study demonstrated favoured uptake of cylindrical or rod shaped particles [63]. This can only be attributed to the predominance of other factors such as the size, the surface properties and the nature of the nanocarrier. Intracellular trafficking seems to also be affected by the shape of the internalised particle. A study on layered doubled hydroxides (LDHs) having rod-like or hexagonal shapes revealed that, although both shapes were internalised by CME and escaped from endosomes,

hexagonal LDHs were localised in the cytoplasm, while rod-like LDHs were localised in the nucleus, probably via active transport mediated by microtubules. This would be beneficial for the intracellular delivery of genes [64]. Finally, it is worth mentioning that nanocarriers with dimensions of high aspect ratio such as rod-like nanowhiskers or carbon nanotubes can enter cells in a non-energy dependent, needle-like manner called nanopenetration .

Mechanical properties. Particles flexibility and deformability play a major role in the biodistribution and circulation half-life of these particles. This effect was demonstrated in many studies using soft and flexible particles that mimic red blood cells (RBCs) which are able to deform and pass through pores and channels that are smaller than their diameter (~ 8 μm) [65-67]. Particles prepared with higher flexibility showed a much longer circulation half-life after intravenous injection and were able to pass through small channels.

Flexibility of the nanoparticles has been proposed to improve the binding ability of nanoparticles to the cell surface and increase the number of surface interactions with the surrounding environment [37, 68]. Hydrogel particles have been used to study the effect of flexibility on cellular uptake by altering cross-linking density. The effect was described to be cell-type dependent. For example, macrophages have shown increased sensitivity to stiff particles which can be linked to the fact that pathogens (e.g. bacteria) have stiffer cell walls than the surrounding tissue [37], whereas HeLa cells were shown to prefer soft particles [69].

Surface properties. In the presence of serum, the surface properties of the nanoparticles will directly influence opsonisation and, in turn, the extent of phagocytosis. Hydrophobic and ionic interactions are the two main driving forces controlling protein adsorption onto the nanoparticle surface [52]. It has been proposed that hydrophobic surfaces acquire higher level of protein adsorption than hydrophilic ones [70]. Therefore, nanoparticles exhibiting hydrophilic polymers on their surface (e.g. polyethyleneglycol (PEG) and polysaccharides) are able to repel opsonins and enhance circulation time [71, 72]. In addition, it has been proven that neutral or negatively charged nanoparticles have low rate of nonspecific cellular

uptake due to reduced plasma protein adsorption and, therefore, longer circulation time [21].

Nanoparticles possessing positively charged surface (e.g. polysaccharide chitosan) have better association with the cell membrane and internalisation rates, due to the negatively charged character of the cell membrane [73]. Particle surface charge plays a major role in the interaction with the endocytic vesicles due to low pH and the presence of enzymes which could trigger the release of the payload in a responsive manner.

Polycations are hypothesized to cause changes in endosomal volume, pH and chloride conductance. Endosomal membrane vacuolar H^+-ATPase pumps protons inside endosomes. If certain materials with protonable (e.g. amine) groups are sequestered in these acidic compartments, the transferred protons will be captured by these groups and decrease the rate of acidification. This proton buffering leads to further influx of protons, as well as their counter ions Cl^-. An osmotic imbalance occurs between the endosome and the cytosol, which in turn leads to a water influx and endosomal swelling and rupture [74, 75]. This proposed mechanism is called the "proton sponge" effect.

Although a positively charged surface of nanocarriers enhances membrane association, internalisation and endosomal escape, those bearing a negative zeta potential can show more specific and efficient uptake, especially when decorated with targeting ligands (the strategy of molecular addressing). According to this strategy, nanoparticles bearing ligands on their surface will be internalised through the same endocytic mechanism as the ligand alone. Moreover, potentiality of stronger cell interactions as compared to ligands alone results from the concentrated ligands on the nanoparticles surface. This strategy has been investigated in order to enhance delivery to a specific cell population and/or to control cellular internalisation. For example, folic acid-decorated nanoparticles have shown a higher affinity to folic acid receptors compared to free folic acids and showed preferential nanoparticles uptake [76, 77].

Anionic polyelectrolytes can also facilitate endosomal escape through what is called fusogenicity. Fusogenicity is the physical interaction between pH-sensitive membrane destabilizers and endosomal membranes. Several anionic polyelectrolytes undergo pH-induced hydrophilic-to-hydrophobic transitions and thus may penetrate

into the hydrophobic tail region of the phospholipids bilayers causing pore formation in the bilayers [75].

Bionano interface. Once the nanoparticles are exposed to a biological environment, they interact with blood proteins and that creates a "protein corona" on the surface of the nanoparticles [78]. This corona represents what is called the "bionano interface" that the cell sees and interacts with. It is one of the determining factors of cellular uptake, subcellular trafficking and biodistribution of nanoparticles [79, 80]. In a biological environment, the cell interacts with a nano-architectured system composed of a) the core (i.e. nanoparticle), b) a hard corona of slowly exchanging proteins surrounding the core and c) a collection of rapidly exchanging and weakly interacting proteins [81, 82]. Kinetically, the protein corona undergoes continuous exchange with the surrounding environment; protein exchange occurs between the nanoparticle surface and biological milieu (e.g. plasma), between the nanoparticle surface and the cell surface and between the free protein molecules in the medium, which have high affinity and can compete for the cell surface [82]. The biological activity of nanoparticles is strongly affected by protein structure. Activity and native structure of proteins can be affected by adsorption on the surface of nanoparticles and this can trigger a distinct signal within the cells [83]. This phenomenon has been exploited to modulate nano-objects targeting and biodistribution in two ways. First, to engineer a surface that creates an interface that exhibits minimal interactions with the surrounding milieu except for desired targets (e.g. PEGylated particles) [84]. Second, to design a surface that can attract certain proteins which can effectively deliver the particle to its desired location; e.g. Tween 80 coated particles bound to Apolipoprotein E (ApoE) in dispersion medium were as effective as ApoE grafted particles for brain delivery [85, 86].

1.6 Polysaccharide-based nanocarriers

It is important that materials used in the preparation of nanocarriers can be functionalised easily, in addition to being well characterised, biocompatible and biodegradable [17]. As polysaccharides (polymers of monosaccharides joined by

glycosidic bonds) possess these characteristics they are commonly used in the preparation of nanoparticles for use in drug delivery [87].

Polysaccharides can be found in abundance in a diverse range of natural sources. For example, alginate and carrageenan have algal origins; cellulose, pectin and guar gum have plant origins; dextran and xanthan gum have microbial origins; and hyaluronan, chondroitin and heparin have animal origins [88]. Correspondingly, there are wide variations in the chemical composition of polysaccharides (Figure 1-5) and in their physicochemical properties, including charge and molecular weight. On the other hand, as common points all these polysaccharides are biocompatible, stable, hydrophilic, and low in toxicity and have reactive sites available for chemical modification [88, 89]. Furthermore, they have the advantage of being inexpensive.

Chitosan

Alginate

Hyaluronan

Dextran

Heparin

In the major disaccharide repreating unit R$_1$and R$_2$=SO$_3$H
Otherwise, R$_1$=H or SO$_3$H and R$_2$=H, SO$_3$H or COCH$_3$

Chondroitin Sulfate

In Chondroitin-4-sulfate R$_1$=SO$_3$H and R$_2$=H
In Chondroitin-6-Sulfate R$_1$=H and R$_2$=SO$_3$H

Amylose

Pullulan

β-Cyclodextrin
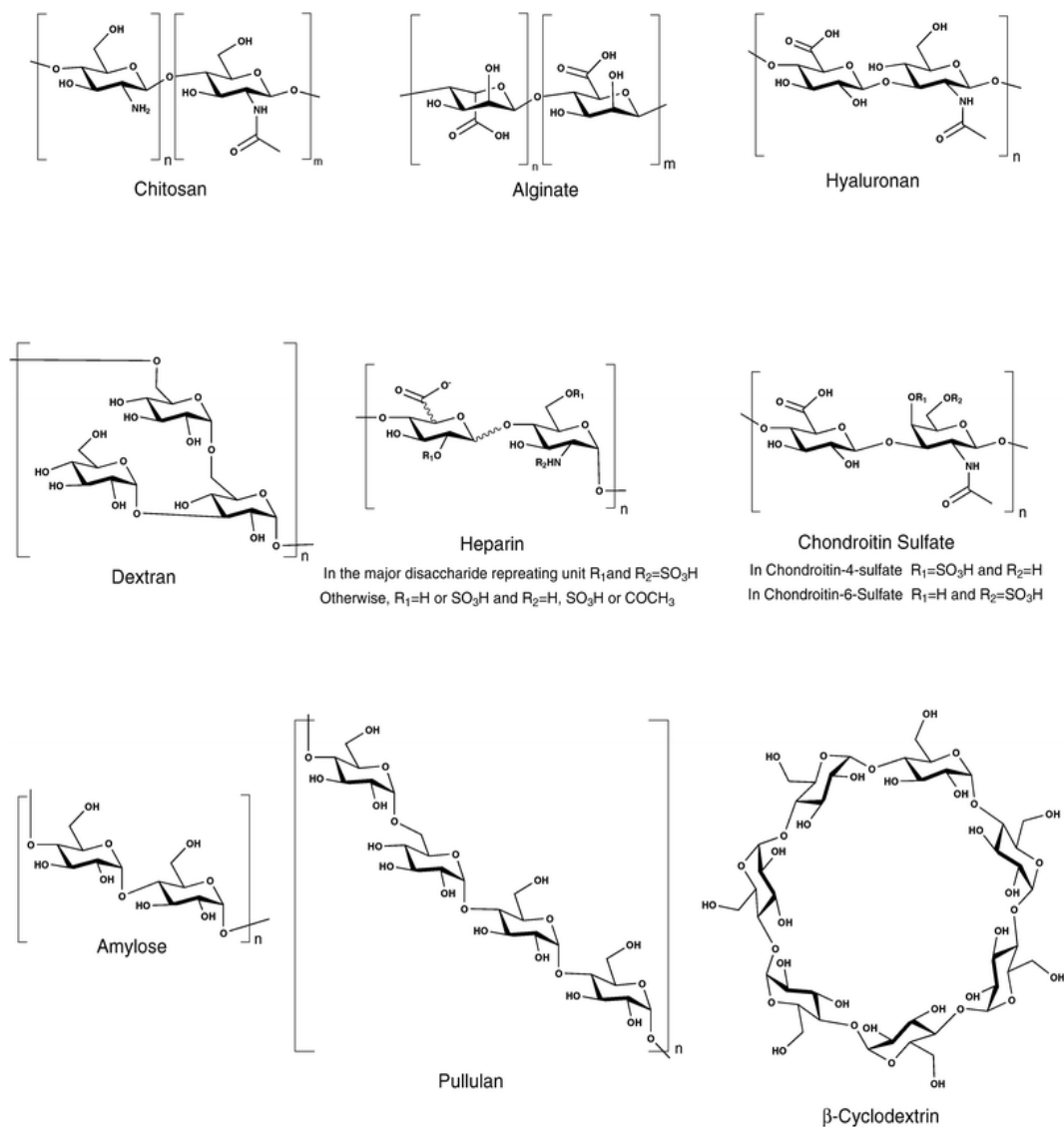
Figure 1- 5 The most commonly used polysaccharides in nanoparticles preparation for drug delivery and their chemical structures. Taken from [87].

Derivatives with determined/tailored properties have been created from the above polysaccharides via chemical functionalisation by predominantly using the free carboxyl and hydroxyl groups found along the backbone of polysaccharides [90, 91]; by using a range of methods, including oxidation, sulfation or grafting of polymer chains, the derivatisation has allowed to modify e.g. solubility, hydrophobicity and biological properties of the functionalised polysaccharides [90].

It is worth mentioning that these materials often show bioadhesive properties, particularly to mucosal surfaces, which is useful in targeting particular cells or organs and extending the time of drug residence [87].

1.6.1   Chitosan-based materials

Chitosan, a copolymer of β-(1→4)-linked D-glucose-2-amine and N-acetyl-D-glucose-2-amine (Figure 1- 5, top left), is a versatile biomaterial derived from the alkaline deacetylation of chitin (essentially poly(β-1,4-N-acetyl-D-glucose-2-amine) which is an abundant polysaccharide naturally present in the exoskeleton of insect and crustacean shells which are the most common source of the commercial forms of chitosan [92]. Chitin deacetylation is generally a heterogeneous and poorly controlled process which can result in polymers with different proportions of deacetylated D-glucose amine residues known as the degree of deacetylation (DD). This means that chitosan is a generic name which can refer to a variety of polymers with different molecular weight (MW) and DD, resulting in different physical, chemical and biological properties [93]. Therefore, MW and DD are the key factors to determine the applicability of chitosan as a biomaterial.

MW of chitosan correlates with the physical size of the polymer chains; since they are generally coiled (at least at acidic pH), the correlation is generally quadratic (size increasing with the square root of the MW). MW is an important factor that

determines chitosan's solubility as increasing the MW will decrease the entropy of mixing per mass unit [94]. Along with chitosan concentration, MW determines the viscosity of chitosan solution [94] which is commonly used to describe commercially available chitosan. Additionally, larger MW appears to decrease the complexation strength with oppositely charged macromolecules (e.g. nucleic acids) [95, 96]; this is the likely cause of the larger hydrodynamic size of the nanoparticles formed by higher MW chitosan with polyanions [97]. Chitosan has also been reported to have antimicrobial activity that is MW dependent [92].

The pKa of chitosan primary amines is in the range 6.2-7, thus they are completely protonated at a pH lower than 4.5 [98]. Due to this ionic character, chitosan is soluble in aqueous solutions at acidic pH; on the other hand, the absence of electrostatic repulsion at basic pH and the resulting formation of inter- and/or intra-molecular hydrogen bonds are at the basis of the poor solubility of chitosan at neutral or basic pH, where it typically crystallises [99]. However, since only the deacetylated amino groups can be protonated, the positive charge density is highly dependent on the DD of the polymer as well as the pH and the ionic strength of the medium. Additionally, this process is more apparent for polymers with high MW, while low MW chitosan typically shows some solubility at neutral pH (higher contribution of the entropy of mixing). Other properties are affected by chitosan DD: for example, mucoadhesion and cellular uptake of chitosan [100]. The higher is DD, the higher is the adsorption through mucosal surfaces due to electrostatic interaction with negatively charged cell membranes [101]. Additionally, chitosan's DD can influence the complexation and the release of polyanionic payloads, and it has been demonstrated that high DD enhances the extent of complexation and retards the release of the payload [102, 103]. As a result of the increased interactions with polyanions, the materials obtained via polyelectrolyte complexation are more compact (less porous) for higher DD; in the case of nanoparticles, this translates into lower hydrodynamic size and higher surface charge [104, 105].

Biocompatibility and degradability of chitosan are also affected by DD [106]. Decreasing DD appears to have beneficial effects on cell viability *in vitro*: this is not surprising if we consider the general toxicity of polycations, which on the other hand is advantageous for the fight against many parasites, bacteria and fungi [107]. In terms of degradability, since chitosan can be degraded by lysozyme through

hydrolysis of its residual N-acetylated residues, the *in vitro* and *in vivo* enzymatic degradation rates are inversely related to DD.

Having in mind applications in pharmaceutics, chitosan has gained approval in Japan, Italy and Finland for dietary applications and its use in wound dressings has been approved by the Food and Drug Administration (FDA) [108]. Chitosan-based nanocarriers can be formed via a variety of preparation methods, including desolvation method, reverse micellar method, emulsion droplet coalescence method and both covalent and ionic cross-linking methods [109] ; the latter are probably the most popular method, specifically in the ionotropic gelation with triphosphate (TPP), due to the ease of performance and the versatility and biocompatibility of TPP [110]. These nanocarriers have been investigated in a range of routes of administration, including oral, nasal, ocular, parenteral and transdermal delivery [87, 111]. More specifically, most research is now focusing in antigen delivery, anticancer drug delivery, peptide/protein delivery and gene delivery [111]; as a proof of the popularity of these systems, almost 10,000 papers (totalling almost 120,000 citations) have been published in this area [111].

1.6.1.1 TPP-mediated ionotropic gelation of chitosan

TPP is an inorganic multi-charged anion (Figure 1- 6) that is largely used in detergents, food industry and biomedical applications [112]. The complexation of sufficiently protonated chitosan with TPP is a mild and simple procedure that does not require the use of organic solvents or covalent cross-linking reagents which are often toxic to cells [113]. Electrostatic complexation allows TPP to bridge chitosan chains through the formation of inter- and intramolecular crosslinks forming a nano-sized three-dimensional (3D) polymeric network; the resulting materials can be defined as hydrogels, since the hydrophilicity of the ionic groups causes the network to be swollen by water [109]. Typically, chitosan/TPP 3D materials are characterized by high water content, soft and rubbery consistency, and low interfacial tension with water or biological fluids [114, 115]. When nanomaterials are prepared, the chitosan/TPP ratio allows to modulate particle size, morphology and surface charge [87].
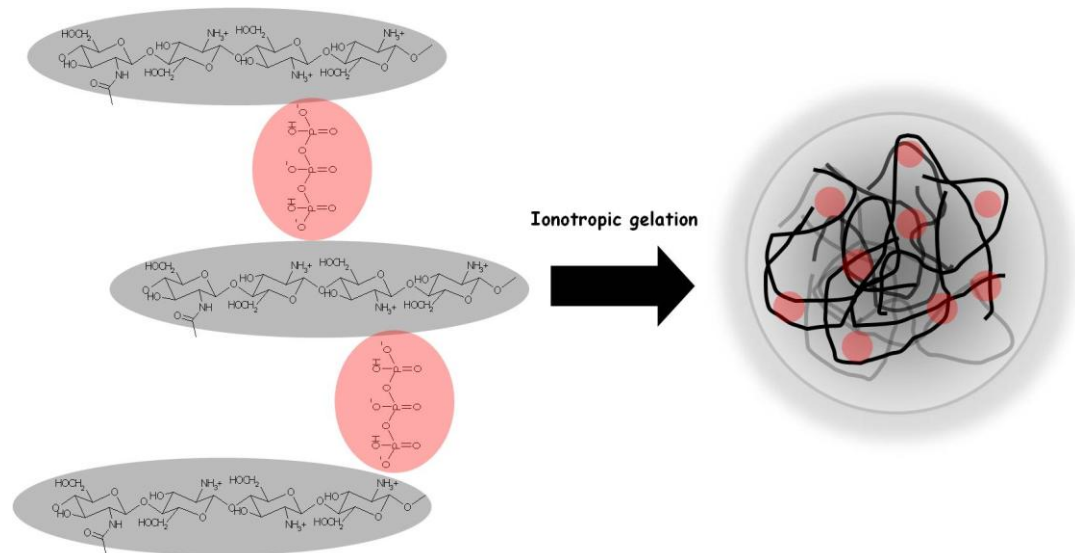
Figure 1- 6. TPP-mediated ionotropic gelation of Chitosan. Negatively charged TPP bridges between positive charges of chitosan chains forming a 3D polymeric network.

It is important to note that the chitosan/TPP complexation is most effective (more rapid and higher cross-link density) in providing gels when the charge of both partners is maximised, a condition that is profoundly dependent on the pH and the ionic strength of the environment [116]. For example, chitosan charge density above pH 6 is generally not sufficient to provide gelation. On the contrary, the minimum pH value for TPP to possess three negative charges is 3. Therefore, for stable and acceptable complexation the value must range between 3 and 5.5 [103].

Chitosan-TPP 3D or nanomaterials can be loaded with drugs either by incorporating them during complexation or by adsorption on the pre-formed materials [117]. The drugs can then be released by three mechanisms: diffusion through the swollen matrix; desorption from the particle surface; or erosion or degradation of the polymeric network [118]. Small molecules can be easily released through the first two mechanisms, while only the erosion mechanism allows macromolecules to be released [117].

1.6.1.2   Chitosan nanoparticles for gene delivery

Research in gene delivery has attracted the attention of scientists around the world as a promising therapeutic strategy to treat inherited as well as acquired diseases by restoring or shutting down a specific cellular function. Uncomplexed ("naked")

therapeutic nucleic acids have shown to be rapidly degraded by endogenous nucleases, and are poorly taken up by targeted cells, showing therefore a low transfection efficiency. Therefore, an appropriate gene delivery vehicle is required for successful gene therapy. There are two types of vectors that can be used for the delivery of genetic materials. One is genetically modified viruses, which are highly efficient vectors but are complex to use and to produce and are often associated with immunogenic responses [119]. The second is synthetic vectors, which are relatively safer, simple to use and easy to produce in large scale. The main disadvantage of these vectors is their low efficiency compared to viral vectors [120]. Synthetic vectors include liposomes, polymer based nanoparticles and complexes of negatively charged nucleic acids with cationic polymers (polyplexes) or cationic lipids (lipoplexes) [121]. Liposomes have shown a poor storage stability, relatively low encapsulation efficiency and short residence in the blood even after PEGylation [122]. Therefore, cationic polymers where amino groups are distributed across their backbone have been exploited extensively as gene carriers [120].

An ideal polymeric carrier should 1) form a complex with nucleic acids in a reversible fashion, 2) protect nucleic acids from degradation by endogenous enzymes, 3) allow prolonged circulation in the body fluid of choice and avoid phagocytosis; i.e. its surface should have a (stealth) protein-repellent character, 4) be taken up by the desired cell population in a selective manner, 5) be able to escape the endocytic pathway and 6) be degraded to a metabolisable or excretable product, showing negligible toxicity throughout its life cycle [21, 22, 120]. Since the late 90's, chitosan-based carriers gained increasing interest as a potential platform for safe and effective delivery of genetic material such as plasmid DNA (pDNA) and small interfering RNA (siRNA) [111, 121]. Chitosan is often used as building block of nucleic acid carriers, since it can complex them rather efficiently through its protonated amines [121]; it is noteworthy that at a given pH, the fraction of protonated amines is higher (= the pKa of the ammonium ions is lower) when the system is complexed with a polyanion, therefore the complexation is effective also at neutral pH where chitosan protonation is typically very low. Through complexation, chitosan can prevent nucleases from accessing the enclosed nucleic acid drugs by steric protection [123]. Additionally, chitosan demonstrates a capacity for pH buffering which is vital for endosomal escape through proton sponge effect (see

Section 1.5), which enables efficient transfection of nucleic acids [124]. Quantitatively, this buffering capacity is lower than that reported for poly(ethylene imine) (PEI) but higher than that observed for polylysine [125]. Moreover, chitosan has shown favourable values of IC_{50} compared to the above mentioned competitors [126, 127].

Chitosan nanocarriers have shown promising transfection efficiency both *in vitro* and *in vivo*. In fact, it has been reported that some chitosan-based formulations have higher tranfection efficiency than commercially available reagents [128-131]. A chitosan-based transfection reagent is already commercially available and development of many other prototypes is undergoing in laboratories [111]. However, several factors have shown to affect transfection efficiency of chitosan nanocarriers [121], of which chitosan MW and DD were the most important. Chitosan MW, as mentioned earlier, has an influence on the size and consequently on cell uptake which can strongly affect transfection efficiency [104, 105, 132]. Moreover, chitosan MW has an effect on the dissociation of nucleic acids from the complex after endocytosis. For example, complexes made of chitosan with MW of 10-50 kDa were shown to have good transfection efficiency compared to higher MW [132]. Chitosan DD can affect transfection efficiency too [133]. Increasing DD can increase nucleic acid loading, cellular uptake and enhance the stability of the complex. However, very high chitosan DD may retard or slow the subcellular release of encapsulated nucleic acids [134].

1.6.2 HA-based nanoparticles

Hayaluronic acid (HA), is a naturally occurring glycosaminoglycan that plays an extracellular structural role. HA is concentrated in regions of high cell division and invasion (e.g. cancer). In addition to its structural role, HA has an instructive role via HA receptors on the cell surface (mainly CD44 and RHAMM) [135]. Other receptors have also been reported [136]. There is a widespread interest in HA as a drug carrier as it is biocompatible, biodegradable, nontoxic and non-inflammatory [137].

In general, three main platforms of HA based nanocarriers have been exploited so far, 1) conjugates of low molecular weight HA to drugs; 2) nanoparticulate carriers where HA is displayed on the surface and drugs are physically incorporated in the bulk; 3) HA nanogels, which, from a structural point of view, are an intermediate system between two other platforms (Figure 1- 7) [137].
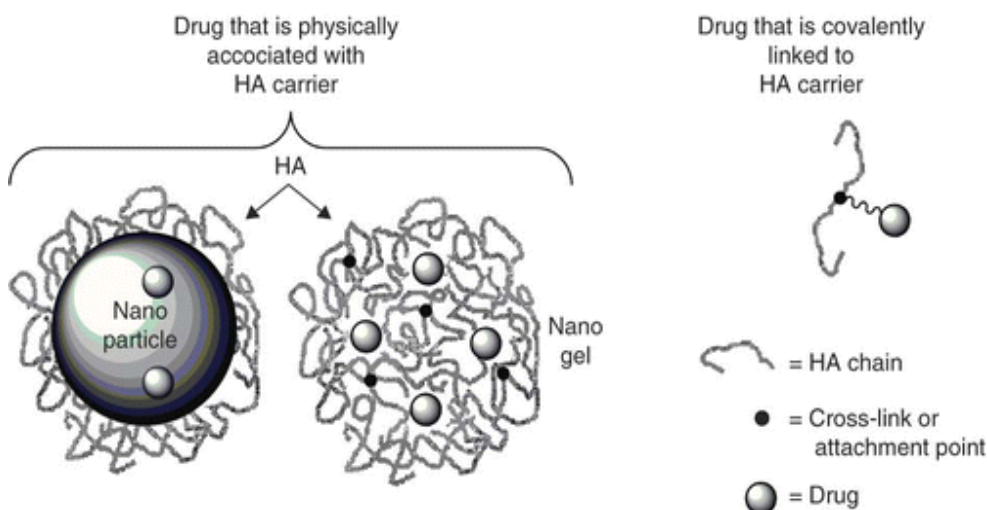
Figure 1- 7 Fundamental types of HA based nanomaterials. Taken from [137].

1.6.2.1 HA-decorated nanoparticles

HA in particular and polysaccharides in general [72, 137] have been exploited as coating materials for several colloidal drug carriers. The rationale behind this has been to provide protein-repellent character to the surface of the nanocarrier to increase blood residence time and diminish phagocytosis and/or to regulate the biodistribution of the nanocarrier to target a specific site in the body where HA receptors are overexpressed. Generally, HA-decorated nanoparticles include submicronic particles with a core of organic or inorganic materials and HA molecules are presented only in the outer shell of the particles. Amphiphilic HA derivatives with micellar structure in an aqueous medium can be considered also as HA-decorated nanoparticles. Nanocarriers are decorated with HA either by chemical or physical means. As examples of nanocarriers decorated with HA, one can mention

chitosan nanoparticles [138-140], polycation/nucleic acid complex [141, 142], iron oxide [143], liposomes [144, 145] and solid polyesters [146].

Chitosan nanoparticles prepared by ionotropic gelation with TPP have been coated with HA either by exploiting the ionic interactions between oppositely charged chitosan and HA [138] or by covalent bonding using a coupling reagent [140]. Positively charged chitosan-TPP nanoparticles (240 nm) have been added to HA solutions with varying parameters such as HA concentration, HA molecular weight and chitosan nanoparticle concentration. The HA-coating was found to markedly reduce the nanoparticle toxicity in a sensitive cell model (J774 macrophages). Moreover, the HA coating considerably slowed down the uptake process [147]. However, HA coating was shown to have a rather modest effect in terms of the mechanism of internalisation.

In order to improve chitosan-TPP nanoparticles stability and targeting, covalent bonding between the chitosan-TPP core and HA has been performed for the purpose of delivering 5-fluorouracil (5FU) to the colon. A solution of TPP and 5FU was added to chitosan solution to form hydrogel nanoparticles. Thereafter, an amide coupling reagent, N-(3-Dimethylaminopropyl)-N-ethylcarbodiimide (EDC), was added to a suspension containing chitosan nanoparticles as well as HA to form amide linkages between the carboxyalte groups of HA and the amino group of chitosan. HA coating was shown to decrease the drug release in different gastrointestinal tract simulated fluids with different pH values, to increase the potency of the drug and to enhance the uptake of the nanoparticles in HT-29 colon cancer cell line [140].

1.6.2.2 The feasibility of targeting CD44

CD44, the most common characterised HA receptor, is a cell-surface proteoglycan that encompasses a heterogeneous group of receptors with different isoforms which range from 80 to 250 kDa in size [136]. CD44 is encoded by a single gene containing 19 exons where 10 of them are variably spliced. The extensive heterogeneity of CD44 is attributed to this alternate splicing [136, 148] and post-translational modifications such as phosphorylation and glycosylation [136, 149].

 CD44 is involved in cell–cell interactions, cell adhesion and migration. CD44 also has a role in growth factor and chemokines binding and presentation [148].

CD44 has four major domains (Figure 1- 8); the distal (hyaluronan-binding) domain, the proximal domain (which is responsible for the alternate splicing to form numerous CD44 variants), the transmembrane domain and the cytoplasmic domain.

It is demonstrated that CD44, the main receptor for HA, is overexpressed in certain conditions, such as several solid tumours [150, 151] and activated inflammatory cells [152, 153]. This would enhance binding and internalisation of HA-attached therapeutics via receptor mediated endocytosis and consequently will allow HA functioning as a homing device. This may increase the potency of the attached (or loaded) drug by two means. First, potency is increased by increasing the uptake through CD44 or by circumventing multidrug resistance efflux pumps. Second, intrinsic activity of the drug can be increased by altering its localisation inside the cell [154]. Indeed, several HA based nanotherapeutics have been developed for CD44-mediated delivery (e.g. HA-anthracyclines [155], HA-quantum dots [156], and HA-nanogels [157]). However, it is worth mentioning that there are some drawbacks in CD44 selective drug delivery. First, CD44 is ubiquitously expressed, although in different amounts, in a large number of mammalian cell types which may decrease cell specificity. Additionally, CD44 present in variable isoforms, interacts with different substrates and is easily saturated due to its slow turnover (24-48 h) allowing only for a limited capacity for receptor mediated drug uptake. Therefore, factors affecting HA-CD44 interactions are of a significant importance to enhance selectivity of drug delivery [158, 159].
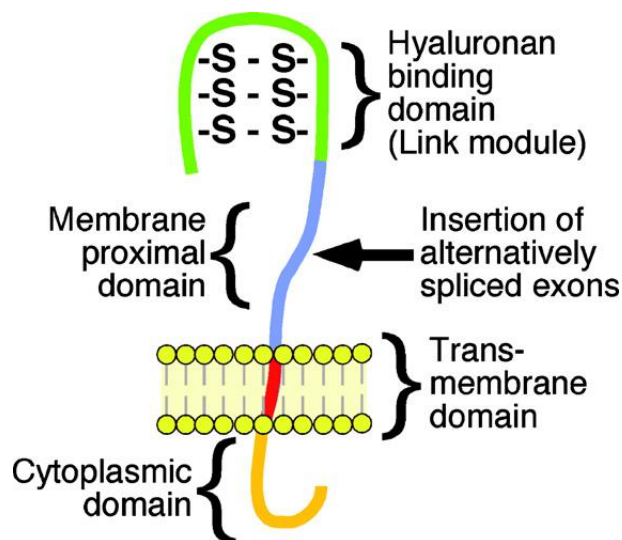
Figure 1- 8 The major domains of the standard form of CD44. Taken from [149].

1.6.2.3 Factors affecting HA-decorated nanoparticles-CD44 interactions

CD44-HA binding is proposed to be regulated by several mechanisms. First, CD44 post-translational modifications, which are not constant across all cells expressing the receptor, greatly influence the affinity of an individual receptor to HA [160]. For example, glycosylated CD44 is a prerequisite for HA binding in certain cell types, while glycosylated CD44 rich in sialic acid decrease HA binding [153, 161, 162]. Furthermore, CD44 expressing lymphocytes do not bind HA until CD44 is deglycosylated upon lymphocytes activation [153, 163]. Last, CD44 must be acylated to internalise via endocytosis [164]. Thus, CD44 post-translational modifications must be considered in the development of HA targeted therapeutics.

A second proposed mechanism is derived from the fact that an individual HA chain contains, within its repetitive structure, multiple CD44 binding sites which will allow an individual HA chain to interact with many receptors on the cell surface simultaneously. Therefore, changes in CD44 density (e.g. over-expression) and arrangement on the cell surface (e.g. clustering) would affect the strength or avidity of such interaction [160]. Indeed, a preferential uptake of HA-decorated nanotherapeutics in CD44-overexpressing cells through CD44-mediated endocytosis has been demonstrated in many cell types [146, 165]

A third mechanism proposes that changes in HA molecular mass have an impact on its binding to CD44 and consequently its biological functions [160]. For example, high molecular weight HA (HMW-HA) is known to be immunosuppressive and anti-angiogenic, whereas low molecular weight HA (LMW-HA) is regarded as immuno-stimulatory and angiogenic [166]. However, the exact MW of HA responsible for stimulation or suppression of immune response is debatable. Carriers which exploited HA MW and its consequent binding to CD44 have been reported in the literature. A small library of liposomes distinguished only by the MW of their surface-grafted HA was used to test HA MW effect on the affinity of these

liposomes to CD44 [167]. The affinity towards CD44 was found to be merely controlled by the MW of the liposomes surface bound HA, from extremely low binding for LMW-HA to binding with high affinity for HMW-HA. This could be ascribed to the fact that carriers consisting of high molecular weight HA were shown to induce CD44-binding and endocytosis by cross-linking multiple receptors [154]. Likewise, short HA oligosaccharides have also been employed on a larger carrier to tune the carrier interactions with CD44 [168, 169]. It is demonstrated that CD44 interacts with HA length of 6 to 8 saccharides at the minimum [170]. A single HA oligosaccharide on a larger carrier can maintain a high enough affinity to an individual CD44. Multiple HA oligosaccharides binding to multiple CD44 receptors at sites of high receptor density create enough avidity for uptake and effective targeting [154]. In conclusion, highlighting the molecular weight dependent interactions of HA-decorated nanocarriers with CD44 would have a great implication on the development of more efficient CD44 targeted therapeutics.

1.7 Scope of the thesis

This research aimed to develop polysaccharide-based nanoparticles for potential use in gene delivery. These nanoparticles would display a core mostly composed of chitosan cross-linked with TPP and a surface where HA would concentrate, thus providing the possibility to target HA receptors (e.g. CD44) and creating a surface with a "protein-repellent" character (Figure 1- 9).
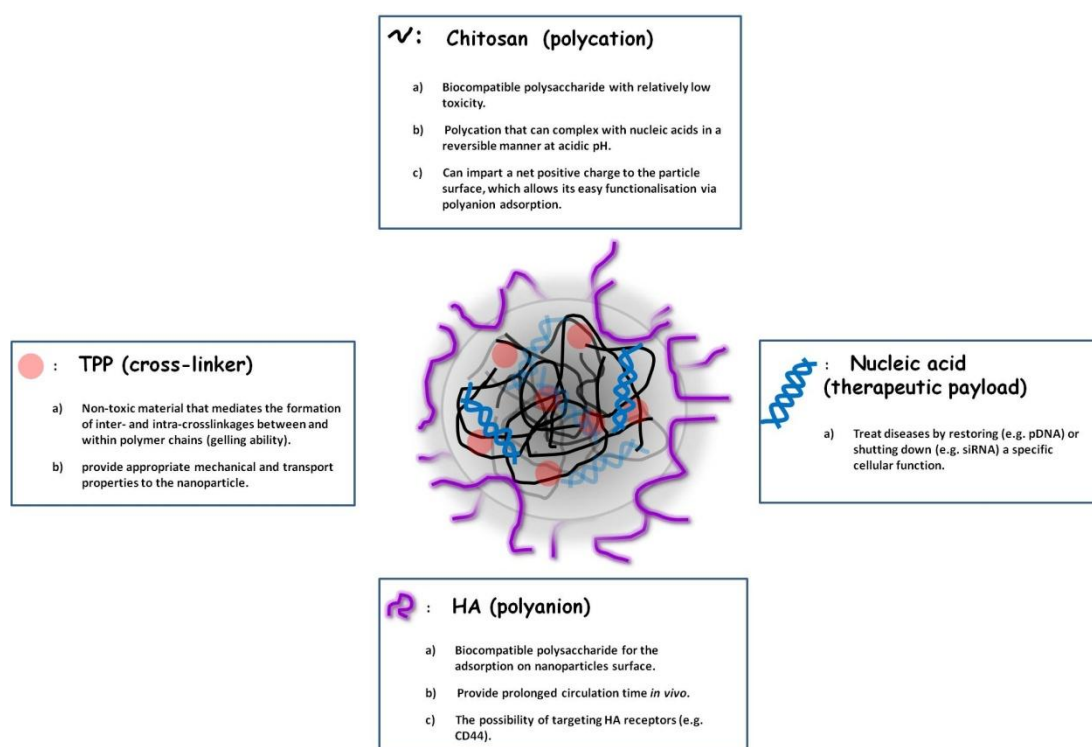
Figure 1- 9 Nanoparticles building blocks, the rationale behind using them and hypothetical nanoparticle structure (middle): TPP cross-links chitosan chains which form a positively charged core of the nanoparticle where nucleic acid is encapsulated and HA can concentrate on the surface.

The specific aims of this thesis were:

Aim 1 (developed in Chapter Two) was to highlight the effect of chitosan molecular weight on the morphology/structure of chitosan-TPP nanoparticles and their nucleic acid encapsulation efficiency and how the resulting differences may influence the

process of HA adsorption on their surfaces. Particular interest was given to investigate the influence of different structures of HA-coated nanoparticles on their stability, protein repellent character and payload release.

Aim 2 (developed in Chapter Three) was to illustrate the influence of nanoparticles morphological differences on HA presentation to cell surface receptors and thus the phenomenon of CD44-mediated internalisation. Cytotoxicity, internalisation mechanism and kinetics of HA-coated chitosan-TPP nanoparticles were investigated in a phagocyte model expressing CD44 (RAW 264.7 macrophages).

Aim 3 (developed in Chapter Four) was to test the feasibility of using HA-coated chitosan-TPP nanoparticles as a CD44-dependent therapeutic approach. Nanoparticle-mediated transfection of nucleic acid payloads to cells with significantly different expression of CD44 was investigated. Additionally, we have studied the possibility for HA-coated nanoparticles to exert a direct anti-inflammatory effect due to the presentation of HA and its binding to cell surface receptors such as CD44. The effect of HA-coated nanoparticles on inflammatory mediators in activated and non-activated macrophages was also analysed.

1.8 References

1. Kim, B.Y.S., J.T. Rutka, and W.C.W. Chan, *Current Concepts: Nanomedicine.* New England Journal of Medicine, 2010. **363**(25): p. 2434-2443.
2. Tirelli, N., *(Bio)Responsive nanoparticles.* Current Opinion in Colloid & Interface Science, 2006. **11**(4): p. 210-216.
3. Feynman, R.P., *There's plenty of room at the bottom.* Engineering and Science 1960. **23**(5): p. 22-36.
4. Feynman, R.P. and C. Sykes, *No Ordinary Genius: The Illustrated Richard Feynman.* 1995: W. W. Norton & Company.
5. Eigler, D.M. and E.K. Schweizer, *Positioning single atoms with a scanning tunneling microscope.* Nature, 1990. **344**(6266): p. 524-526.
6. Junno, T., et al., *Controlled manipulation of nanoparticles with an atomic force microscope.* Applied Physics Letters, 1995. **66**(26): p. 3627-3629.
7. Euliss, L.E., et al., *Imparting size, shape, and composition control of materials for nanomedicine.* Chemical Society Reviews, 2006. **35**(11): p. 1095-1104.
8. De Jong, W.H. and P.J.A. Borm, *Drug delivery and nanoparticles: Applications and hazards.* International Journal of Nanomedicine, 2008. **3**(2): p. 133-149.
9. Farokhzad, O.C. and R. Langer, *Impact of Nanotechnology on Drug Delivery.* Acs Nano, 2009. **3**(1): p. 16-20.
10. Cho, K.J., et al., *Therapeutic nanoparticles for drug delivery in cancer.* Clinical Cancer Research, 2008. **14**(5): p. 1310-1316.
11. Hillaireau, H. and P. Couvreur, *Nanocarriers' entry into the cell: relevance to drug delivery.* Cellular and Molecular Life Sciences, 2009. **66**(17): p. 2873-2896.
12. Anne, S. and R. Thomas, *"Solid Lipid Nanoparticles"*, in *Nanocarrier Technologies*. 2006. p. 41.
13. Muller, R.H., K. Mader, and S. Gohla, *Solid lipid nanoparticles (SLN) for controlled drug delivery - a review of the state of the art.* European Journal of Pharmaceutics and Biopharmaceutics, 2000. **50**(1): p. 161-177.
14. Torchilin, V., et al., *Pharmaceutical Micelles: Combining Longevity, Stability, and Stimuli Sensitivity*, in *Multifunctional Pharmaceutical Nanocarriers*. 2008, Springer New York. p. 263-308.
15. Nishiyama, N. and K. Kataoka, *Current state, achievements, and future prospects of polymeric micelles as nanocarriers for drug and gene delivery.* Pharmacology & Therapeutics, 2006. **112**(3): p. 630-648.
16. Faraji, A.H. and P. Wipf, *Nanoparticles in cellular drug delivery.* Bioorganic & Medicinal Chemistry, 2009. **17**(8): p. 2950-2962.
17. Peer, D., et al., *Nanocarriers as an emerging platform for cancer therapy.* Nature Nanotechnology, 2007. **2**(12): p. 751-760.
18. Zhang, L., et al., *Nanoparticles in medicine: Therapeutic applications and developments.* Clinical Pharmacology & Therapeutics, 2008. **83**(5): p. 761-769.
19. Lyon, A.R., et al., *Gene therapy: targeting the myocardium.* Heart, 2008. **94**(1): p. 89-99.

20.   Yildiz, I., S. Shukla, and N.F. Steinmetz, *Applications of viral nanoparticles in medicine.* Current Opinion in Biotechnology, 2011. **22**(6): p. 901-908.

21.   Alexis, F., et al., *Factors affecting the clearance and biodistribution of polymeric nanoparticles.* Molecular Pharmaceutics, 2008. **5**(4): p. 505-515.

22.   Whitehead, K.A., R. Langer, and D.G. Anderson, *Knocking down barriers: advances in siRNA delivery.* Nature Reviews Drug Discovery, 2009. **8**(2): p. 129-138.

23.   Aderem, A. and D.M. Underhill, *Mechanisms of phagocytosis in macrophages.* Annual Review of Immunology, 1999. **17**: p. 593-623.

24.   Rabinovitch, M., *Professional and non-professional phagocytes: an introduction.* Trends in Cell Biology, 1995. **5**(3): p. 85-87.

25.   Vonarbourg, A., et al., *Parameters influencing the stealthiness of colloidal drug delivery systems.* Biomaterials, 2006. **27**(24): p. 4356-4373.

26.   Owens, D.E. and N.A. Peppas, *Opsonization, biodistribution, and pharmacokinetics of polymeric nanoparticles.* International Journal of Pharmaceutics, 2006. **307**(1): p. 93-102.

27.   Groves, E., et al., *Molecular mechanisms of phagocytic uptake in mammalian cells.* Cellular and Molecular Life Sciences, 2008. **65**(13): p. 1957-1976.

28.   Vachon, E., et al., *CD44 is a phagocytic receptor.* Blood, 2006. **107**(10): p. 4149-4158.

29.   Caron, E. and A. Hall, *Identification of two distinct mechanisms of phagocytosis controlled by different Rho GTPases.* Science, 1998. **282**(5394): p. 1717-1721.

30.   Swanson, J.A. and S.C. Baer, *Phagocytosis by zippers and triggers.* Trends in Cell Biology, 1995. **5**(3): p. 89-93.

31.   Harris, J.M. and R.B. Chess, *Effect of pegylation on pharmaceuticals.* Nature Reviews Drug Discovery, 2003. **2**(3): p. 214-221.

32.   Khalil, I.A., et al., *Uptake pathways and subsequent intracellular trafficking in nonviral gene delivery.* Pharmacol Rev, 2006. **58**(1): p. 32-45.

33.   Mukherjee, S., R.N. Ghosh, and F.R. Maxfield, *Endocytosis.* Physiological Reviews, 1997. **77**(3): p. 759-803.

34.   Bareford, L.A. and P.W. Swaan, *Endocytic mechanisms for targeted drug delivery.* Advanced Drug Delivery Reviews, 2007. **59**(8): p. 748-758.

35.   Stromhaug, P.E., et al., *Differences between fluid-phase endocytosis (pinocytosis) and receptor-mediated endocytosis in isolated rat hepatocytes.* European Journal of Cell Biology, 1997. **73**(1): p. 28-39.

36.   Matveev, S., et al., *The role of caveolae and caveolin in vesicle-dependent and vesicle-independent trafficking.* Adv Drug Deliv Rev, 2001. **49**(3): p. 237-50.

37.   Conner, S.D. and S.L. Schmid, *Regulated portals of entry into the cell.* Nature, 2003. **422**(6927): p. 37-44.

38.   Harris, J., et al., *Caveolae and caveolin in immune cells: distribution and functions.* Trends Immunol, 2002. **23**(3): p. 158-64.

39.   Lamaze, C. and S.L. Schmid, *The emergence of clathrin-independent pinocytic pathways.* Curr Opin Cell Biol, 1995. **7**(4): p. 573-80.

40.   Ferrari, A., et al., *Caveolae-mediated internalization of extracellular HIV-1 tat fusion proteins visualized in real time.* Mol Ther, 2003. **8**(2): p. 284-94.

41.   Sobo, K., et al., *Late Endosomal Cholesterol Accumulation Leads to Impaired Intra-Endosomal Trafficking.* Plos One, 2007. **2**(9).

42.   Morachis, J.M., E.A. Mahmoud, and A. Almutairi, *Physical and Chemical Strategies for Therapeutic Delivery by Using Polymeric Nanoparticles.* Pharmacological Reviews, 2012. **64**(3): p. 505-519.

43.   Nagayama, S., et al., *Time-dependent changes in opsonin amount associated on nanoparticles alter their hepatic uptake characteristics.* International Journal of Pharmaceutics, 2007. **342**(1-2): p. 215-221.

44.   Fang, C., et al., *In vivo tumor targeting of tumor necrosis factor-alpha-loaded stealth nanoparticles: Effect of MePEG molecular weight and particle size.* European Journal of Pharmaceutical Sciences, 2006. **27**(1): p. 27-36.

45.   Rappaport, J., et al., *Transport of phosphorothioate oligonucleotides in kidney - implications for molecular therapy.* Kidney International, 1995. **47**(5): p. 1462-1469.

46.   Hobbs, S.K., et al., *Regulation of transport pathways in tumor vessels: Role of tumor type and microenvironment.* Proceedings of the National Academy of Sciences of the United States of America, 1998. **95**(8): p. 4607-4612.

47.   Aderem, A., *How to eat something bigger than your head.* Cell, 2002. **110**(1): p. 5-8.

48.   Wetzel, M.G. and E.D. Korn, *Phagocytosis of latex beads by acanthamoeba castellanii (NEFF): isolation of phagocytic vesicles and their membranes.* Journal of Cell Biology, 1969. **43**(1): p. 90-104.

49.   Schafer, V., et al., *Phagocytosis of nanoparticles by human-immunodeficiency-virus (HIV)-infected macrophages - a possibility for antiviral drug targeting.* Pharmaceutical Research, 1992. **9**(4): p. 541-546.

50.   Tabata, Y. and Y. Ikada, *Effect of the size and surface-charge of polymer microspheres on their phagocytosis by macrophage.* Biomaterials, 1988. **9**(4): p. 356-362.

51.   Moghimi, S.M. and J. Szebeni, *Stealth liposomes and long circulating nanoparticles: critical issues in pharmacokinetics, opsonization and protein-binding properties.* Progress in Lipid Research, 2003. **42**(6): p. 463-478.

52.   Heath, T.D., N.G. Lopez, and D. Papahadjopoulos, *The effects of liposome size and surface-charge on liposome-mediated delivery of methotrexate-gamma-aspartate to cells-invitro.* Biochimica Et Biophysica Acta, 1985. **820**(1): p. 74-84.

53.   Allen, T.M., et al., *Uptake of liposomes by cultured mouse bone-marrow macrophages - influence of liposome composition and size.* Biochimica Et Biophysica Acta, 1991. **1061**(1): p. 56-64.

54.   Zauner, W., N.A. Farrow, and A.M.R. Haines, *In vitro uptake of polystyrene microspheres: effect of particle size, cell line and cell density.* Journal of Controlled Release, 2001. **71**(1): p. 39-51.

55.   Mayor, S. and R.E. Pagano, *Pathways of clathrin-independent endocytosis.* Nature Reviews Molecular Cell Biology, 2007. **8**(8): p. 603-612.

56.   Desai, M.P., et al., *The mechanism of uptake of biodegradable microparticles in Caco-2 cells is size dependent.* Pharmaceutical Research, 1997. **14**(11): p. 1568-1573.

57.   Rejman, J., et al., *Size-dependent internalization of particles via the pathways of clathrin-and caveolae-mediated endocytosis.* Biochemical Journal, 2004. **377**: p. 159-169.

58.   Harush-Frenkel, O., et al., *Surface charge of nanoparticles determines their endocytic and transcytotic pathway in polarized MDCK cells.* Biomacromolecules, 2008. **9**(2): p. 435-443.

59.   Decuzzi, P., et al., *Size and shape effects in the biodistribution of intravascularly injected particles.* Journal of Controlled Release, 2010. **141**(3): p. 320-327.

60.   Geng, Y., et al., *Shape effects of filaments versus spherical particles in flow and drug delivery.* Nature Nanotechnology, 2007. **2**(4): p. 249-255.

61.   Champion, J.A. and S. Mitragotri, *Role of target geometry in phagocytosis.* Proceedings of the National Academy of Sciences of the United States of America, 2006. **103**(13): p. 4930-4934.

62.   Chithrani, B.D., A.A. Ghazani, and W.C.W. Chan, *Determining the size and shape dependence of gold nanoparticle uptake into mammalian cells.* Nano Letters, 2006. **6**(4): p. 662-668.

63.   Gratton, S.E.A., et al., *The effect of particle design on cellular internalization pathways.* Proceedings of the National Academy of Sciences of the United States of America, 2008. **105**(33): p. 11613-11618.

64.   Xu, Z.P., et al., *Subcellular compartment targeting of layered double hydroxide nanoparticles.* Journal of Controlled Release, 2008. **130**(1): p. 86-94.

65.   Peretz S, Regev O. *Carbon nanotubes as nanocarriers in medicine*. Current Opinion in Colloid & Interface Science Dec;17(6):360-368.

66.   Haghgooie, R., M. Toner, and P.S. Doyle, *Squishy Non-Spherical Hydrogel Microparticles.* Macromolecular Rapid Communications, 2010. **31**(2): p. 128-134.

67.   Merkel, T.J., et al., *Using mechanobiological mimicry of red blood cells to extend circulation times of hydrogel microparticles.* Proceedings of the National Academy of Sciences of the United States of America, 2011. **108**(2): p. 586-591.

68.   Doshi, N., et al., *Red blood cell-mimicking synthetic biomaterial particles.* Proceedings of the National Academy of Sciences of the United States of America, 2009. **106**(51): p. 21495-21499.

69.   Matter, K. and I. Mellman, *Mechanisms of cell polarity - sorting and transport in epithelial-cells.* Current Opinion in Cell Biology, 1994. **6**(4): p. 545-554.

70.   You, J.O. and D.T. Auguste, *Nanocarrier Cross-Linking Density and pH Sensitivity Regulate Intracellular Gene Transfer.* Nano Letters, 2009. **9**(12): p. 4467-4473.

71.   Jeon, S.I., et al., *Protein surface interactions in the presence of polyethylene oxide .1. simplified theory.* Journal of Colloid and Interface Science, 1991. **142**(1): p. 149-158.

72.   Vonarbourg, A., et al., *Parameters influencing the stealthiness of colloidal drug delivery systems.* Biomaterials, 2006. **27**(24): p. 4356-4373.

73.   Lemarchand, C., R. Gref, and P. Couvreur, *Polysaccharide-decorated nanoparticles.* European Journal of Pharmaceutics and Biopharmaceutics, 2004. **58**(2): p. 327-341.

74.   Mao, S., et al., *Uptake and transport of PEG-graft-trimethyl-chitosan copolymer-insulin nanocomplexes by epithelial cells.* Pharmaceutical Research, 2005. **22**(12): p. 2058-2068.

75. Kang, H.C., Lee, M., and Bae, Y. H, *Polymeric gene delivery vectors*, in *Nanotechnology in Therapeutics: Current Technology and Application*, J.Z.H. N. A. Peppas, and and J. B. Thomas, Editors. 2007, Horizon Bioscience. p. 131–161.

76. Cho, Y.W., J.D. Kim, and K. Park, *Pollycation gene delivery systems: escape from endosomes to cytosol.* Journal of Pharmacy and Pharmacology, 2003. **55**(6): p. 721-734.

77. Stella, B., et al., *Design of folic acid-conjugated nanoparticles for drug targeting.* Journal of Pharmaceutical Sciences, 2000. **89**(11): p. 1452-1464.

78. Lee, R.J. and P.S. Low, *Folate-mediated tumor-cell targeting of liposome-entrapped doxorubicin in-vitro.* Biochimica Et Biophysica Acta-Biomembranes, 1995. **1233**(2): p. 134-144.

79. Mahon, E., et al., *Designing the nanoparticle-biomolecule interface for "targeting and therapeutic delivery".* Journal of Controlled Release, 2012. **161**(2): p. 164-174.

80. Chithrani, B.D. and W.C.W. Chan, *Elucidating the mechanism of cellular uptake and removal of protein-coated gold nanoparticles of different sizes and shapes.* Nano Letters, 2007. **7**(6): p. 1542-1550.

81. Dobrovolskaia, M.A., et al., *Preclinical studies to understand nanoparticle interaction with the immune system and its potential effects on nanoparticle biodistribution.* Molecular Pharmaceutics, 2008. **5**(4): p. 487-495.

82. Cedervall, T., et al., *Understanding the nanoparticle-protein corona using methods to quantify exchange rates and affinities of proteins for nanoparticles.* Proceedings of the National Academy of Sciences of the United States of America, 2007. **104**(7): p. 2050-2055.

83. Walczyk, D., et al., *What the Cell "Sees" in Bionanoscience.* Journal of the American Chemical Society, 2010. **132**(16): p. 5761-5768.

84. Deng, Z.J., et al., *Nanoparticle-induced unfolding of fibrinogen promotes Mac-1 receptor activation and inflammation.* Nature Nanotechnology, 2010. **6**(1): p. 39-44.

85. Otsuka, H., Y. Nagasaki, and K. Kataoka, *PEGylated nanoparticles for biological and pharmaceutical applications.* Advanced Drug Delivery Reviews, 2003. **55**(3): p. 403-419.

86. Kreuter, J., *Influence of the surface properties on nanoparticle-mediated transport of drugs to the brain.* Journal of Nanoscience and Nanotechnology, 2004. **4**(5): p. 484-488.

87. Kreuter, J., et al., *Apolipoprotein-mediated transport of nanoparticle-bound drugs across the blood-brain barrier.* Journal of Drug Targeting, 2002. **10**(4): p. 317-325.

88. Mizrahy, S. and D. Peer, *Polysaccharides as building blocks for nanotherapeutics.* Chemical Society Reviews, 2012. **41**(7): p. 2623-2640.

89. Sinha, V.R. and R. Kumria, *Polysaccharides in colon-specific drug delivery.* International Journal of Pharmaceutics, 2001. **224**(1-2): p. 19-38.

90. Baldwin, A.D. and K.L. Kiick, *Polysaccharide-Modified Synthetic Polymeric Biomaterials.* Biopolymers, 2010. **94**(1): p. 128-140.

91. Yang, J.-S., Y.-J. Xie, and W. He, *Research progress on chemical modification of alginate: A review.* Carbohydrate Polymers, 2011. **84**(1): p. 33-39.

92.   Mukhopadhyay, P., et al., *Strategies for effective oral insulin delivery with modified chitosan nanoparticles: A review.* Progress in Polymer Science, 2012. **37**(11): p. 1457-1475.

93.   Qin, C.Q., et al., *Water-solubility of chitosan and its antimicrobial activity.* Carbohydrate Polymers, 2006. **63**(3): p. 367-374.

94.   Illum, L., *Chitosan and its use as a pharmaceutical excipient.* Pharmaceutical Research, 1998. **15**(9): p. 1326-1331.

95.   Kasaai, M.R., J. Arul, and C. Charlet, *Intrinsic viscosity-molecular weight relationship for chitosan.* Journal of Polymer Science Part B-Polymer Physics, 2000. **38**(19): p. 2591-2598.

96.   Xu, Y.M. and Y.M. Du, *Effect of molecular structure of chitosan on protein delivery properties of chitosan nanoparticles.* International Journal of Pharmaceutics, 2003. **250**(1): p. 215-226.

97.   Mi, F.L., et al., *Chitosan-polyelectrolyte complexation for the preparation of gel beads and controlled release of anticancer drug. I. Effect of phosphorous polyelectrolyte complex and enzymatic hydrolysis of polymer.* Journal of Applied Polymer Science, 1999. **74**(7): p. 1868-1879.

98.   Csaba, N., M. Koeping-Hoeggard, and M. Jose Alonso, *Ionically crosslinked chitosan/tripolyphosphate nanoparticles for oligonucleotide and plasmid DNA delivery.* International Journal of Pharmaceutics (Kidlington), 2009. **382**(1-2): p. 205-214.

99.   Kumar, M., et al., *Chitosan chemistry and pharmaceutical perspectives.* Chemical Reviews, 2004. **104**(12): p. 6017-6084.

100.   Nishimura, S.I., et al., *Chemospecific manipulations of a rigid polysaccharide - syntheses of novel chitosan derivatives with excellent solubility in common organic-solvents by regioselective chemical modifications.* Macromolecules, 1991. **24**(17): p. 4745-4748.

101.   Lehr, C.M., et al., *Invitro evaluation of mucoadhesive properties of chitosan and some other natural polymers.* International Journal of Pharmaceutics, 1992. **78**(1): p. 43-48.

102.   Schipper, N.G.M., K.M. Varum, and P. Artursson, *Chitosans as absorption enhancers of poorly absorbable drugs: Influence of molecular weight and degree of acetylation.* European Journal of Pharmaceutical Sciences, 1996. **4**(SUPPL.): p. S153.

103.   Richardson, S.C.W., H.J.V. Kolbe, and R. Duncan, *Potential of low molecular mass chitosan as a DNA delivery system: biocompatibility, body distribution and ability to complex and protect DNA.* International Journal of Pharmaceutics, 1999. **178**(2): p. 231-243.

104.   Shu, X.Z. and K.J. Zhu, *The influence of multivalent phosphate structure on the properties of ionically cross-linked chitosan films for controlled drug release.* European Journal of Pharmaceutics and Biopharmaceutics, 2002. **54**(2): p. 235-243.

105.   Huang, M., E. Khor, and L.Y. Lim, *Uptake and cytotoxicity of chitosan molecules and nanoparticles: Effects of molecular weight and degree of deacetylation.* Pharmaceutical Research, 2004. **21**(2): p. 344-353.

106.   Liu, X.D., et al., *The influence of polymeric properties on chitosan/siRNA nanoparticle formulation and gene silencing.* Biomaterials, 2007. **28**(6): p. 1280-1288.

107. Ren, D.W., et al., *The enzymatic degradation and swelling properties of chitosan matrices with different degrees of N-acetylation.* Carbohydrate Research, 2005. **340**(15): p. 2403-2410.

108. Kean, T. and M. Thanou, *Biodegradation, biodistribution and toxicity of chitosan.* Advanced Drug Delivery Reviews, 2010. **62**(1): p. 3-11.

109. Janes, K.A., P. Calvo, and M.J. Alonso, *Polysaccharide colloidal particles as delivery systems for macromolecules.* Advanced Drug Delivery Reviews, 2001. **47**(1): p. 83-97.

110. Hamidi, M., A. Azadi, and P. Rafiei, *Hydrogel nanoparticles in drug delivery.* Advanced Drug Delivery Reviews, 2008. **60**(15): p. 1638-1649.

111. Gan, Q., et al., *Modulation of surface charge, particle size and morphological properties of chitosan-TPP nanoparticles intended for gene delivery.* Colloids and Surfaces B: Biointerfaces, 2005. **44**(2-3): p. 65-73.

112. Garcia-Fuentes, M. and M.J. Alonso, *Chitosan-based drug nanocarriers: Where do we stand?* Journal of Controlled Release, 2012. **161**(2): p. 496-504.

113. Madsen, T., H. Buchardt Boyd, D. Nylén, A. Rathmann Pedersen, G.I. Petersen, and F. Simonsen, *Environmental and Health Assessment of Substances in Household Detergents and Cosmetic Detergent Products.* Environmental Project No. 615. CETOX, 2001.

114. Berger, J., et al., *Structure and interactions in covalently and ionically crosslinked chitosan hydrogels for biomedical applications.* European Journal of Pharmaceutics and Biopharmaceutics, 2004. **57**(1): p. 19-34.

115. Blanco, M.D., et al., *5-fluorouracil release from copolymeric hydrogels of itaconic acid monoester .1. Acrylamide-co-monomethyl itaconate.* Biomaterials, 1996. **17**(11): p. 1061-1067.

116. Ratner, B.D. and A.S. Hoffman, *Synthetic hydrogels for biomedical applications.* Acs Symposium Series, 1976(31): p. 1-36.

117. Mi, F.L., et al., *Kinetic study of chitosan-tripolyphosphate complex reaction and acid-resistive properties of the chitosan-tripolyphosphate gel beads prepared by in-liquid curing method.* Journal of Polymer Science Part B-Polymer Physics, 1999. **37**(14): p. 1551-1564.

118. Soppimath, K.S., et al., *Biodegradable polymeric nanoparticles as drug delivery devices.* Journal of Controlled Release, 2001. **70**(1-2): p. 1-20.

119. Gan, Q. and T. Wang, *Chitosan nanoparticle as protein delivery carrier - Systematic examination of fabrication conditions for efficient loading and release.* Colloids and Surfaces B-Biointerfaces, 2007. **59**(1): p. 24-34.

120. Nabel, G.J., et al., *Direct Gene-Transfer with DNA Liposome Complexes in Melanoma - Expression, Biologic Activity, and Lack of Toxicity in Humans.* Proceedings of the National Academy of Sciences of the United States of America, 1993. **90**(23): p. 11307-11311.

121. Li, S. and L. Huang, *Nonviral gene therapy: promises and challenges.* Gene Therapy, 2000. **7**(1): p. 31-34.

122. Mao, S.R., W. Sun, and T. Kissel, *Chitosan-based formulations for delivery of DNA and siRNA.* Advanced Drug Delivery Reviews, 2010. **62**(1): p. 12-27.

123. Ishida, T., et al., *Accelerated blood clearance of PEGylated liposomes following preceding liposome injection: Effects of lipid dose and PEG*

surface-density and chain length of the first-dose liposomes. Journal of Controlled Release, 2005. **105**(3): p. 305-317.

124. Huang, M., et al., *Transfection efficiency of chitosan vectors: Effect of polymer molecular weight and degree of deacetylation.* Journal of Controlled Release, 2005. **106**(3): p. 391-406.

125. Chang, K.L., et al., *Efficient Gene Transfection by Histidine-Modified Chitosan through Enhancement of Endosomal Escape.* Bioconjugate Chemistry, 2010. **21**(6): p. 1087-1095.

126. Ishii, T., Y. Okahata, and T. Sato, *Mechanism of cell transfection with plasmid/chitosan complexes.* Biochimica Et Biophysica Acta-Biomembranes, 2001. **1514**(1): p. 51-64.

127. Fischer, D., et al., *In vitro cytotoxicity testing of polycations: influence of polymer structure on cell viability and hemolysis.* Biomaterials, 2003. **24**(7): p. 1121-1131.

128. Sgouras, D. and R. Duncan, *Methods for the evaluation of biocompatibility of soluble synthetic-polymers which have potential for bio-medical use: use of the tetrazolium-based colorimetric assay (mtt) as a preliminary screen for evaluation of invitro cytotoxicity.* Journal of Materials Science-Materials in Medicine, 1990. **1**(2): p. 61-68.

129. Rojanarata, T., et al., *Chitosan-Thiamine Pyrophosphate as a Novel Carrier for siRNA Delivery.* Pharmaceutical Research, 2008. **25**(12): p. 2807-2814.

130. Tripathi, S.K., et al., *Linear polyethylenimine-graft-chitosan copolymers as efficient DNA/siRNA delivery vectors in vitro and in vivo.* Nanomedicine-Nanotechnology Biology and Medicine, 2012. **8**(3): p. 337-345.

131. Gwak, S.J., et al., *Chitosan/TPP-Hyaluronic Acid Nanoparticles: A New Vehicle for Gene Delivery to the Spinal Cord.* Journal of Biomaterials Science-Polymer Edition, 2011. **23**(11): p. 1437-1450.

132. Wang, B.Q., et al., *Effects of hydrophobic and hydrophilic modifications on gene delivery of amphiphilic chitosan based nanocarriers.* Biomaterials, 2011. **32**(20): p. 4630-4638.

133. Sato, T., T. Ishii, and Y. Okahata, *In vitro gene delivery mediated by chitosan. Effect of pH, serum, and molecular mass of chitosan on the transfection efficiency.* Biomaterials, 2001. **22**(15): p. 2075-2080.

134. Koping-Hoggard, M., et al., *Chitosan as a nonviral gene delivery system. Structure-property relationships and characteristics compared with polyethylenimine in vitro and after lung administration in vivo.* Gene Therapy, 2001. **8**(14): p. 1108-1121.

135. Kiang, T., et al., *The effect of the degree of chitosan deacetylation on the efficiency of gene transfection.* Biomaterials, 2004. **25**(22): p. 5293-5301.

136. Toole, B.P. and M.G. Slomiany, *Hyaluronan: A constitutive regulator of chemoresistance and malignancy in cancer cells.* Seminars in Cancer Biology, 2008. **18**(4): p. 244-250.

137. Knudson, C.B. and W. Knudson, *Hyaluronan-binding proteins in development, tissue homeostasis, and disease.* Faseb Journal, 1993. **7**(13): p. 1233-1241.

138. Ossipov, D.A., *Nanostructured hyaluronic acid-based materials for active delivery to cancer.* Expert Opinion on Drug Delivery, 2010. **7**(6): p. 681-703.

139. Nasti, A., et al., *Chitosan/TPP and Chitosan/TPP-hyaluronic Acid Nanoparticles: Systematic Optimisation of the Preparative Process and*

Preliminary Biological Evaluation. Pharmaceutical Research, 2009. **26**(8): p. 1918-1930.

140. Schmitt, F., et al., *Chitosan-based nanogels for selective delivery of photosensitizers to macrophages and improved retention in and therapy of articular joints.* Journal of Controlled Release, 2010. **144**(2): p. 242-250.

141. Jain, A. and S.K. Jain, *In vitro and cell uptake studies for targeting of ligand anchored nanoparticles for colon tumors.* European Journal of Pharmaceutical Sciences, 2008. **35**(5): p. 404-416.

142. Ito, T., N. Iida-Tanaka, and Y. Koyama, *Efficient in vivo gene transfection by stable DNA/PEI complexes coated by hyaluronic acid.* Journal of Drug Targeting, 2008. **16**(4): p. 276-281.

143. Ito, T., et al., *Hyaluronic acid and its derivative as a multi-functional gene expression enhancer: Protection from non-specific interactions, adhesion to targeted cells, and transcriptional activation.* Journal of Controlled Release, 2006. **112**(3): p. 382-388.

144. Lee, H., et al., *Synthesis, characterization, and in vivo diagnostic applications of hyaluronic acid immobilized gold nanoprobes.* Biomaterials, 2008. **29**(35): p. 4709-4718.

145. Peer, D. and R. Margalit, *Tumor-targeted hyaluronan nanoliposomes increase the antitumor activity of liposomal doxorubicin in syngeneic and human xenograft mouse tumor models.* Neoplasia, 2004. **6**(4): p. 343-353.

146. Peer, D. and R. Margalit, *Loading mitomycin C inside long circulating hyaluronan targeted nano-liposomes increases its antitumor activity in three mice tumor models.* International Journal of Cancer, 2004. **108**(5): p. 780-789.

147. Hyung, W., et al., *Novel hyaluronic acid (HA) coated drug carriers (HCDCs) for human breast cancer treatment.* Biotechnology and Bioengineering, 2008. **99**(2): p. 442-454.

148. Zaki, N.M., A. Nasti, and N. Tirelli, *Nanocarriers for Cytoplasmic Delivery: Cellular Uptake and Intracellular Fate of Chitosan and Hyaluronic Acid-Coated Chitosan Nanoparticles in a Phagocytic Cell Model.* Macromolecular Bioscience, 2011. **11**(12): p. 1747-1760.

149. Bajorath, J., et al., *Identification of CD44 residues important for hyaluronan binding and delineation of the binding site.* Journal of Biological Chemistry, 1998. **273**(1): p. 338-343.

150. Toole, B.P. and M.G. Slomiany, *Hyaluronan, CD44 and Emmprin: Partners in cancer cell chemoresistance.* Drug Resistance Updates, 2008. **11**(3): p. 110-121.

151. Ghosh, S.C., S.N. Alpay, and J. Klostergaard, *CD44: a validated target for improved delivery of cancer therapeutics.* Expert Opinion on Therapeutic Targets, 2012. **16**(7): p. 635-650.

152. Negi, L.M., et al., *Role of CD44 in tumour progression and strategies for targeting.* Journal of Drug Targeting, 2012. **20**(7): p. 561-573.

153. Katoh, S., et al., *Cutting edge: An inducible sialidase regulates the hyaluronic acid binding ability of CD44-bearing human monocytes.* Journal of Immunology, 1999. **162**(9): p. 5058-5061.

154. Katoh, S., et al., *Glycosylation of CD44 negatively regulates its recognition of hyaluronan.* Journal of Experimental Medicine, 1995. **182**(2): p. 419-429.

155. Platt, V.M. and F.C. Szoka, *Anticancer therapeutics: Targeting macromolecules and nanocarriers to hyaluronan or CD44, a hyaluronan receptor.* Molecular Pharmaceutics, 2008. **5**(4): p. 474-486.

156. Cera, C., et al., *Water-soluble polysaccharide anthracycline conjugates - biological-activity.* Anti-Cancer Drug Design, 1992. **7**(2): p. 143-151.

157. Kim, J., K. Park, and S.K. Hahn, *Effect of hyaluronic acid molecular weight on the morphology of quantum dot-hyaluronic acid conjugates.* International Journal of Biological Macromolecules, 2008. **42**(1): p. 41-45.

158. Lee, H., et al., *Target-specific intracellular delivery of siRNA using degradable hyaluronic acid nanogels.* Journal of Controlled Release, 2007. **119**(2): p. 245-252.

159. Aguiar, D.J., W. Knudson, and C.B. Knudson, *Internalization of the hyaluronan receptor CD44 by chondrocytes.* Experimental Cell Research, 1999. **252**(2): p. 292-302.

160. Ouasti, S., et al., *The CD44/integrins interplay and the significance of receptor binding and re-presentation in the uptake of RGD-functionalized hyaluronic acid.* Biomaterials, 2012. **33**(4): p. 1120-1134.

161. Wolny, P.M., et al., *Analysis of CD44-Hyaluronan Interactions in an Artificial Membrane System: insights into the distinct binding properties of high and low molecular weight hyaluronan.* Journal of Biological Chemistry, 2010. **285**(39): p. 30170-30180.

162. Rochman, M., et al., *The CD44 receptor of lymphoma cells: Structure-function relationships and mechanism of activation.* Cell Adhesion and Communication, 2000. **7**(4): p. 331-347.

163. Skelton, T.P., et al., *Glycosylation provides both stimulatory and inhibitory effects on cell surface and soluble CD44 binding to hyaluronan.* Journal of Cell Biology, 1998. **140**(2): p. 431-446.

164. Hathcock, K.S., et al., *CD44 expression on activated b-cells - differential capacity for cd44-dependent binding to hyaluronic-acid.* Journal of Immunology, 1993. **151**(12): p. 6712-6722.

165. Thankamony, S.P. and W. Knudson, *Acylation of CD44 and its association with lipid rafts are required for receptor and hyaluronan endocytosis.* Journal of Biological Chemistry, 2006. **281**(45): p. 34601-34609.

166. Coradini, D., et al., *Inhibition of hepatocellular carcinomas in vitro and hepatic metastases in vivo in mice by the histone deacetylase inhibitor HA-But.* Clinical Cancer Research, 2004. **10**(14): p. 4822-4830.

167. Stern, R., A.A. Asari, and K.N. Sugahara, *Hyaluronan fragments: An information-rich system.* European Journal of Cell Biology, 2006. **85**(8): p. 699-715.

168. Mizrahy, S., et al., *Hyaluronan-coated nanoparticles: The influence of the molecular weight on CD44-hyaluronan interactions and on the immune response.* Journal of Controlled Release, 2011. **156**(2): p. 231-238.

169. Eliaz, R.E. and F.C. Szoka, *Liposome-encapsulated doxorubicin targeted to CD44: A strategy to kill CD44-overexpressing tumor cells.* Cancer Research, 2001. **61**(6): p. 2592-2601.

170. Eliaz, R.E., S. Nir, and F.C. Szoka, *Interactions of hyaluronan-targeted liposomes with cultured cells: Modeling of binding and endocytosis.* Liposomes, Pt D, 2004. **387**: p. 16-33.

171.   Lesley, J., et al., *Hyaluronan binding by cell surface CD44.* Journal of Biological Chemistry, 2000. **275**(35): p. 26967-26975.

Chapter Two

Structural characterisation of hyaluronic acid-coated chitosan nanoparticles: molecular weight-dependent effects on particle morphology and functional behaviour[a]

Abstract

Chitosan nanoparticles are popular carriers for the delivery of macromolecular payloads, e.g. nucleic acids. In this study, nanoparticles were prepared via complexation with triphosphate (TPP) anions and were successively coated with hyaluronic acid (HA). Key variables of the preparative process (e.g. chitosan and HA molecular weight) were optimised in view of the maximisation of loading with DNA, of the ζ potential and of the dimensional stability, and the resulting particles showed excellent storage stability.

We have specifically focused on the influence of chitosan molecular weight on the properties of the nanoparticles. In particular, we have showed that increasing chitosan molecular weight provided increasingly porous (= lower cross-link density) chitosan-TPP particles, which responded with larger dimensional changes in response to variations in osmotic pressure or upon drying. The variable porosity of the chitosan-TPP nanoparticles also had a profound effect on the mode of HA adsorption; HA was apparently able to deeply penetrate within the more porous nanoparticles composed of high molecular weight (684 kDa) chitosan, while it formed a corona around the more densely cross-linked ones produced from low molecular weight chitosan (25 kDa). Atomic Force Microscopy (AFM) allowed not only to highlight the presence of this corona, but also to estimate its apparent thickness to about 20-30 nm (in a dry state). This different mode of adsorption could have a significant effect on the way HA is presented to cell receptors, and therefore on the kinetics and possibly also on the mechanism of nanoparticle uptake.

Finally, it is worth mentioning that chitosan molecular weight (at least when > 25 kDa) did not appear to significantly affect DNA loading efficiency, nor the presence of loaded DNA caused appreciable differences in the process of HA adsorption. However, the different response to chitosanase allowed to obtain enzymatically triggered DNA release only for high molecular weight chitosan.

[a] **AFM imaging and analysis were conducted by Mr. Roberto Donno.**

2.1 Introduction

Chitosan, a linear random copolymer of β-1,4- D-glucose-2-amine and N-acetyl-D-glucose-2-amine, is a versatile biomaterial derived from the deacetylation of chitin, which is abundantly present in crustacean shells [1], in insect exoskeletons [2] and also in fungal cell walls [3]. Chitosan is a biocompatible molecule [4], generally regarded as a degradable material [5] and employed in a wide range of applications from tissue engineering [5] to food science[6], specifically including micro- and nano-carrier-mediated delivery of payloads, generally of macromolecular nature [7, 8]. In this area, the ionotropic gelation with triphosphate (TPP) is possibly the most popular preparative method for chitosan nanoparticles [8], due to the ease of performance and the rather benign character both of the polyanion and of the process (absence of chemical reaction, use of only mildly acidic water solutions, etc.). Chitosan-TPP nanoparticles typically exhibit a cationic surface, which results in a quick and unselective cellular uptake, above all in phagocytic cells [9]. However, the use of chemically modified chitosan or, alternatively, nanoparticle decoration with polyanions [10, 11] have been developed for preferential uptake of the nanoparticles in specific cell types. For example, mannosylated and galactosylated chitosans were used to target dendritic cells and hepatocytes respectively [12, 13].

The chitosan / TPP weight ratio is possibly the most important variable to control particle size, morphology and surface charge [14, 15]. However, chitosan concentration and molecular weight, ionic strength and pH of the medium also play a significant role [16-20] and have been shown to affect the long-term stability of the particles [21-23]. In particular, it is worth pointing out that a different degree of deacetylation and molecular weight confer to chitosan considerably different physico-chemical properties, which affect its complexation ability [24], the toxicity of its nanoparticles (reportedly lower with decreasing the degree of deacetylation and molecular weight) [25], their dimensions (lower with decreasing the molecular weight)[26], and their encapsulation efficiency (lower with decreasing the molecular weight and with increasing the degree of deacetylation), and ultimately also the efficiency of payload delivery e.g. of nucleic acids (higher with lower molecular weight) [27] or of proteins (again higher with lower molecular weight) [28].

Our group has previously optimised the conditions of chitosan/TPP electrostatic complexation in diluted solution; *inter alia* showing the importance of variables such as the order of addition and mixing of the solutions with identical or different pH [29]. The resulting nanoparticles can be further coated with hyaluronic acid (HA) to render their surface anionic and in principle biofunctional. HA decoration of (nano)material surfaces has been shown to provide a certain resistance to protein adsorption [30, 31], which is accompanied by prolonged circulation times [32], and therefore confer a relative "stealth" character. Indeed, we have confirmed such effects on HA-coated chitosan nanoparticles, which in macrophages exhibited a 2-3 orders of magnitude lower uptake than their parent uncoated nanoparticles [9]. An additional advantage of the presence of surface bound HA is the possibility to target cells overexpressing HA receptors, such as CD44 [33], which is a possible strategy to target activated inflammatory cells [34, 35] or certain types of tumours [36, 37].

In the present study, we have explored the effect of chitosan molecular weight on the morphology/structure of chitosan-TPP nanoparticles, and how the resulting differences may influence the process of HA adsorption.

Finally, using salmon sperm DNA (average size of $\leq$ 2,000 bp $\approx$ 1.2-1.3$\times$10^3 kDa) as a model payload, we have also assessed whether loaded particles would exhibit significant differences in the coating process.

2.2 Materials and methods

2.2.1 Materials

Middle viscous chitosan (CS, average viscosimetric molecular weight ($\overline{M_v}$) = 684 kDa), Quantipro BCA assay kit, bovine serum albumin (BSA), foetal bovine serum (FBS), sodium nitrite ($NaNO_2$), 1 M hydrochloric acid (HCl), 1 M sodium hydroxide (NaOH), sodium pentabasic (TPP) and Chitosanase from *Streptomyces griseus* were obtained from Sigma-Aldrich (Gillingham, UK); 10 mM phosphate buffered saline (PBS) was prepared from appropriate tablets (Oxoid, Basingtoke, UK); hyaluronic acid (HA) with $\overline{M_v}$ = 15, 60, 360, and 1000 kDa was obtained from Medipol SA (Lausanne, Switzerland). Salmon sperm DNA was purchased from Invitrogen (CA, USA). PicoGreen® reagent was obtained from Molecular Probes (OR, USA). Glacial acetic acid and sodium acetate were purchased from VWR BDH Chemicals (Poole, UK). The other chemicals were of reagent grade and were used as received.

2.2.2 Preparative procedures

Chitosan purification depolymerisation and characterisation are described in Supplementary Information, Section 2.6.1 and Figure 2-SI 1 and Figure 2-SI 2.

Preparation of chitosan/TPP (CS-TPP) nanoparticles. CS-TPP nanoparticles were prepared according to a previously reported procedure [29]. The pH of a 0.069 % wt. CS solution in 4.6 mM HCl was adjusted to 5 by the addition of appropriate volumes of NaOH 0.1 M and the solution was sonicated for 40 min. TPP was prepared as a 0.1 % wt. solution in deionised water, correcting the pH to 5 using appropriate volumes of HCl 0.1 M. Both solutions were filtered through a 0.22 μm pore size filter. For a final volume of 3 mL of CS-TPP nanoparticles, 214 μL of TPP solution were pipetted into 2786 μL of CS solution, where the final concentrations of CS and TPP are 0.064 and 0.0071 % wt., respectively, resulting in a 9:1 mass ratio of CS:TPP. The complexation was carried under magnetic agitation (750 rpm), for 30 min at 25 °C. The final dispersion was sonicated for 40 minutes and then left undisturbed for additional 16 h. The nanoparticle dispersion was then dialysed against deionised water (MWCO 1000 kDa). For further experiments, the

concentration of nanoparticle dispersions was assessed by sampling a known volume after dialysis and measuring the residual weight after freeze drying.

Preparation of CS-TPP//HA nanoparticles. In a typical experiment, 2 mL of a 0.025 % wt. dispersion of CS-TPP nanoparticles in 100 mM acetic buffer at pH = 5 were added under vigorous magnetic stirring (30 min, 1,200 rpm) to an equal volume of a 1.5, 1.0, 0.5 or 0.1 mg/mL solution of 1000, 360, 60 or 15 kDa hyaluronic acid in the same buffer. The dispersions were then dialysed against deionised water or PBS, typical MW cut-off (MWCO) 1000 kDa.

The procedures for the **encapsulation of DNA and BSA** are described in Supplementary Information, Section 2.6.2, Figure 2-SI 3, Figure 2-SI 4 and Figure 2-SI 5, and Table 2-SI 1.

2.2.3 Characterisation

Nuclear Magnetic Resonance (^{1}H NMR). The samples were prepared by dissolving 10 mg of CS in 0.5 mL of 0.5M DCl in D_2O. ^{1}H NMR spectra were recorded at room temperature on a JEOL EX300 300 MHz NMR spectrometer (Bruker Avance 300, Coventry, UK).

^{1}H NMR: δ = 1.75-1.85 (acetamide CH_3), δ = 2.82-3.00 (H2), δ = 3.17-3.8 (H3, H4, H5, H6) ppm (for the assignment of the protons, see Supplementary Information, Figure 2-SI 1).

Viscometry. Viscosity measurements were performed at 25 °C in a 0.25 M acetic acid/0.25 M sodium acetate solution using a falling ball automated microviscometer (Anton Parr, Graz, Austria) equipped with a 1.6 mm internal diameter capillary tube at an inclination angle of 30°. $\overline{M_v}$ was calculated assuming the parameters of the Mark-Houwink equation for CS to be equal to K = 1.57×10^{-5} L.g^{-1} and a = 0.79 [38]. For the determination of molecular weight, see Supplementary Information, Figure 2-SI 2.

Dynamic Light Scattering (DLS). Hydrodynamic diameter (Z-average size), size polydispersity (PDI), derived count rate (DCR) and ζ potential measurements were always performed on three independent samples at a temperature of 25 °C using a Zetasizer Nano ZS instrument (Model ZEN3600, Malvern Instruments Ltd., UK) equipped with a solid state HeNe laser (λ = 633 nm) at a scattering angle of 173°.

Atomic Force Microscopy (AFM). A drop ($\approx$ 50 µL) of a 50 µg/mL nanoparticle dispersion in deionised water was deposited on a mica surface and dried overnight at room temperature. A Molecular Force Probe 3D AFM (MFP- 169 3D, Asylum Research, Santa Barbara, CA) equipped with a 90 µm scanner and silicon cantilevers (model AC240TS, Olympus; spring constant 2 N/m) was employed in contact mode with a scan rate of 1 Hz.

Analysis of AFM data. A) <u>Substrate</u>. The original images (without flattening or filtering) were analysed with Igor-pro software (Asylum Research AFM software, Version 101010+1202, Wavemetrics, Portland, OR) in order to calculate the root mean square (RMS) roughness of flat areas (no nanoparticles), which typically had a value close to 0.5 nm.

B) <u>Chitosan/TPP nanoparticles and CS(684)-TPP//HA nanoparticles</u>. The RMS value of the substrate was used to determine a threshold (the nanoparticle "border") that allows to discriminate nanoparticles from the surface and thus also to calculate their individual volume. Using a typical population of around 200 nanoparticles from AFM height images (Figure 2- 1A), volume distributions were calculated and fitted with different probability distributions using the Statistic Toolbox of MATLAB (MATLAB version 7.12.0, Natick, Massachusetts: The MathWorks Inc.). The final best-fit model was selected on the basis of the Akaike Information Criterion (AIC). For each model, the log-likelihood parameter (measured with MATLAB) was used to calculate the AIC value, expressed as in Equation 1.

$$AIC = 2k - 2\ln(L) \qquad \textbf{Equation 1}$$

where k represents the number of parameters in the statistical model and L is the likelihood function for the estimated model (ln(L) = log-likelihood). The model with the lowest AIC is the one that better fits the data. The best fitting was obtained using the lognormal distribution (solid line Figure 2- 1B) described as in Equation 2 [1-3].

$$P(V) = \frac{1}{V\sigma\sqrt{2\pi}} e^{\frac{-(lnV-\mu)^2}{2\sigma^2}} \qquad \textbf{Equation 2}$$

, where V is the volume and μ and σ are the distribution parameters related to the mean value of the distribution V_m as described in Equation 3.

$$V_m = e^{\mu + \frac{\sigma^2}{2}} \qquad \textbf{Equation 3}$$

Finally, using the volume of each nanoparticle it is possible to calculate its diameter if it had a spherical geometry (Figure 2- 1C), as it would be in a water dispersion;

clearly, this does not take into account the dimensional variation due to swelling. From the corresponding diameter distributions it is then possible to estimate a mean diameter of the particles. The resulting values would not reflect the average dimension of the nanoparticles in water, but allow an easy comparison of their dimensions.

C) CS(25)-TPP//HA nanoparticles. Due to the clear presence of a flattened external area (the nanoparticle "corona"), two different thresholds can be employed (Figure 2- 1 D-F), which allows to separately calculate the volume distributions of the nanoparticle corona and of the core, using the methods described in B).
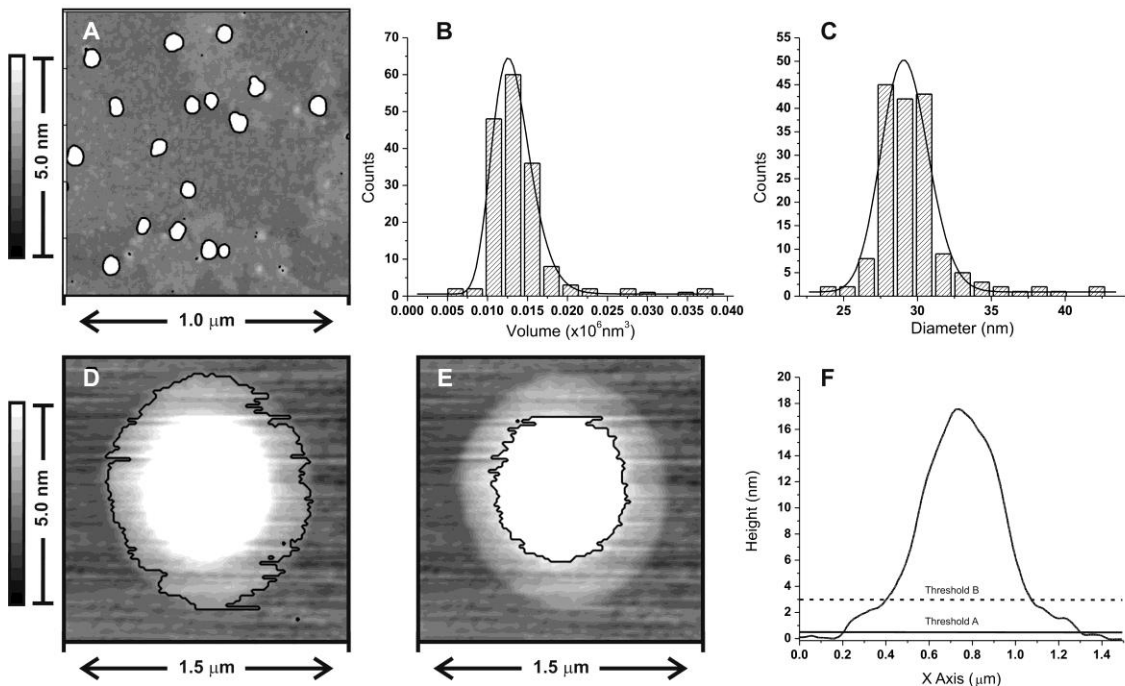
Figure 2- 1 *A*. Height images of CS(25)-TPP nanoparticles deposited on a mica substrate. *B*. Volume distribution CS(25)-TPP nanoparticles (population ≈ 200 particles); the solid line represents its fitting with a lognormal distribution function. *C*. Diameter distribution for the same population, which was obtained converting the individual volumes in diameters under the assumption of a spherical geometry; the solid line represents its fitting with a lognormal distribution function. *D*. The image shows an HA-coated CS(25)-TPP nanoparticle assuming a flattened morphology when deposited on mica. The entire nanoparticle was segmented using the average roughness (RMS) of the regions with no nanoparticle as a threshold (RMS = 500 pm; the RMS of pure mica is typically 60 pm). *E*. An additional segmentation was performed using a higher threshold, 3 nm. *F*. Profile of the nanoparticle, where the two thresholds are highlighted. Correspondingly, neglecting any contribution from HA possibly covering the central region (the segmented white area in Figure 2- 1E), it is possible to selectively calculate the volume for the entire nanoparticle (threshold A = $V_{CS-TPP//HA}$), its core (threshold B = V_{CS-TPP}) and the HA corona (obtained by the difference: $V_{CS-TPP//HA}$ - V_{CS-TPP}).

Protein adsorption. 500 µL of a 0.5 mg/mL nanoparticle dispersion in deionised water were incubated for 30 min with equal volumes of FBS at 37 ^{o}C, then

centrifuged (13,000 rpm, 60 min) and the resulting precipitate was washed three times with 1 mL deionised water to remove proteins not firmly adsorbed onto the surface of nanoparticles. The protein content in the precipitate was then quantified using the Quantipro BCA assay kit. Briefly, 100 µL of reconstituted precipitate were added to 100 µL of Quantipro solution. After 2 hours incubation at 37 °C, the absorbance was recorded at 562 nm and the amount of protein was calculated using a protein standard curve using 1 mL of 50% FBS (no nanoparticle) as a blank. The value of protein adsorption was expressed in relation to the nanoparticle content (wt. of protein / wt. of nanoparticle).

DNA release. HA-coated nanoparticles were prepared at a final DNA concentration of 1 µg/mL, dialysed as described above and incubated shaking at 37 °C in 10 mM PBS buffer (pH = 7.4) or in 100 mM acetate buffer (pH = 5) with 0.7 U chitosanase per mg of nanoparticle. At predetermined incubation times, samples were centrifuged (13,000 rpm for 60 min) and the supernatants assayed for the presence of DNA using the PicoGreen® reagent. The amount of DNA released was expressed as a percentage to the total DNA encapsulated within the nanoparticles.

2.3 Results and discussion

2.3.1 Chitosan/TPP nanoparticles with variable chitosan molecular weight

We have produced chitosan samples with variable molecular weight via nitrous acid oxidative degradation, controlling their size with sodium nitrite concentration [39]; the resulting polymers with $\overline{M_v}$ = 10, 25 and 70 kDa exhibited minimal differences in the degree of deacetylation (Figure 2- 2A), ensuring that any difference in their performance could be ascribed to differences in molecular weight.
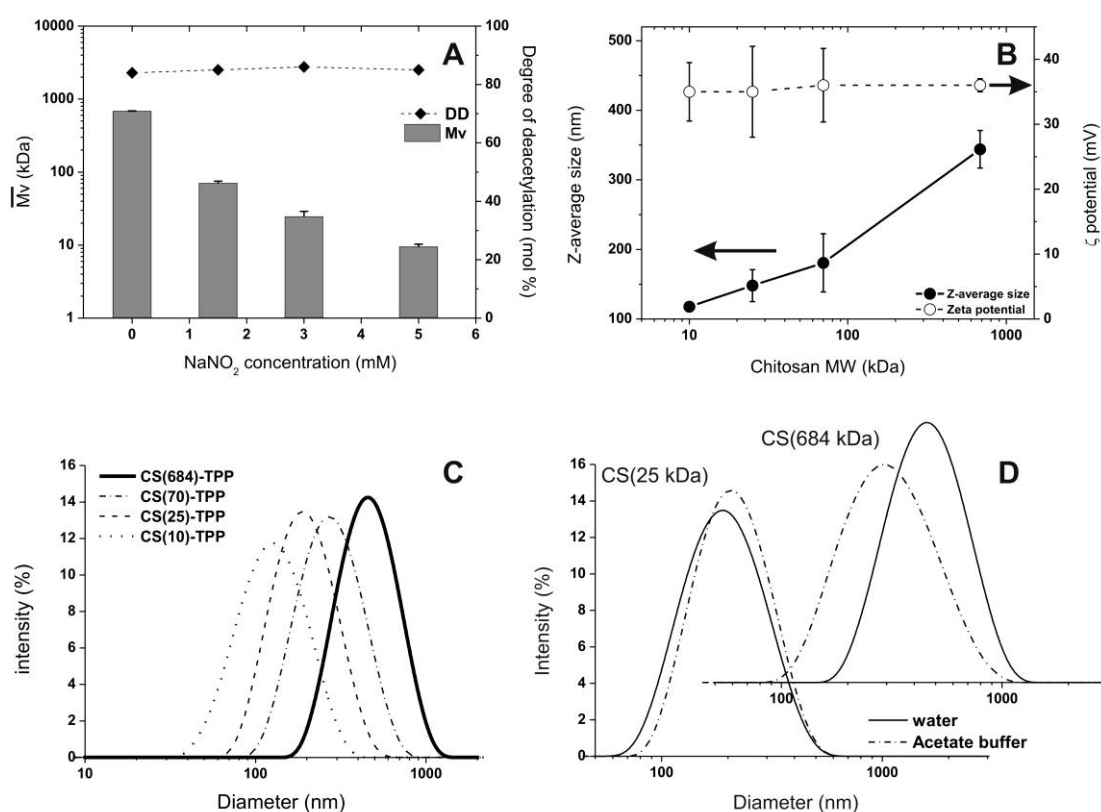
Figure 2- 2 *A.* Viscosity average molecular weight ($\overline{M_v}$, bars) and degree of deacetylation (determined by ^{1}H NMR, symbols) of chitosan after depolymerisation with sodium nitrite. *B.* Z-average size (closed symbols) and ζ-potential (open symbols) of CS-TPP nanoparticles as a function of chitosan MW. *C.* Size distribution of CS-TPP nanoparticles prepared from CS with different MWs. The numbers between brackets indicate chitosan molecular weight expressed in kDa. *D.* Size distribution of CS/TPP nanoparticles produced from low and high MW chitosan in deionised water (solid line) and in high ionic strength medium (0.1M Acetate buffer, pH 5; dashed line).

The electrostatic complexation of chitosan ($\overline{M_v}$ = 477 kDa) with triphosphate (TPP) was performed in a diluted solution at pH = 5, adopting conditions that we had previously optimised [29]. The ζ potential of the resulting nanoparticles was not affected by chitosan molecular weight (Figure 2- 2B, open symbols); on the other hand, the particle average diameter gradually increased with increasing molecular weight (Figure 2- 2B, closed symbols), although the overall shape of the size distribution was not altered (Figure 2- 2C). We ascribe this effect to a less effective complexation of TPP by chitosan with increasing size, as already seen in chitosan/TPP microparticles (lower TPP content with increasing chitosan molecular weight [39]). Accordingly, aggregates composed by a given (constant) number of macromolecules would feature a lower cross-linking density for larger chitosan molecular weight, hence also a larger size and a higher swelling degree.

Swelling, however, should depend on the surrounding environment; indeed, a higher ionic strength buffer (0.1 M acetate buffer, Figure 2- 2D) shrank high MW chitosan nanoparticles to one third of their original volume, while it left unaltered the size of low MW chitosan ones; therefore, proving the higher cross-linking density of the latter. Additionally, no significant dimensional difference could be recorded between 25 kDa (Figure 2- 3A and C) and 684 kDa (Figure 2- 3B and D) chitosan nanoparticles after drying; therefore, ascribing their dimensional difference in water primarily to differential swelling caused by a chitosan molecular weight-dependent cross-link density.
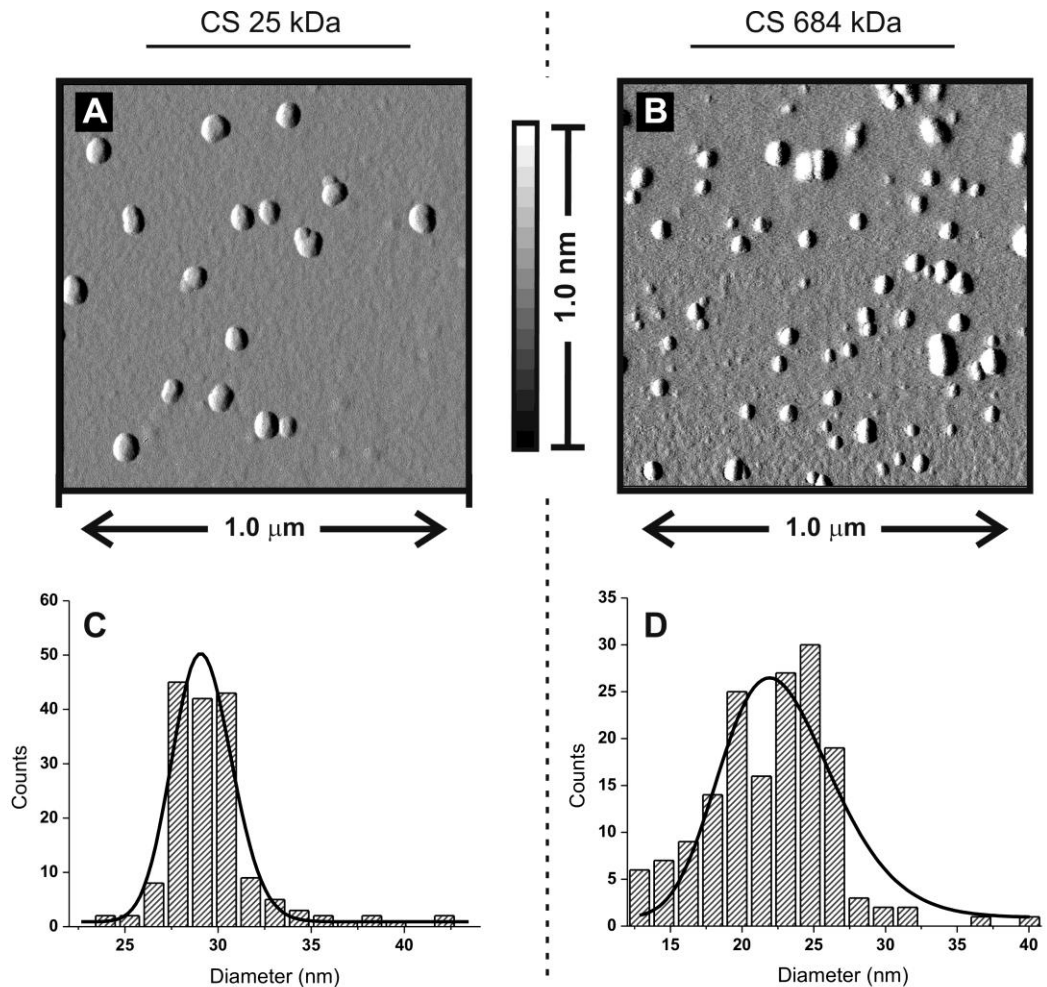
Figure 2- 3 *A* and *B*. Deflection images of 25 and 684 kDa chitosan/TPP nanoparticles deposited on a mica surface and dried overnight at room temperature. The size of the nanoparticles appears very similar, although nanoparticles from higher molecular weight chitosan seem more disperse in size. *C* and *D*. The analysis of AFM height images allowed the generation of volume distributions; forcing the flattened nanoparticles in a spherical geometry, it is then possible to calculate the hypothetical diameter distribution of the dry nanoparticles (see Figure 2- 1 B and C). The size distributions of the nanoparticles obtained from high and low molecular chitosan show a very substantial overlap, suggesting a rather similar solid content per nanoparticle and therefore attributing their different size in water to a different swelling degree due to different cross-link density.

2.3.2 Selection of chitosan molecular weight (payload encapsulation)

We have studied the encapsulation of a model nucleic acid (salmon sperm DNA) as a function of chitosan molecular weight, with the aim to identify the minimum chitosan size that would leave DNA loading, nanoparticle overall size and ζ potential unaltered. The encapsulation efficiency was assessed by measuring the amount of uncomplexed DNA after nanoparticle preparation; typically, we were able to use

DNA/chitosan ratios up to 25% wt. before observing detrimental effects on particle size or ζ potential, and thus on their stability (see Supplementary Information, Figure 2-SI 4).

For salmon sperm DNA/chitosan > 25% wt., nanoparticle stability was compromised and precipitation was recorded for all chitosan molecular weights; on the other hand, for DNA/chitosan $\leq$ 25% wt., the encapsulation efficiency was significantly lowered only with 10 kDa chitosan (Table 2- 1 and section 2.6.2 in supplementary information). The size of loaded nanoparticles did not appear to show a significant dependency on chitosan molecular weight (Figure 2- 4, left), but the ζ potential sharply decreased for 10 kDa chitosan even at very low loadings (Figure 2- 4, right). This effect is likely due to a higher affinity of low molecular chitosan for DNA (i.e. a better complexation with chitosan amines because of the reduced size of the macromolecular coil) [40, 41], which is essentially the same phenomenon recorded above for TPP complexation. As a result, we have selected the sample with 25 kDa molecular weight for any further comparison between high and low MW chitosan.

The different complexation ability of high (684 kDa) and low (25 kDa) molecular weight chitosan can also be seen using differently charged payloads. For example, albumin bears a partial positive charge at pH = 5 (pH used for loading), and is better encapsulated employing 25 kDa chitosan (see Supplementary Information, Figure 2-SI 4 and Figure 2-SI 5, and Table 2-SI 1).

Table 2- 1 DNA encapsulation efficiencies of chitosan-TPP nanoparticles loaded with different amounts of DNA.

DNA / chitosan (% wt.)	DNA encapsulation efficiency (% wt.)			
Chit. MW:	684 kDa	70 kDa	25 kDa	10 kDa
2	>99.9	>99.9	>99.9	83.0 ± 0.2
9	>99.9	98.6 ± 2.0	>99.9	96.2 ± 0.5
17	99.3 ± 1.2	99.0 ± 1.7	99.6 ± 0.7	90.0 ± 6.0
25	90.7 ± 3.7	92.7 ± 6.6	97.0 ± 4.4	89.0 ± 1.5
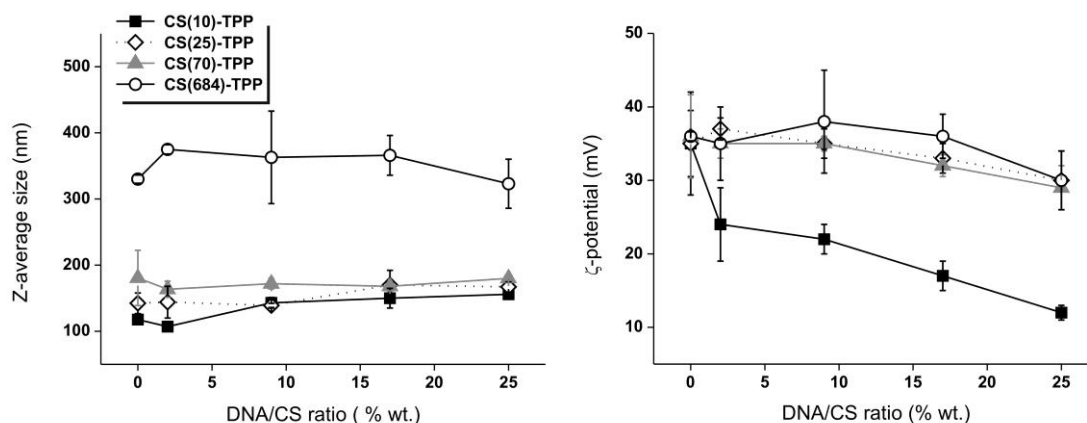
Figure 2- 4 Dependency of Z-average size (***left***) and ζ potential (***right***) on the DNA/chitosan weight ratio for DNA-loaded nanoparticles prepared from chitosan with variable molecular weight. The ζ potential appeared to be a more sensitive marker of the effects of the encapsulation on the nanoparticle properties.

2.3.3 HA adsorption on nanoparticles

Using 684 and 25 kDa chitosan-TPP nanoparticles and employing HA molecular weight and concentration as experimental variables, we have studied the HA surface adsorption at pH = 5, which was deemed to be a good compromise between the maximisation of chitosan positive charge (amine protonation) and of HA negative charge (deprotonation of carboxylic groups) (Figure 2- 5). Since HA is unlikely to fully uncoil upon adsorption, its size determines the amount of negative charge that each macromolecule will provide to the surface, thus specifically influencing the evolution of ζ potential in the early stages of the adsorption; on the other hand, HA concentration will dictate the rate of adsorption. The two parameters in combination, therefore, determine the speed at which the ζ potential of the nanoparticles will pass from positive to negative values.

The combination of low molecular weight and/or low concentration of HA, i.e. the conditions for a slow inversion of the surface charge, were generally detrimental to nanoparticle stability (both chitosan molecular weights), with aggregation for any concentration of 15 kDa HA and partial aggregation for 60 kDa at the lowest concentration used (0.1 mg/mL).

On the other hand, negatively charged, stable and spherical nanoparticles (Figure 2-SI 6) could be easily obtained with a more rapid inversion using moderate or high

HA concentration ($\geq$ 0.5 mg/mL) and/or molecular weight. The following points apply to these conditions.

For both chitosan nanopartices, and basically for all HA molecular weights, increasing HA concentration in solution corresponded to increasingly negative ζ potential and thus possibly to a larger amount of adsorbed HA; this link between concentration of HA on the nanoparticle surface and in solution could indicate a certain equilibrium character of the adsorption process.
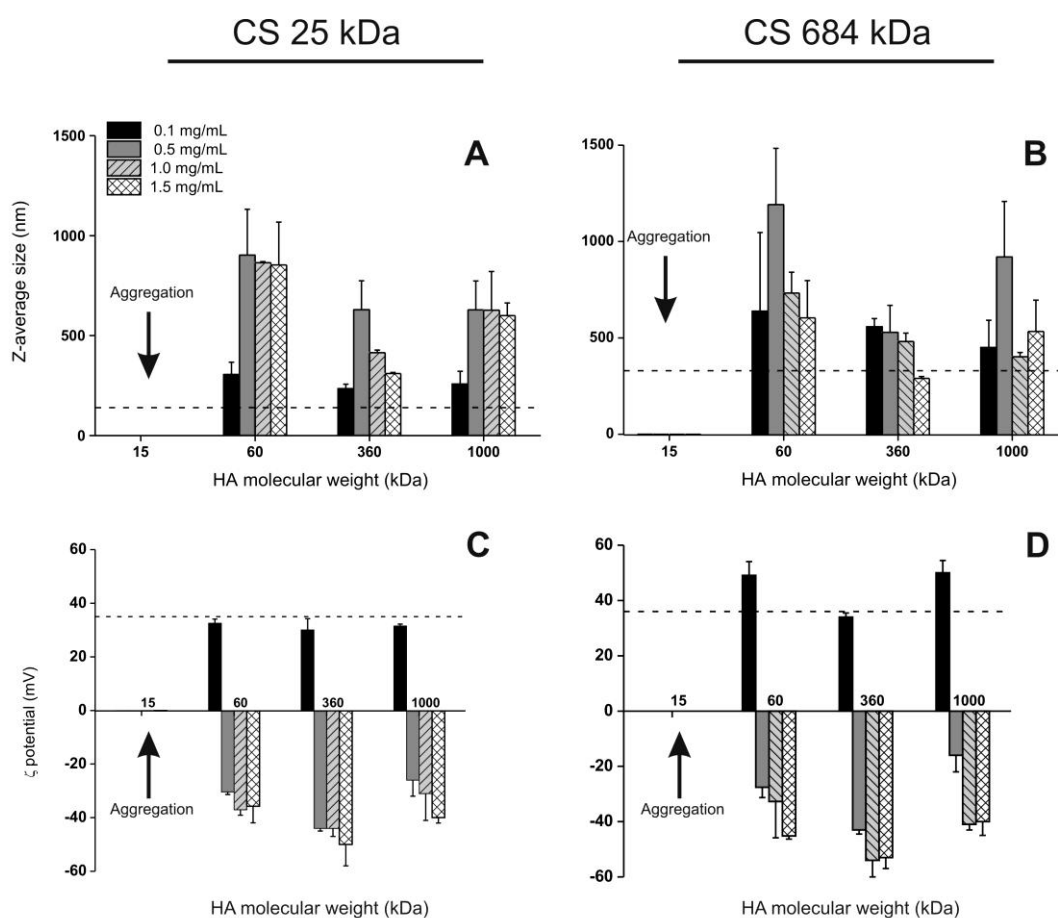
Figure 2- 5 Z-average size (**A** and **B**) and ζ potential (**C** and **D**) for 25 kDa (**A** and **C**) and 684 kDa (**B** and **D**) chitosan/TPP nanoparticles after HA adsorption as a function of HA molecular weight and concentration (0.1 – 1.5 mg/mL). The dashed lines report the values of Z-average size and ζ potential before adsorption. All measurements were performed after dialysis, in deionised water.

The particle size considerably increased upon HA adsorption from dilute solution. However, increasing HA concentration progressively decreased the average size and 684 kDa chitosan coated nanoparticles were not much larger than their parent

uncoated particles. However, AFM showed that, despite this moderate increase in hydrodynamic size, coated nanoparticles increased their dry volume by at least two orders of magnitude (Figure 2- 6A and B). In our interpretation, this is due to HA penetration in the nanoparticles, which would act as a cross-linker; in comparison to uncoated particles, the HA-coated ones would therefore have a smaller size in solution, but on the other hand, would not shrink much upon drying. HA would penetrate easier in the more porous 684 kDa chitosan nanoparticles, and indeed the 25 kDa chitosan coated particles appeared larger with both DLS and AFM, with the latter technique showing the presence of a corona, which is absent in higher MW chitosan particles (Figure 2- 6C and D). It was further possible (see Materials and Methods, Figure 2- 1D-F, and Supplementary Information, Table 2-SI 2) to separately estimate the average volume of the 25 kDa chitosan nanoparticle core and of their corona (Figure 2- 7, left). By transferring the volume data into a hypothetical spherical geometry, it was finally possible to estimate the thickness of the corona in a dry nanoparticle: this value was always in the range of 20-25 nm, independent of the actual size of the nanoparticle, and is compatible with the dimensions of 360 kDa HA [42].

It is worth mentioning that using another microscopy technique (i.e. TEM), indistinguishable dimensions have been obtain for dried 25 kDa chitosan nanoparticle (Figure 2-SI 6). Additionally, TEM revealed nanoparticles with a core-shell like structure further support the conclusion of the presences of a HA-corona around a CS-TPP core.

Using accumulative information from three different nanoparticles characterisation techniques (i.e. DLS, AFM and TEM), we conclude that the corona was likely composed predominantly of surface bound HA, given the difficulty of its penetration into the less porous / more densely cross-linked low molecular weight chitosan-TPP nanoparticles.
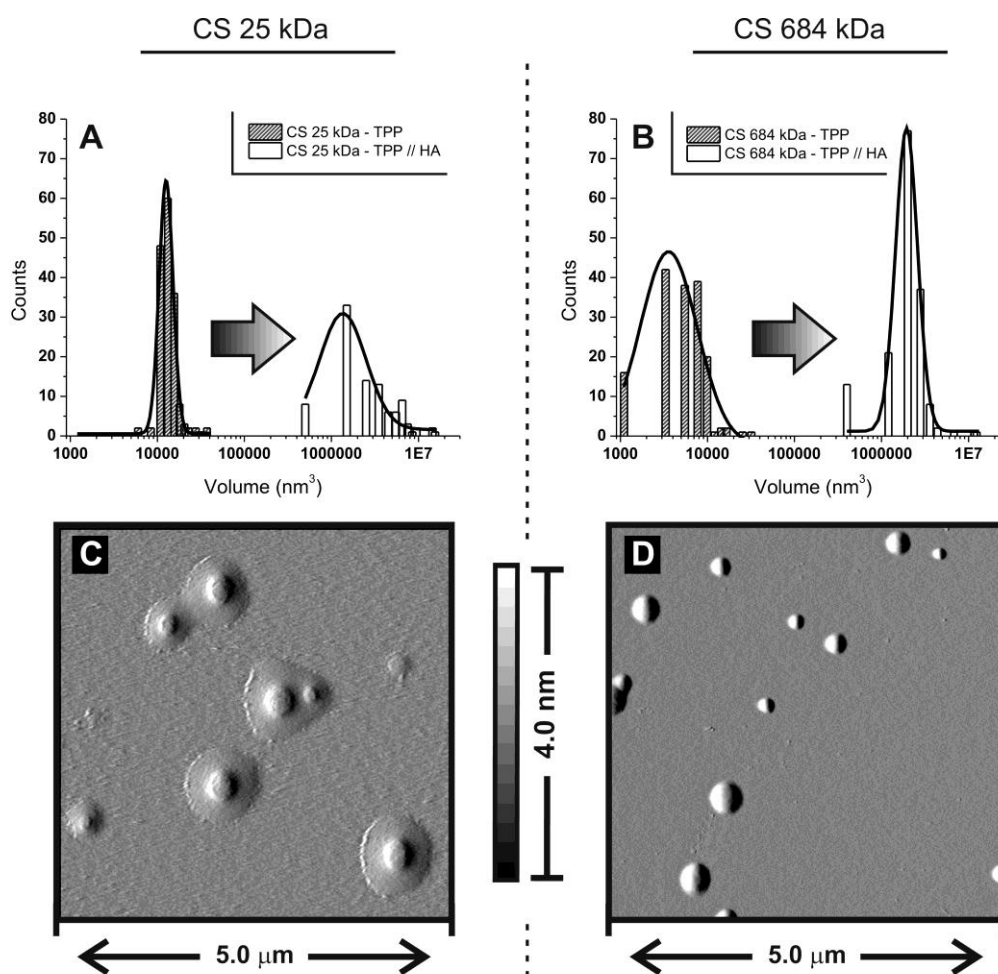
Figure 2- 6 *A* and *B*. Volume distributions (from the analysis of AFM height images) of chitosan nanoparticles before (grey bars) and after HA coating (HA 360 kDa, 1.5 mg/mL; white bars); the curves clearly show a dramatic increase in the dry volume of the nanoparticles as a result of the HA coating process. *C* and *D*. Deflection images of HA-coated 25 and 684 kDa chitosan-TPP nanoparticles deposited on a mica surface and dried overnight at room temperature. The nanoparticles produced from low molecular weight chitosan appeared surrounded by a thin (2-3 nm, see Figure 2-1F) corona.

Indistinguishable results were obtained for DNA-loaded nanoparticles (DNA / chitosan = 25% wt.). HA-coated 25 kDa chitosan nanoparticles presented a substantially identical corona (see Supplementary Information Table 2-SI 2 and Figure 2-SI 7), which was absent for the corresponding 684 kDa chitosan nanoparticles and for both uncoated parent nanoparticles.
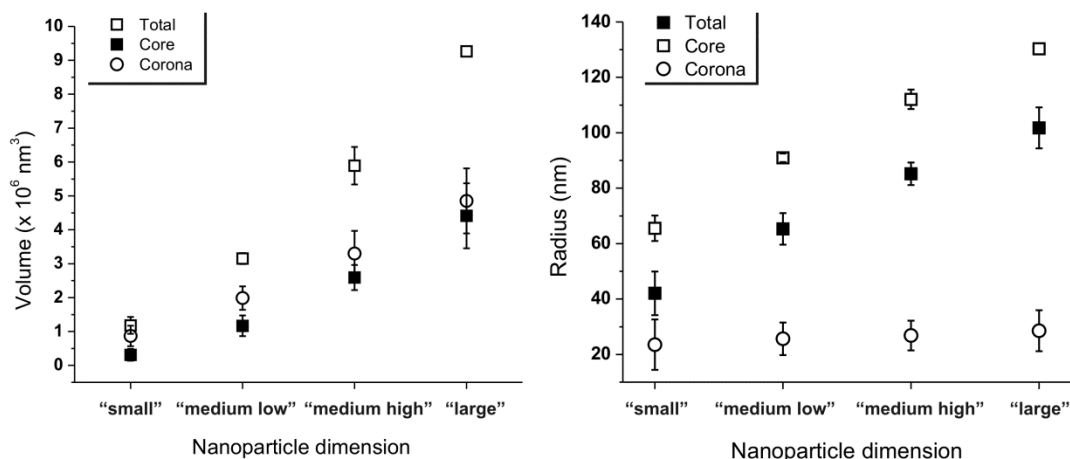
Figure 2- 7 *Left:* The overall volume distribution of HA-coated 25 kDa chitosan nanoparticles was divided in four sub-populations characterised by increasing nanoparticle volume ("small" = 0 - $7x10^5$ nm^3; "medium low" = $7x10^5$ - $1.9x10^6$ nm^3, "medium high" = $1.9x10^6$ - $3.3x10^6$ nm^3, "large" > $3.3x10^6$ nm^3). The average volume of each nanoparticle sub-population and the average volumes of the cores and of the thin coronas surrounding the nanoparticles are reported. *Right:* The distributions of the nanoparticle total volume and of the volume of their cores were also used to calculate the total radius, the radius of the nanoparticle core and the thickness of the corona, under the assumption of spherical nanoparticle geometry.

2.3.4 Stability, protein uptake and enzymatically-triggered payload release

The different morphology of adsorbed HA may significantly affect nanoparticle properties, for example their stability (see Section 2.6.4 of Supplementary Information). Although all HA-coated nanoparticles could be stored in aqueous dispersion for prolonged amounts of time (at least 4 weeks at 4 °C in deionised water), freeze-dried (with cryoprotectants), or filtered without significant variations in their size distribution (pore size down to 0.4 µm), those based on low MW chitosan exhibited a higher resistance towards agglomeration caused by depletion interactions or by pH increase (see Supplementary Information, Figure 2-SI 8A and B). On the contrary, they aggregated more upon freeze drying without cryoprotectants, possibly because of the increased likelihood of entanglements between dandling HA chains.

The unspecific uptake of serum proteins was evaluated by isolating large aggregates (centrifugation) obtained upon exposing the nanoparticles to 50% FBS, and

measuring their protein content. It is likely that the latter value overestimates the amount of adsorbed proteins by compounding it to that of proteins denatured during centrifugation; however, this method allows a good relative estimation of the influence of surface chemistry on the unspecific interactions with proteins, as demonstrated e.g. with PEGylation of polyester nanoparticles [43]. Protein uptake largely decreased upon decoration with HA, which further demonstrates the efficacy of coating in reducing unspecific interactions in a biological medium (Figure 2- 8A). Importantly, a decrease was also observed for low MW chitosan nanoparticles, both coated and uncoated; while the reduction for the HA-coated nanoparticles is easily attributable to the presence of the thick HA corona, that for the uncoated nanoparticles can possibly be ascribed to the lower accessibility of the chitosan cationic sites due to their higher complexation with TPP (higher cross-link density).
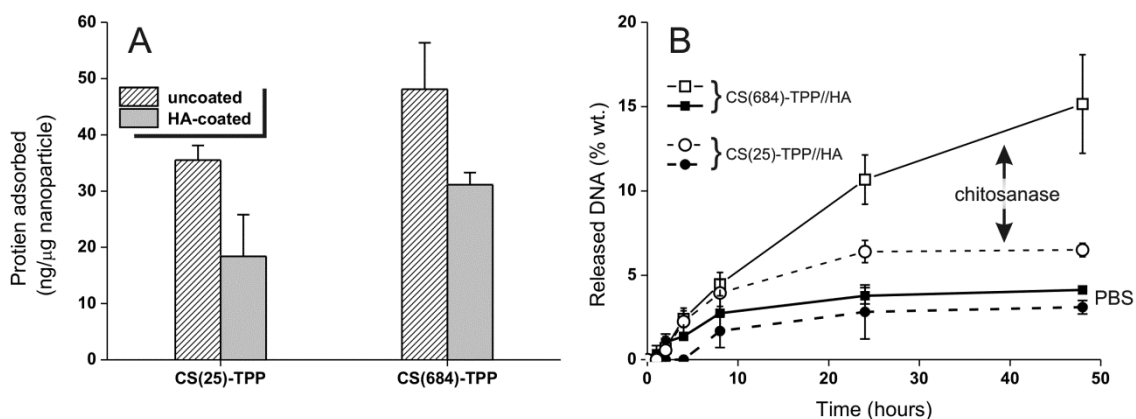
Figure 2- 8 *A.* Serum protein adsorption on nanoparticles before and after HA coating upon exposure to 50% FBS; proteins were quantified on aggregates isolated via centrifugation. Low MW chitosan significantly lowered protein adsorption for coated and uncoated nanoparticles, although with rather high standard errors. *B.* Release of DNA at 37 °C from HA-coated nanoparticles in PBS at pH = 7 (black symbols) and in the presence of chitosanase in acetate buffer at pH = 5 (white symbols). DNA/chitosan = 2% wt., DNA concentration: 1 µg/mL. The small difference recorded for CS(25)-TPP//HA is ascribed to the different pH.

The enzyme chitosanase has been used to reduce the strength of complexation between chitosan and nucleic acids, therefore inducing the release of the latter. For example, nucleic acids could be more efficiently released from chitosan nanoparticles by co-transfection with a bacterial chitosanase gene [44], while RNA can be more efficiently recovered through the chitosanase-mediated digestion of intracellular complexes [45]. Here, we have used chitosanase as a tool to probe the

facility of unpacking of the nanoparticle bulk. The enzymatic degradation of chitosan caused a significant DNA release only for 684 kDa chitosan nanoparticles (Figure 2-8B), while the 25 kDa chitosan nanoparticles followed a time profile analogous to control experiments. This effect is unlikely to be due to the enzyme not being active on low molecular weight chitosan since the typical end products of chitosanases are much smaller oligomers (< 10 units) [46, 47]; on the contrary, the lack of degradability is likely to be ascribed to the lower accessibility of chitosan because of a higher density of cross-links and/or the barrier properties of the HA corona.

2.4 Conclusions

We believe to have for the first time rationalised some of the molecular weight-dependent effects recorded for chitosan nanoparticles. In particular, the larger size typically recorded for high molecular weight chitosan nanoparticles appear to be due to their lower cross-link density; literature reports indicating stronger interactions with TPP with lower molecular weight were complemented by our measurements indicating higher swelling/shrinkage capacities for an identical size in the dry state. Most interestingly, the different compaction of the chitosan-TPP core seems to be responsible for very significant differences in the adsorption of the polyanionic HA on its surface. On lower molecular weight chitosan nanoparticles, HA formed a thick (20-30 nm) outer layer, which appears also to have significant effects on their stability; for example, these nanoparticles were much less sensitive to the presence of excess HA causing aggregation likely via depletion interactions (see Supplementary Information, Figure 2-SI 8A and B). On the contrary, HA appeared to diffuse more deeply in the bulk of high molecular weight chitosan nanoparticles and did not build any observable corona; either the absence of the latter or the inherently higher porosity of the chitosan matrix allowed these nanoparticles to be degraded by chitosanase, whereas no apparent enzymatic sensitivity was recorded for 25 kDa chitosan nanoparticles.

The different mode of HA adsorption is also likely to significantly influence the presentation of HA (more tightly bound in high MW chitosan nanoparticles) and thus to have significant effects on the interactions that may preside the receptor-mediated internalisation of these nanoparticles.

2.5 References

1.   Kurita, K., Chitin and chitosan: Functional biopolymers from marine crustaceans. Marine Biotechnology, 2006. 8(3): p. 203-226.

2.   Kramer, K.J. and D. Koga, Insect chitin - physical state, synthesis, degradation and metabolic-regulation. Insect Biochemistry, 1986. 16(6): p. 851-877.

3.   Lipke, P.N. and R. Ovalle, Cell wall architecture in yeast: New structure and new challenges. Journal of Bacteriology, 1998. 180(15): p. 3735-3740.

4.   Rao, S.B. and C.P. Sharma, Use of chitosan as a biomaterial: Studies on its safety and hemostatic potential. Journal of Biomedical Materials Research, 1997. 34(1): p. 21-28.

5.   Suh, J.K.F. and H.W.T. Matthew, Application of chitosan-based polysaccharide biomaterials in cartilage tissue engineering: a review. Biomaterials, 2000. 21(24): p. 2589-2598.

6.   Shahidi, F., J.K.V. Arachchi, and Y.J. Jeon, Food applications of chitin and chitosans. Trends in Food Science & Technology, 1999. 10(2): p. 37-51.

7.   Agnihotri, S.A., N.N. Mallikarjuna, and T.M. Aminabhavi, Recent advances on chitosan-based micro- and nanoparticles in drug delivery. Journal of Controlled Release, 2004. 100(1): p. 5-28.

8.   Garcia-Fuentes, M. and M.J. Alonso, Chitosan-based drug nanocarriers: Where do we stand? Journal of Controlled Release, 2012. 161(2): p. 496-504.

9.   Zaki, N.M., A. Nasti, and N. Tirelli, Nanocarriers for Cytoplasmic Delivery: Cellular Uptake and Intracellular Fate of Chitosan and Hyaluronic Acid-Coated Chitosan Nanoparticles in a Phagocytic Cell Model. Macromolecular Bioscience, 2011. 11(12): p. 1747-1760.

10.   Borges, O., et al., Uptake studies in rat Peyer's patches, cytotoxicity and release studies of alginate coated chitosan nanoparticles for mucosal vaccination. Journal of Controlled Release, 2006. 114(3): p. 348-358.

11.   Borges, O., et al., Preparation of coated nanoparticles for a new mucosal vaccine delivery system. International Journal of Pharmaceutics, 2005. 299(1-2): p. 155-166.

12.   Kim, T.H., et al., Receptor-mediated gene delivery into antigen presenting cells using mannosylated chitosan/DNA nanoparticles. Journal of Nanoscience and Nanotechnology, 2006. 6(9-10): p. 2796-2803.

13.   Kim, T.H., et al., Galactosylated chitosan/DNA nanoparticles prepared using water-soluble chitosan as a gene carrier. Biomaterials, 2004. 25(17): p. 3783-3792.

14.   Hamidi, M., A. Azadi, and P. Rafiei, Hydrogel nanoparticles in drug delivery. Advanced Drug Delivery Reviews, 2008. 60(15): p. 1638-1649.

15.   Gan, Q., et al., Modulation of surface charge, particle size and morphological properties of chitosan-TPP nanoparticles intended for gene delivery. Colloids and Surfaces B-Biointerfaces, 2005. 44(2-3): p. 65-73.

16.   Tsai, M.-L., et al., The storage stability of chitosan/tripolyphosphate nanoparticles in a phosphate buffer. Carbohydrate Polymers, 2011. 84(2): p. 756-761.

17.   Fan, W., et al., Formation mechanism of monodisperse, low molecular weight chitosan nanoparticles by ionic gelation technique. Colloids and Surfaces B: Biointerfaces, 2012. 90(0): p. 21-27.

18.   Ajun, W., et al., Preparation of aspirin and probucol in combination loaded chitosan nanoparticles and in vitro release study. Carbohydrate Polymers, 2009. 75(4): p. 566-574.

19.   Huang, Y. and Y. Lapitsky, Monovalent Salt Enhances Colloidal Stability during the Formation of Chitosan/Tripolyphosphate Microgels. Langmuir, 2011. 27(17): p. 10392-10399.

20.   Zhang, H., et al., Monodisperse chitosan nanoparticles for mucosal drug delivery. Biomacromolecules, 2004. 5(6): p. 2461-2468.

21.   Jonassen, H., A.L. Kjoniksen, and M. Hiorth, Stability of Chitosan Nanoparticles Cross-Linked with Tripolyphosphate. Biomacromolecules, 2012. 13(11): p. 3747-3756.

22.   Morris, G.A., et al., The effect of prolonged storage at different temperatures on the particle size distribution of tripolyphosphate (TPP) - chitosan nanoparticles. Carbohydrate Polymers, 2011. 84(4): p. 1430-1434.

23.   Lopez-Leon, T., et al., Physicochemical characterization of chitosan nanoparticles: electrokinetic and stability behavior. Journal of Colloid and Interface Science, 2005. 283(2): p. 344-351.

24.   Sabnis, S. and L.H. Block, Chitosan as an enabling excipient for drug delivery systems - I. Molecular modifications. International Journal of Biological Macromolecules, 2000. 27(3): p. 181-186.

25.   Huang, M., E. Khor, and L.Y. Lim, Uptake and cytotoxicity of chitosan molecules and nanoparticles: Effects of molecular weight and degree of deacetylation. Pharmaceutical Research, 2004. 21(2): p. 344-353.

26.   Janes, K.A. and M.J. Alonso, Depolymerized chitosan nanoparticles for protein delivery: Preparation and characterization. Journal of Applied Polymer Science, 2003. 88(12): p. 2769-2776.

27.   Csaba, N., M. Koeping-Hoeggard, and M. Jose Alonso, Ionically crosslinked chitosan/tripolyphosphate nanoparticles for oligonucleotide and plasmid DNA delivery. International Journal of Pharmaceutics (Kidlington), 2009. 382(1-2): p. 205-214.

28.   Kim, T.H., et al., Release of albumin from chitosan-coated pectin beads in vitro. International Journal of Pharmaceutics, 2003. 250(2): p. 371-383.

29.   Nasti, A., et al., Chitosan/TPP and Chitosan/TPP-hyaluronic Acid Nanoparticles: Systematic Optimisation of the Preparative Process and Preliminary Biological Evaluation. Pharmaceutical Research, 2009. 26(8): p. 1918-1930.

30.   Croll, T.I., et al., A blank slate? Layer-by-layer deposition of hyaluronic acid and chitosan onto various surfaces. Biomacromolecules, 2006. 7(5): p. 1610-1622.

31.   Lord, M.S., et al., Protein adsorption on derivatives of hyaluronic acid and subsequent cellular response. Journal of Biomedical Materials Research Part A, 2009. 91A(3): p. 635-646.

32.   Peer, D. and R. Margalit, Loading mitomycin C inside long circulating hyaluronan targeted nano-liposomes increases its antitumor activity in three mice tumor models. International Journal of Cancer, 2004. 108(5): p. 780-789.

33.   Ouasti, S., et al., The CD44/integrins interplay and the significance of receptor binding and re-presentation in the uptake of RGD-functionalized hyaluronic acid. Biomaterials, 2012. 33(4): p. 1120-1134.

34.   Katoh, S., et al., Glycosylation of cd44 negatively regulates its recognition of hyaluronan. Journal of Experimental Medicine, 1995. 182(2): p. 419-429.

35. Katoh, S., et al., Cutting edge: An inducible sialidase regulates the hyaluronic acid binding ability of CD44-bearing human monocytes. Journal of Immunology, 1999. 162(9): p. 5058-5061.

36. Ossipov, D.A., Nanostructured hyaluronic acid-based materials for active delivery to cancer. Expert Opinion on Drug Delivery, 2010. 7(6): p. 681-703.

37. Ghosh, S.C., S.N. Alpay, and J. Klostergaard, CD44: a validated target for improved delivery of cancer therapeutics. Expert Opinion on Therapeutic Targets, 2012. 16(7): p. 635-650.

38. Kasaai, M.R., J. Arul, and C. Charlet, Intrinsic viscosity-molecular weight relationship for chitosan. Journal of Polymer Science Part B-Polymer Physics, 2000. 38(19): p. 2591-2598.

39. Ungphaiboon, S., et al., Materials for microencapsulation: what toroidal particles ("doughnuts") can do better than spherical beads. Soft Matter, 2010. 6(17): p. 4070-4083.

40. Ma, P.L., et al., New Insights into Chitosan-DNA Interactions Using Isothermal Titration Microcalorimetry. Biomacromolecules, 2009. 10(6): p. 1490-1499.

41. Maurstad, G., S. Danielsen, and B.T. Stokke, The influence of charge density of chitosan in the compaction of the polyanions DNA and xanthan. Biomacromolecules, 2007. 8(4): p. 1124-1130.

42. La Gatta, A., et al., A complete hyaluronan hydrodynamic characterization using a size exclusion chromatography-triple detector array system during in vitro enzymatic degradation. Analytical Biochemistry, 2010. 404(1): p. 21-29.

43. Ameller, T., et al., Polyester-poly(ethylene glycol) nanoparticles loaded with the pure antiestrogen RU 58668: Physicochemical and opsonization properties. Pharmaceutical Research, 2003. 20(7): p. 1063-1070.

44. Zuo, A., et al., Improved transfection efficiency of CS/DNA complex by co-transfected chitosanase gene. International Journal of Pharmaceutics, 2008. 352(1-2): p. 302-308.

45. Alameh, M., et al., Chitosanase-based method for RNA isolation from cells transfected with chitosan/siRNA nanocomplexes for real-time RT-PCR in gene silencing. International Journal of Nanomedicine, 2010. 5: p. 473-481.

46. Pan, S.K. and S.J. Wu, Preparation of water-soluble chitosan by hydrolysis with commercial glucoamylase containing chitosanase activity. European Food Research and Technology, 2011. 233(2): p. 325-329.

47. Lee, Y.S., et al., Cloning, purification, and characterization of chitosanase from Bacillus sp DAU101. Applied Microbiology and Biotechnology, 2006. 73(1): p. 113-121.

2.6 Supplementary information

2.6.1 Nitrite-mediated chitosan degradation

Purification of chitosan. 5 g of CS were dissolved in 400 mL of a 2% w/v acetic acid solution. Complete dissolution was achieved after stirring for 16 h. The solution was then boiled for 15 min in order to denature and precipitate any proteic contaminant. The mixture was centrifuged at 4,500 rpm for 10 min and the supernatant was then removed and filtered through 1 µm pore size filters. In order to precipitate CS from the aqueous phase, the pH of the solution was then corrected to 9 with 1 M NaOH. After centrifugation, the precipitate was redispersed and sedimented twice using water at pH = 9 as a dispersing medium. The dispersion was then purified via ultrafiltration using a 3 kDa MWCO membrane with pure water until the conductivity and pH values of the waste water reached the values of pure water. The sample was then freeze dried and stored at 4 °C.

Depolymerisation of chitosan. CS oligomers were prepared by oxidative degradation of CS ($\overline{M_v}$ = 684 kDa) using sodium nitrite in acidic solution. CS (1% w/v) was dissolved in 0.1 M HCl solution under magnetic stirring. Appropriate amounts of $NaNO_2$ were slowly added to the CS solution to obtain $NaNO_2$ concentrations of 1.5, 3 and 5 mM, stirring the solutions at room temperature for 12 hours. Upon raising the pH to 8.0 with 1 M NaOH the solution became milky and was then purified via ultrafiltration (MWCO: 3 kDa) and freeze dried.
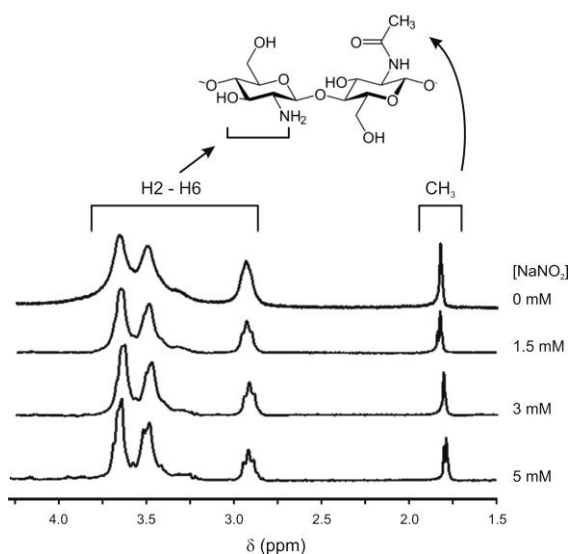
Figure 2-SI 1 ^{1}H-NMR spectra of chitosan in 0.5 M DCl/D_2O as a function of the concentration of sodium nitrite after a 12 hr depolymerisation (chitosan 1 % wt. in the reaction environment). The DD of all chitosan samples was calculated as %DD= 1-[(I_{CH3}/3) / (I_{H2-H6})/6)]*100, where (I_{CH3}) and (I_{H2-H6}) are the integrals of the acetyl group protons and of the H2, H3, H4, H5 and H6 protons respectively, as shown in the figure.
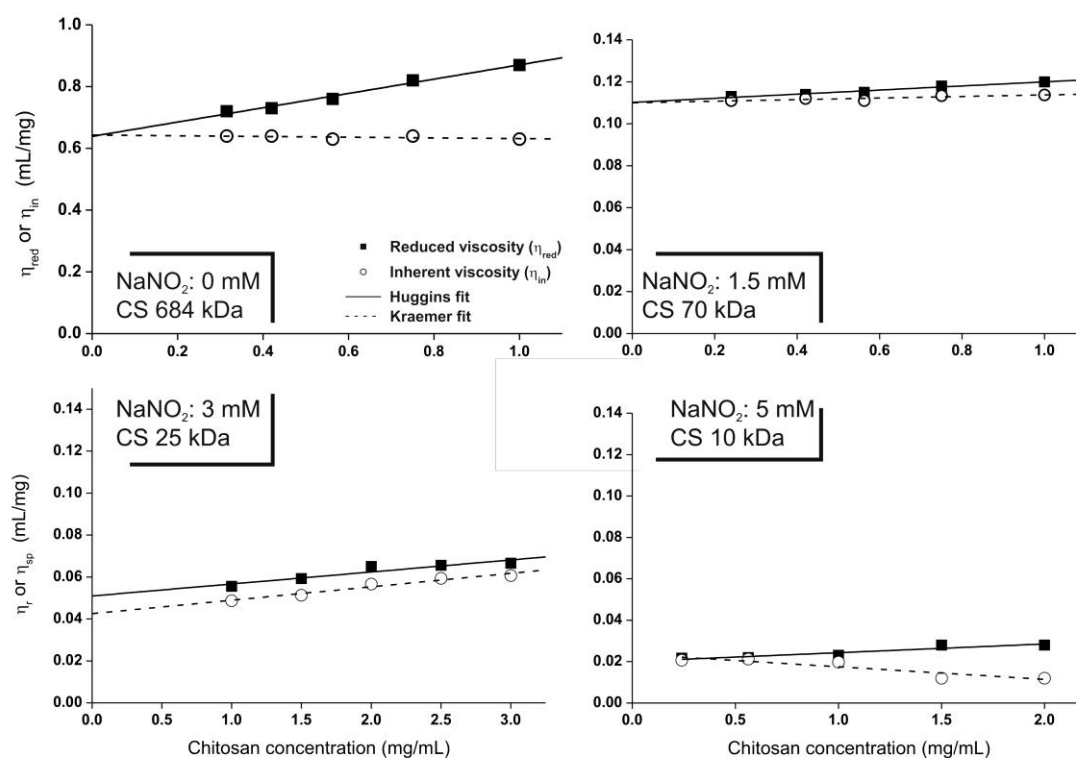
Figure 2-SI 2 Plots of reduced and inherent viscosity of chitosan before and after depolymerisation with sodium nitrite at the concentrations 1.5, 3 and 5 mM for 12 hrs. The intrinsic viscosity was calculated as the intercept of Huggins and Kraemer plots with the ordinate axis (at concentration = 0) for the two samples with the highest molecular weight, or as the intercept of the Huggins plot with the ordinate axis for the two samples with the lowest molecular weight. The intrinsic viscosities were then used to calculate the viscosimetric average molecular weight using the Mark-Houwink equation.

2.6.2 Loading of salmon sperm DNA and bovine serum albumin in CS/TPP nanoparticles

Encapsulation of macromolecules in CS-TPP nanoparticles. Salmon sperm DNA and BSA were used as a model nucleic acid and protein respectively to assess the encapsulation efficiency of CS-TPP nanoparticles. Variable amounts of DNA and BSA were used, respectively corresponding to 2, 9, 17, 25 % wt. and 10, 20 % wt. in relation to the amount of chitosan used during nanoparticles preparation. DNA and BSA were dissolved in the TPP solution prior to nanoparticle formation, which was then carried out as previously described. The encapsulation efficiency was calculated from the amount of non-encapsulated material recovered in the supernatant after precipitation of the nanoparticles at pH = 7.4 and centrifugation of the nanoparticles (4,500 rpm, 5 minutes). The amount of DNA was determined by UV spectrophotometry at 260 nm using a BioTek Synergy 2 multiwell plate reader, while BSA was quantified using the Quantipro BCA assay kit (for calibration curves, see Figure 2-SI 3). For the latter, 100 µL of supernatant were added to 100 µL of Quantipro solution. After 2 hours incubation at 37 °C, the absorbance was recorded at 562 nm and the amount of protein was calculated using a protein standard curve. The supernatant of non-loaded nanoparticles was used as a negative control and the encapsulation efficiency (EE) was calculated as *EE = (A-B)/A×100*, where *A* is the total amount of macromolecule and B is the amount of macromolecule recovered in the supernatant.
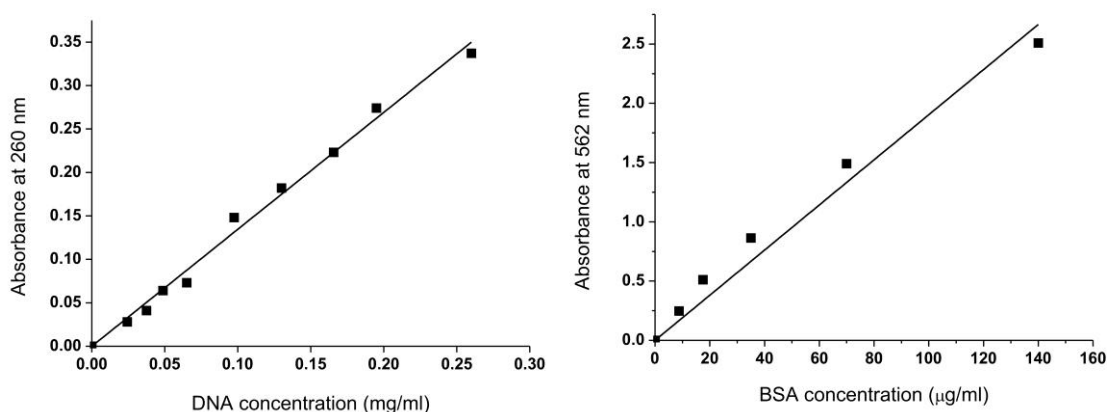
Figure 2-SI 3 Calibration curves for the estimation of the concentration of salmon sperm DNA by direct readings of its absorbance at 260 nm (left) and of BSA through the BCA assay (right). In both cases, the readings were performed using a 0.1 %wt. solution of TPP (in deionised water brought to pH = 5 by the addition of HCl).
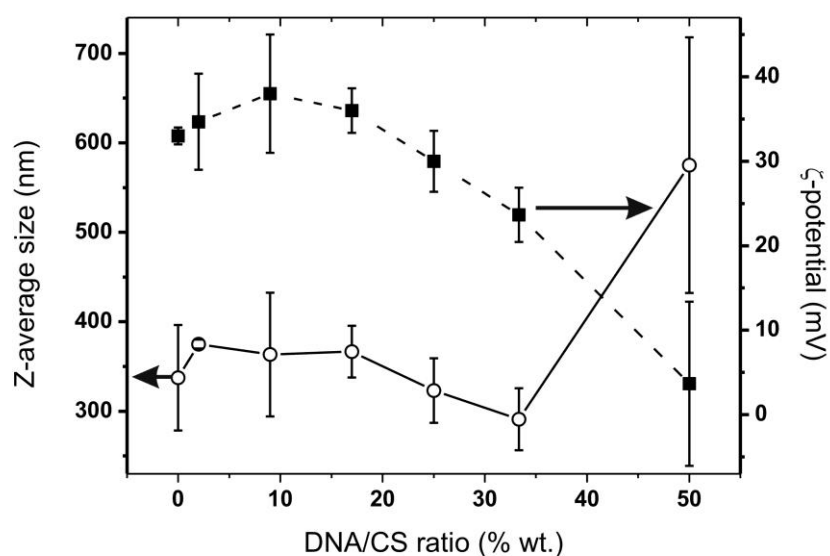
Figure 2-SI 4 Z-average size (circles) and ζ potential (squares) of CS(684)-TPP nanoparticles as a function of the theoretical DNA loading (weight ratio between DNA and chitosan in the feed). The decrease of ζ potential for DNA/CS > 25% wt. was taken as an indication of a decrease in nanoparticle stability due to excessive loading.
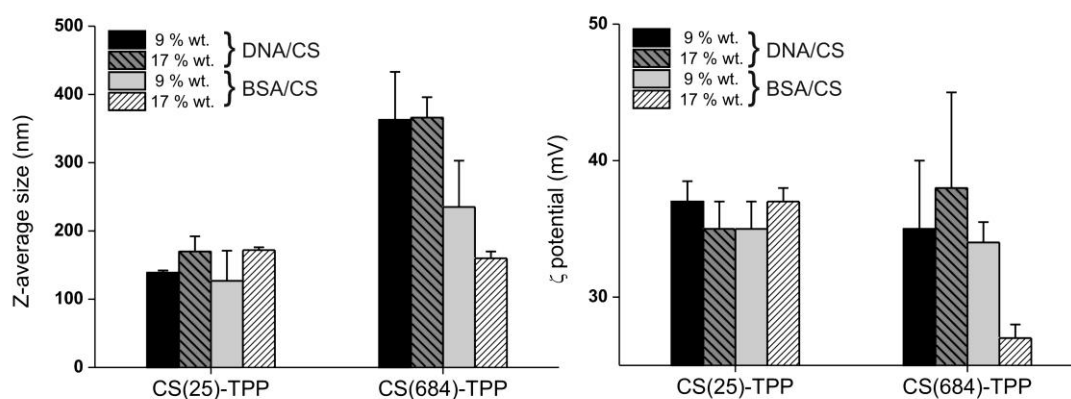
Figure 2-SI 5 Z-average size (*left*) and ζ potential (*right*) of CS(25)-TPP and CS(684)-TPP nanoparticles at two different theoretical loadings.

Table 2-SI 1 Comparison of the encapsulation efficiency (%) for BSA and DNA in CS-TPP nanoparticles prepared from chitosan with two different molecular weights.

Payload /CS (% wt.)	DNA		BSA	
	CS(684)-TPP	CS(10)-TPP	CS(684)-TPP	CS(25)-TPP
9	>99.9	96 ± 0.5	47 ± 3	49 ± 2
17	99.3 ± 1.2	90 ± 6.0	29 ± 3	47 ± 5

2.6.3 Characterisation of HA-coated nanoparticles
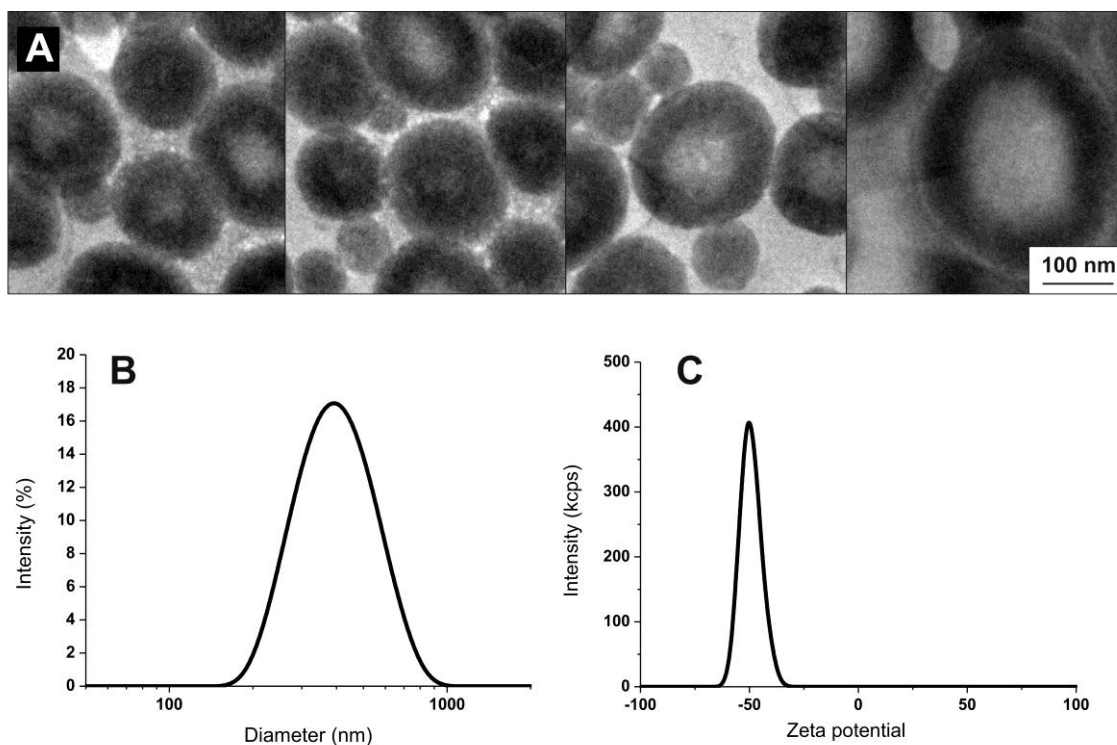
Figure 2-SI 6 TEM images (*A*) size distribution (*B*) and ζ potential distribution (*C*) of HA-decorated nanoparticles (25 kDa chitosan, CS-TPP 9:1, 360 kDa HA 1.5 mg/mL).

Transmission electron microscopy (TEM). A 2% aqueous phosphotungstic acid solution (adjusted to pH 7.3 using NaOH 1 M) was used as a contrast enhancing solution. The grids (mesh 300 Cu, diameter 3.05 mm) were covered with a formvar film and then coated with carbon (Agar Scientific, Essex, UK). 100 μL of the sample at a concentration of 50 μg/mL were mixed with 100 μl of the contrast solution. 10 μL of the resulting solution were deposited on top of the grid. The grid was then freeze-dried to gently evacuate the water from the nanoparticles. A transmission electron microscope Philips CM200 HRTEM operating at 200 kV was used to obtain images of the samples.

Table 2-SI 2 Mean volumes and diameters for uncoated and HA-coated chitosan-TPP nanoparticles, as calculated from the volumes measured via AFM height images on an average of 200 nanoparticles.

		Volume			Diameter		
		Mean (nm^3)	M	σ	Mean (nm)	M	σ
CS(684)-TPP		6300	8.55	0.61	21	3.05	0.20
CS(684)-TPP // HA		2.28×10^6	14.47	0.58	157	5.03	0.19
CS(25)-TPP		14016	9.51	0.25	30	3.38	0.08
CS(25)-TPP // HA	Total	3.54×10^6	14.75	0.80	176	5.13	0.26
	Core	1.42×10^6	13.65	1.01	124	4.76	0.33
CS(25)-TPP // HA (DNA loaded)	Total	4.06×10^6	15.04	0.59	190	5.22	0.19
	Core	1.27×10^6	13.25	1.26	112	4.63	0.42
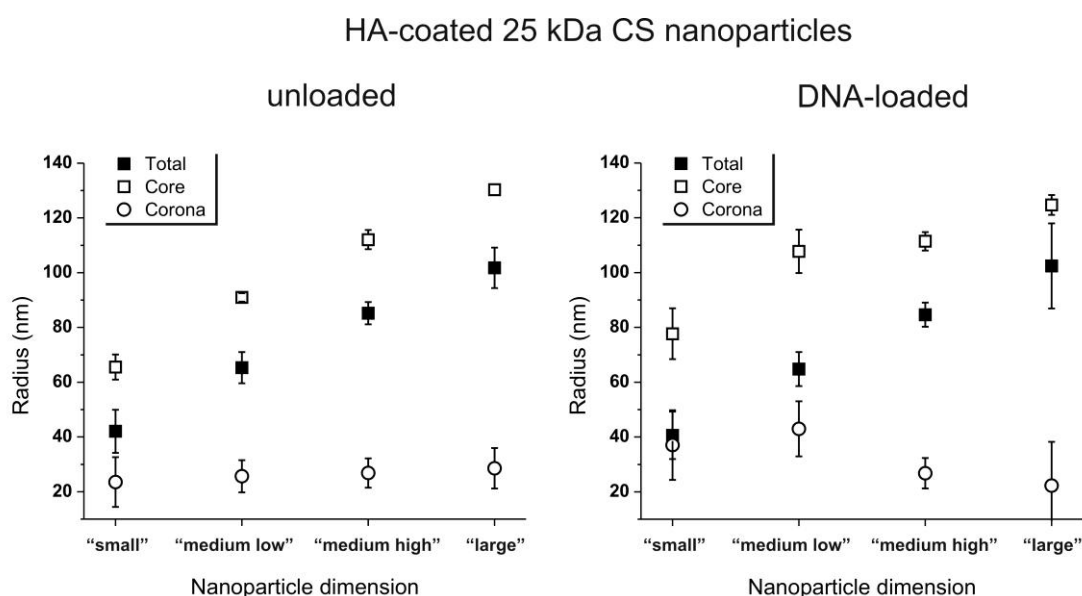
Figure 2-SI 7 Comparison of the dimensional data for coated 25 kDa chitosan nanoparticles with or without salmon sperm DNA (DNA/chitosan = 25% wt.). The linear dimensions (radii) are obtained from the volume of the dry nanoparticles assuming a spherical morphology instead of their flattened shape on the mica substrate.

2.6.4 Stability of HA-coated nanoparticles

The applicability of a nano-carrier depends on its behaviour during e.g. storage or sterilisation, therefore we have investigated the conditions to maximise its colloidal stability.

Stability in water. Coated nanoparticles significantly agglomerated if excess HA was not removed after preparation; for example, agglomeration took place in a manner that is inversely related to the efficiency of HA removal via dialysis membranes with different MWCO sizes (Figure 2-SI 8A). Since this effect was less noticeable for 25 kDa chitosan nanoparticles, we are inclined to ascribe agglomeration to depletion interactions [1], whose influence should be less noticeable for softer and more penetrable colloids.

Also, the pH of the dispersing medium had a significant influence on nanoparticle stability; its gradual increase to neutrality in 10 mM buffers was detrimental to stability (Figure 2-SI 8B), possibly because of detachment of HA due to the reduced degree of protonation of the underlying amines. Also in this case, the magnitude of the effect was lower for low molecular weight chitosan particles, probably because of its better complexation ability (smaller molecule, higher number of interacting site per coil), which also maximises its interactions with HA.

On the other hand, nanoparticles dispersed in deionised water (pH = 5.5 − 6 after dialysis) appeared to have a marked stability, which was studied for up 28 days. At room temperature, after 5 − 7 days, both 25 and 684 kDa chitosan HA-coated nanoparticles showed clear signs of agglomeration (increase in average size, Figure 2-SI 8C; increase in breadth of size distribution, Figure 2-SI 8D) and precipitation (decrease in scattering, Figure 2-SI 8E), which for 25 kDa chitosan nanoparticles were also accompanied by a significant reduction of the magnitude of the ζ potential (Figure 2-SI 8F). This destabilisation may be due to HA detachment, which can be a result of reorganisation and compaction of the chitosan-TPP bulk; the latter phenomenon should be slowed down at low temperature and indeed at 4 °C no change in the colloidal dispersions could be recorded for up to 4 weeks.

Stability upon filtration. The filtration through < 0.5 µm pores, most commonly 0.22 µm, is one of the most common sterilisation methods for nanoparticle dispersions. In our case, sterile filtration is questionable since the majority of HA-

coated nanoparticles have hydrodynamic sizes above 400 nm. However, neither nanoparticle size (Figure 2-SI 9, left) nor scattering intensity (Figure 2-SI 9, right) decreased upon filtration with pore sizes down to 0.44 μm; a significant amount of nanoparticles (62% for 684 kDa chitosan and 22% for 25 kDa chitosan) even passed through a 0.22 μm pore size, thus showing a considerable deformability. Thus, HA-coated nanoparticles can be sterile filtered down to 0.44 μm, which is generally sufficient to avoid bacterial contamination; on the other hand, an aseptic preparation would be needed to ensure the absence of viral contaminants.

Stability upon freeze drying. Freeze drying in the absence of a cryoprotectant caused very significant agglomeration, with an average size, after redispersion in deionised water, about 1.5 and 3.5 times larger than their original diameter for 25 kDa and 684 kDa chitosan HA-coated nanoparticles respectively (Figure 2-SI 10). However, the addition of glucose or sucrose as cryoprotectant allowed reconstitution of the nanoparticles in water without significant alterations to their size distribution.
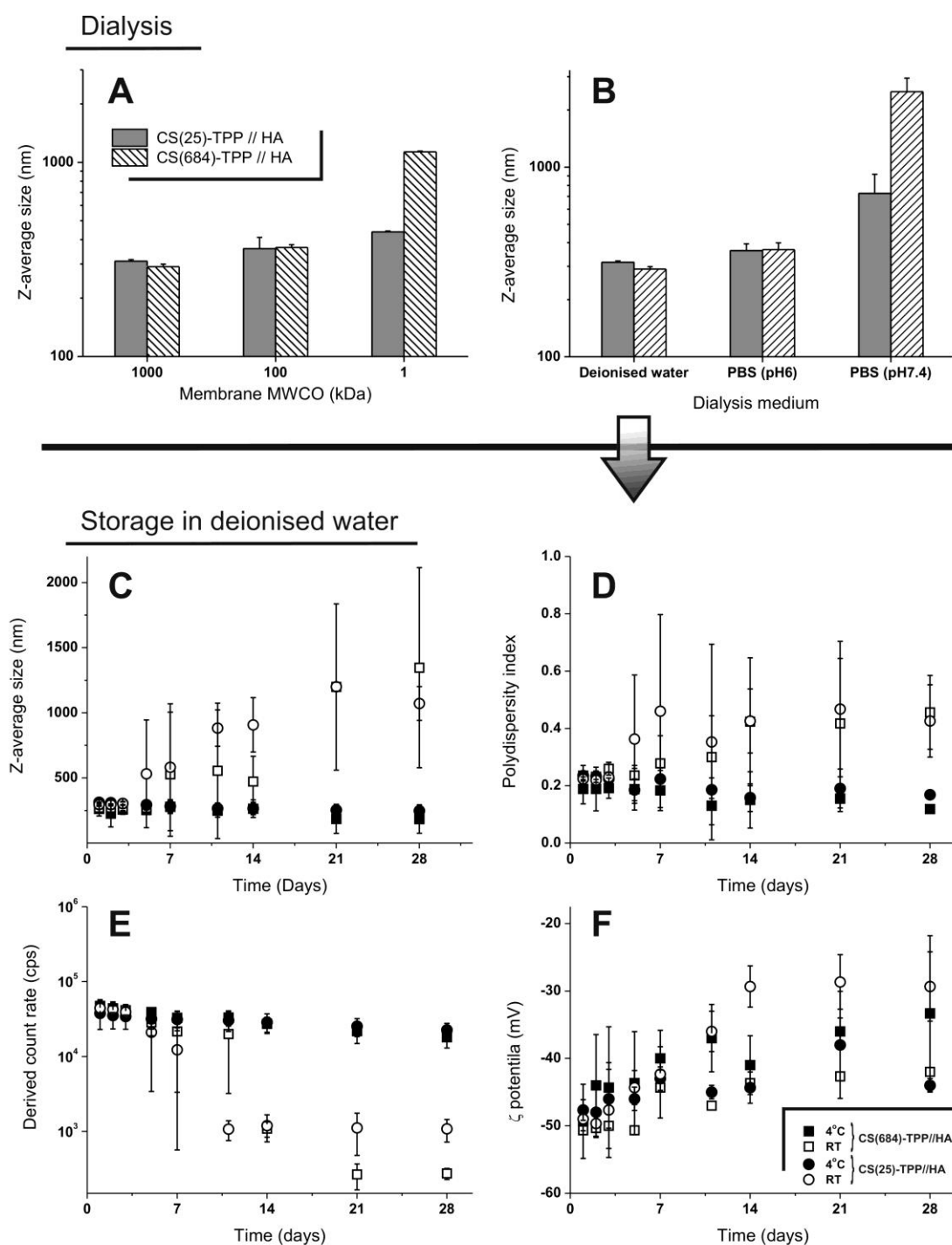
Figure 2-SI 8 *A.* Z-average size of HA-coated nanoparticles prepared in 0.1 M acetic buffer (pH 5) and then dialysed against deionised water using membranes with different molecular MWCO values; in all cases the size was recorded when the conductivity of the dialysate was indistinguishable from that of deionised water. *B.* The same particles in A were dialysed against different media for an identical time (24 h). *C – F.* Z-average size (*C*), polydispersity index (PDI) (*D*), derived count rate (DCR) (*E*) and ζ-potential (*F*) of HA-coated nanoparticles in deionised water stored at 4 °C and at room temperature over a period of 28 days.
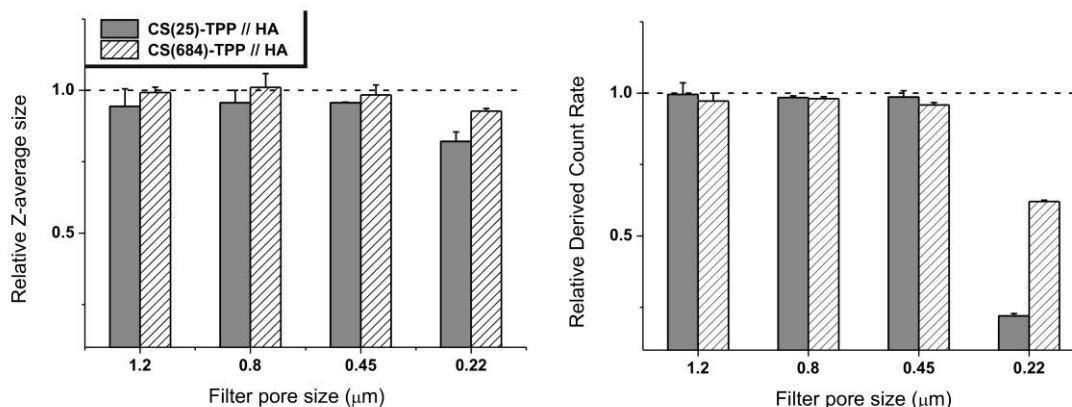
Figure 2-SI 9 Size (*left*) and scattering intensity (*right*) after filtration through different pore sizes. The data are expressed in relation to non-filtered nanoparticles suspension.
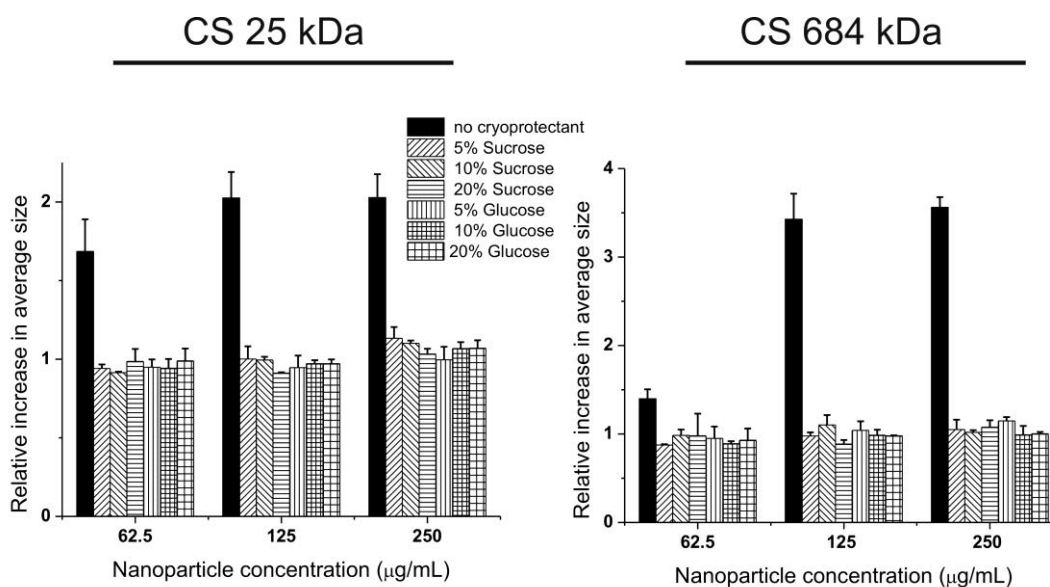
Figure 2-SI 10 Variations in the Z-average size upon freeze-drying and reconstitution in deinoised water for HA-coated 25 kDa (left) and 684 kDa (right) chitosan nanoparticles.

Filtration. Nanoparticles were freshly prepared as described above and then filtered through 1.2 μm, 0.8 μm, 0.45 μm, and 0.22 μm hydrophilic syringe filters (Minisart, Sartorius, Goettingen, Germany) prior to DLS analysis.

Storage. 0.5 mg/mL HA-decorated nanoparticles in deionised water were stored at 4 °C or at room temperature for one month, performing DLS analysis at specific time points (1, 2, 3, 5, 7, 11, 14, 21, 28 days).

Freeze-drying. 2 mL of purified nanoparticle suspension (0.25, 0.125, or 0.062 mg/mL) were freeze-dried with or without a cryoprotectant (5%, 10% or 20% glucose or sucrose; freezing temperature: -80 °C, drying for up to 72 h). The

particles were then redispersed in 2 mL of deionised water and dialysed against deionised water (MWCO 1,000 kDa) in order to remove the cryoprotectant. Z-average size was then measured as indicated above and the result was expressed as the ratio of the Z-average size after (D_f) to that before Freeze-drying (D_i).

Supplementary reference

1.   Ye, X., et al., *Depletion interactions in colloid-polymer mixtures.* Physical Review E, 1996. **54**(6): p. 6500-6510.

Chapter Three

Receptor-mediated uptake of hyaluronic acid (HA)-coated nanoparticles: HA presentation modulates affinity and endocytosis kinetics[a]

Abstract

The natural turnover of free hyaluronic acid (HA) is predominantly based on its CD44-mediated internalization in leukocytes. In a phagocytic cell model (RAW 264.7 murine macrophages) we here provide conclusive evidence that this receptor-mediated mechanism endocytosis is responsible also of the uptake of materials where HA is used as a coating agent, in this case chitosan/triphosphate nanoparticles on the surface of which HA is electrostatically adsorbed. Alginate-coated nanoparticles were used as a control and they appeared to undergo a qualitatively similar endocytic process, which was mediated by a different scavenging receptor yet to be identified.

In this general picture, an important, modulating role appears to be played by how receptors can cluster around individual nanoparticles. The CD44 slow representation (24-48 hours) enforces a limit in the amount of available HA internalisation receptors; therefore, a higher affinity, and hence a higher degree of clustering, would yield a lower number of internalised nanoparticles. Indeed, HA presentation can be varied by acting on nanoparticle structure/morphology, and our data suggest that a better presentation may be linked to both higher affinity and lower capacity/uptake rate.

Paradoxically, this result would suggest that particles with a lower affinity for CD44 may allow a more efficient HA-mediated delivery of payloads.

[a] **Cellular interactions studies were partially conducted by Ms. Shima Karimi under my guidance.**

3.1 Introduction

Hyaluronic acid (HA), a major glycosoaminoglycan (GAG) constituent of extracellular matrices, is increasingly seen as a potential agent to target conditions (e.g. several solid tumours) characterised by the overexpression of its main receptor, CD44 [1, 2]. A variety of HA-based carriers have been used for the purpose of targeting tumoural cells, e.g. HA-butirrate [3], HA-paclitaxel [4] conjugates, self-assembled [5], PLGA-based [6] or disulfide cross-linked nanoparticles [7], and PEGylated HA derivatives [8]. This field has been recently reviewed by Choi et al. [9] and Ossipov et al. [10]. In the majority of cases, the role of CD44 in the internalisation of HA-based carrier structures is inferred from the preferential internalisation in CD44 (over)expressing cell lines: for example, from the comparison of MDA-MB-231 vs. ZR-75-1 breast cancer cell lines [11], of HepB3 and HepG2 hepatoma cell lines [12], or of SCC7 squamous cell carcinoma cells and fibroblasts or HA-saturated cells [5]. Two important caveats exist: a) the slow representation of CD44 and hence its ease of saturation is a cause of concern, since, as we have recently shown, this drawback cannot be circumvented by the addition of ancillary internalisation ligands [13]; b) CD44 is heavily expressed not only by tumoural cells, but also by inflammatory cells [14], e.g. playing a major role in the clearance of apoptotic cells by macrophages [15]; the expression of CD44 by ubiquitous cells such as leukocytes may be seen as a problem, since it inherently reduce the targeting efficiency of tumoural cells, but may also open new avenues by allowing to target (activated) leukocytes.

A yet unanswered question is whether inflammatory cells would be able to recognise HA when it is present on the surface of a nano-carrier, since its binding to leukocyte CD44 is affected by several morphological variables, such as HA molecular weight [16] and spatial arrangement (e.g. HA cables vs. pericellular coats [17, 18]), or the possibility of receptor clustering around it [19]. Previous literature studies have suggested that HA-coated nanoparticles can be internalised in a receptor-mediated fashion [20, 21], but a final proof is still lacking. Further, if we hypothesise that internalisation is mediated by a slowly represented receptor, the extent of its clustering around individual nanoparticles determines their uptake rate and affinity: high level of clustering would correspond to high affinity, but this will limit the

overall capacity, thus determining an apparently slow uptake (Scheme 3- 1). In turn, the degree of receptor clustering would depend on nanoparticle dimension and on the accessibility of HA residues and their individual affinity for the receptors.
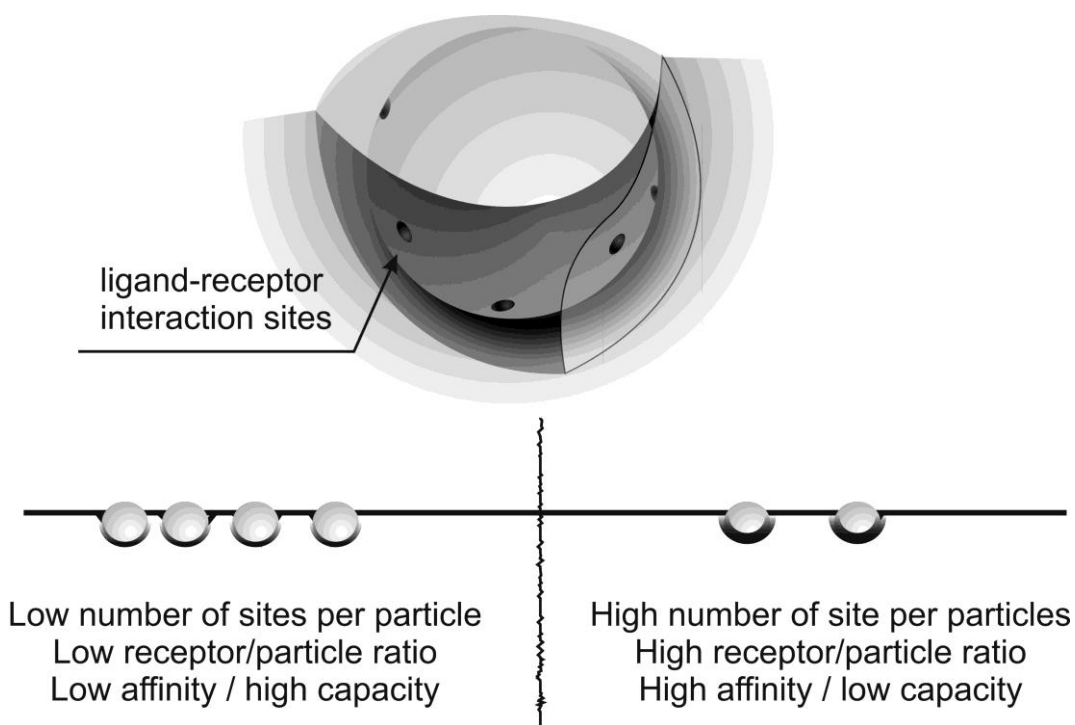
Scheme 3- 1 Under conditions of slow receptor representation, the amount of available receptors is a crucial factor to determine the uptake kinetics of e.g. an HA-coated nanoparticle. A limited number of interaction sites, e.g. because of poor presentation of HA, would allow the internalisation of a larger amount of less strongly bound nanoparticles (left); on the contrary, high strength of interactions due to the clustering of many receptors around each nanoparticle may lead to a small number of nanoparticles being internalised.

In this study, we have used the polyelectrolyte complexation of chitosan with triphosphate (TPP) to produce nanoparticles, which were then employed as a cationic core to complex HA and deliver HA-coated chitosan/TPP nanoparticles (CS-TPP//HA). The electrostatic adsorption of HA on CS-TPP nanoparticles can be modulated by several variables of the preparative process [22], possibly influencing its mode of presentation and its interactions with cell receptors. Therefore, we have investigated the effect of chitosan molecular weight and of two different preparative methods on the toxicity, internalisation kinetics and mechanism of CS-TPP//HA nanoparticles in a phagocyte model (RAW 264.7 macrophages). In addition, nanoparticles coated by an anionic, non-CD44 binding polysaccharide of similar size (alginate, CS-TPP//Alg) were used as a control.

In terms of molecular weight, we have employed chitosan with $\overline{M_v} = 684$ kDa (~85% deacetylated), 325 kDa (~92% deacetylated) and 25 kDa (~85% deacetylated, produced through nitrite controlled degradation of the highest molecular weight). Chitosan size is likely to influence the internal structure of the nanoparticles: higher molecular weight is likely to be less efficiently cross-linkable and therefore to produce more porous particles (larger dimensional variations in response to changes in ionic strength); in turn, this can lead to better HA penetration as opposed to surface adsorption, therefore influencing its presentation to cell receptors.

In terms of preparative method, we have followed two procedures, whose key differences are summarised in Table 3- 1.

Table 3- 1 Key differences between the two preparative methods

	Addition of TPP	pH during CS/TPP complexation	pH during coating	Removal of excess of coating agent via dialysis
Method A	Injection into chitosan solution	5.0	5.0	Yes
Method B	Dropwise addition	4.0	7.2	No

Method A was optimised in a previous study [22] and implemented with chitosan of $\overline{M_v} = 684$, 325 and 24 kDa; by using the same pH = 5 for all solutions, it allows to minimise the influence of different mixing conditions, while by minimising the charge density on both cationic and anionic components, it provides the conditions for a likely slower but more controlled complexation. On the contrary, method B, implemented with chitosan of $\overline{M_v} = 325$ kDa, provides a higher charge density to chitosan (in TPP complexation) and to the anionic coating agent (in nanoparticle coating); therefore, possibly increasing the speed of complexation. Further, the different mode of addition of TPP (injection of the liquid into chitosan solution in method A vs. its dropwise addition in method B) may result in different mixing kinetics and thus contribute to structural differences in the nanoparticle structure. Last, method B is performed under fully aseptic conditions and the nanoparticles can be directly applied to cell experiments, while in method A they are purified by dialysis and then sterile-filtered; method B is therefore more rapid and robust with

less variables being introduced, but the presence of non-adsorbed HA (or alginate) may affect the results.

3.2 Materials and methods

3.2.1 Materials

Chemicals. Middle-viscous chitosan of $\overline{M_v}$ = 684 kDa (Mark-Houwink coefficients: (K = 1.57 × 10^{-5} L.g^{-1} and a = 0.79) [23]) and degree of deacetylation 85 % was purchased from Sigma (Sigma-Aldrich, Gillingham, UK). Lower molecular weight chitosan ($\overline{M_v}$ = 25 kDa was obtained by oxidative degradation of middle-viscous chitosan (1% w/v in 0.1 M HCl) using 3 mM sodium nitrite. All chitosan samples were purified as described in previous reports. Chitosan of $\overline{M_v}$ = 325 kDa (degree of deacetylation 92 %), sodium alginate ($\overline{M_v}$ = 400 kDa) and hyaluronic acid (HA; $\overline{M_v}$ = 360 kDa) were provided by Medipol (Medipol SA., Ecublens, Switzerland). Sodium triphosphate pentabasic (TPP), dimethyl sulfoxide (DMSO) and Rhodamine B isothiocyanate (RITC) were purchased from Sigma-Aldrich (Gillingham, UK). CellTiter 96® AQ$_{\text{ueous}}$ one solution cell proliferation assay (MTS) [3-(4,5-dimethylthiazol-2-yl)-5-(3-carboxymethoxyphenyl)-2-(4-sulfophenyl)-2H-tetrazolium] kit was purchased from Promega (Madison, WN, USA).

Cell culture. RAW 264.7 macrophages (ECACC, UK), Dulbecco's modified eagle medium (DMEM), the quantipro BCA assay kit, TritonX-100, antibiotic-antimycotic solution, sodium pyruvate, D-glucose, 4',6-diamidino-2-phenylindole (DAPI) and endocytosis portals inhibitors (cytochalasin D, filipin, 5-(N-ethyl-N-isopropyl)amiloride (EIPA), nocodazole, chloropromazin, bafilomycin A1 and sodium azide) were purchased from Sigma-Aldrich. Foetal bovine serum (FBS), LysoTracker Green DND-26, L-glutamine and anti-fade mounting gel were purchased from Invitrogen (Paisley, UK). Monoclonal antibody anti-CD44 [KM81] and paraformaldehyde were respectively brought from Abcam (Cambridge, UK) and VWR (Lutterworth, UK).

3.2.2 Fluorescent Labelling of Chitosan

An amount of chitosan corresponding to 0.48 mmol of amine groups (100 mg for CS684) were dissolved in 18 mL of 0.10 M acetic acid solution and the pH was then adjusted to 4 with 0.1 M NaOH. 10 mg of RITC (0.019 mmol of isothiocyanate groups) dissolved in 2 mL of DMSO were added slowly to the chitosan solution using a dropping funnel. The reaction was left under stirring for 12 hours protected

from light. The reaction mixture was then diluted with 20 mL of deionised water and dialysed against deionised water using a RC dialysis membrane of MWCO 10 kDa (SpectraPor, Spectrum Laboratories Inc., Rancho Dominguez CA, USA) until the conductivity and pH values of the waste water reached the values of pure water. The sample was then freeze-dried and stored at 4 °C. The degree of functionalisation was determined by measuring the fluorescence intensity of the RITC-chitosan solution, using a calibration of fluorescein (λ_{ex} = 540 nm; λ_{em} = 620 nm). Typically, 1.2 - 1.7 % mol of D-glucosamine units were derivatised.

3.2.3 Preparation of nanoparticles

Method A. A 0.069 % wt. RITC-labeled chitosan solution was prepared by dissolving purified RITC-labeled chitosan in 4.6 mM HCl. The pH was adjusted to 5 by the addition of appropriate volumes of 0.1 M NaOH. The solution was kept under magnetic stirring overnight and sonicated for 40 min. TPP was prepared as a 0.1 % wt. solution in deionised water, correcting the pH to 5 using appropriate volumes of HCl 0.1 M. Both solutions were filtered through a 0.22 μm pore size filter. The nanoparticles were prepared by addition of the TPP solution 0.1% wt. to the chitosan solution in a 1:9 TPP to chitosan mass ratio, e.g. for a final volume of 3 mL of nanoparticle solution, 214 μL of TPP solution is added to 2786 μL of chitosan solution, where the final concentrations of chitosan and TPP are 0.064 and 0.0071 % wt., respectively. The complexation was carried under magnetic agitation (750 rpm), for 30 min at 25 °C. The final dispersion was sonicated for 40 min and then left undisturbed for additional 16 hours. Then the nanoparticle dispersion was dialysed against deionised water (MWCO 1,000 kDa) before being surface decorated by HA (360 kDa) or sodium alginate (400 kDa). For the surface coating process, 5 mL of a 0.025 % wt. dispersion of CS-TPP nanoparticles in 100 mM acetate buffer at pH = 5 were added under vigorous magnetic stirring (30 min, 1,200 rpm) to an equal volume of HA or sodium alginate both at a concentration of 0.15 % wt. in the same buffer. The dispersions were then dialysed against deionised water (MWCO 1,000 kDa).

Method B. The preparative method is based on a patented aseptic process [24]. RITC-labeled chitosan (345 kDa) was dissolved in deionised water (final concentration is 0.1 % w/v) by the addition of 1 M HCl until the pH was stabilised

below 4. The dispersion was kept under magnetic stirring until complete dissolution. TPP 0.1% (w/v) in deionised water at pH ≈ 6.5 was added dropwise to the chitosan solution, in a 1:9 TPP to chitosan mass ratio while keeping the pH under 4 by the addition of proper volumes of 0.1 M HCl. The suspension was kept under stirring for an hour and then diluted with deionised water at a 1:1 (v/v) ratio. The dispersion was then added dropwise to 0.1% (w/v) sterile filtered aqueous HA or alginate solutions at a volume ratio of 1:1 (v/v) under vigorous agitation. 0.1 M NaOH was used to adjust the pH of the final nanoparticle suspension to 7.2. Finally, the suspension was kept under magnetic stirring for one additional hour at room temperature.

3.2.4 Physico-chemical characterisation

Hydrodynamic diameter (Z-average size), size polydispersity (PDI) and ζ potential measurements were always performed on three independent samples at a temperature of 25 °C using a Zetasizer Nano ZS instrument (Model ZEN3600, Malvern Instruments Ltd., UK) equipped with a solid state HeNe laser (λ = 633 nm) and measuring at a scattering angle of 173°.

Atomic Force Microscopy (AFM) images were acquired at 25 °C in air using a Molecular Force Probe 3D AFM (MFP-3D, Asylum Research, Santa Barbara, CA). Silicon cantilever (model NP-S10, Bruker) with a nominal spring constant, tip radius, tip height and resonance frequency, of 0.06 N/m, 20 nm, 2.5-8 μm, 18 kHz respectively, was used. Contact mode images of several regions were acquired (512x512 pixels per inch), at a scan frequency of 1 Hz and a gain of 10.

3.2.5 Cellular interactions of nanoparticles

General cell culture. RAW 264.7 macrophages were maintained as semi-adherent cell culture in standard conditions for cell culture (37 °C, 5% CO_2, in humidified atmosphere) in Dulbecco's modified eagle minimal essential medium (DMEM) supplemented with 10% heat-inactivated foetal bovine serum (FBS), 2×10^{-3} M glutamine, 100 U·mL^{-1} penicillin and 100 U·mL^{-1} streptomycin. Cells were detached by scrapping and adjusted to the required concentration of viable cells, by counting in a hemocytometer.

Cell viability assays. RITC-labeled chitosans were incorporated in nanoparticle preparation methods A and B as described above. Nanoparticles with required

concentrations (750, 500, 325, 200, 100, 10, 1 and 0 μg/mL) were prepared in full phenol red-free medium (10% FBS, 1% L-glutamate, 1% antibiotic/antimitotic) (see Supplementary Information).

RAW 264.7 macrophages of passages 10-15 were seeded in a 96-well plate at a density of 10,000 cells/well and cultured in DMEM medium containing 10% FBS, 1 % antibiotic/antimitotic solution, and 1 % L-glutamate and incubated under standard sterile conditions for cell culture (5% CO_2, 37 °C) until 70% confluency. The medium was then removed and the cells were washed with PBS. The cells were then incubated with nanoparticles in full phenol-red free DMEM in standard conditions for cell culture for 0, 1, 2, 4, 8, 16 and 24 hours. At the completion of the incubation, the cells were washed with PBS and incubated further for two hours in serum-free medium containing MTS 5 % (v/v). Cell viability was measured colorimetrically using the conversion of MTS to a soluble coloured formazan. The absorbance readings were acquired with a Synergy2 Biotek plate reader using Gen5 software. The quantity of formazan produced as measured by the absorbance at 490 nm is proportional to both the number and the metabolic activity of living cells in culture. Cell viability measurements were normalised by the amount of total protein content in each well. Total protein content was quantified using the Quantipro BCA assay kit. Briefly, the cells were washed with PBS, and incubated for 15 min, in 100 μL cell lysis buffer (0.5% triton X-100 in 0.2 M NaOH), to which 100 μL of Quantipro solution (prepared following the instructions of the manufacturer) was added. After 2 hours incubation at 37 °C, the absorbance was recorded. Cell viability was expressed as the ratio of the absorbance reading for nanoparticle treated cells to that for control non-treated cells.

Quantification of cellular uptake (fluorimetry). RITC-labeled chitosan samples were incorporated in nanoparticle preparation methods A and B to highlight the effect of the preparative procedures, chitosan molecular weight and surface chemistry on the cellular fate of nanoparticles. Following the same procedure as previously described for cell viability studies, the uptake experiments were performed on concentrations ranging from 10 to 250 μg/mL of nanoparticles in full phenol red-free DMEM medium. After specified incubation times (1, 2, 4, 8, 16 and 24 hours), the supernatant solution was removed and the cells were washed three times with PBS and lysed with 100 μL of 0.5% Triton X-100 in 0.2 M NaOH. The

amount of membrane bound and internalised nanoparticles was estimated on the basis of the fluorescence of the cell lysates (λ_{exc} = 540 nm; λ_{emi} = 620 nm); nanoparticles dispersed in cell lysates were used to provide a calibration for the fluorescence data. The amount of internalised nanoparticles was normalised by the total protein content, which was quantified using the Quantipro BCA assay kit as described previously. For Michaelis-Menten fitting, the amount of nanoparticles internalised after 2 and 8 hours was divided by the exposure time to respectively provide an initial uptake rate and an overall uptake rate.

Intracellular localisation. RAW 264.7 macrophages in full DMEM medium were seeded in slide-flasks at a density of 300,000 cells per flask and incubated for 24 hour in standard conditions for cell culture. The medium was then removed and the cells were washed with PBS. The cells were then incubated with nanoparticles in full phenol red-free DMEM at a final concentration of 250 µg/mL for 4 hours. At the completion of incubation, the medium was discarded and cells were washed with PBS. Cells were then incubated with 0.2 % wt. trypan blue solution for one minute at room temperature and washed further three times with PBS. LysoTracker Green (100 nM) in plain phenol red-free DMEM was then incubated with the cells for 10 minutes in standard conditions for cell culture. The medium was carefully discarded and the cells were washed with PBS and fixed with 4% wt. paraformaldehyde in PBS for 30 minutes at room temperature. Fixed cells were washed with PBS and incubated with DAPI for nuclei staining. Cells were then washed with PBS and mounted using an anti-fade mounting gel. The slides were observed under a microscope (Delta Vision RT deconvolution microscope, Applied Precision, Issaquah, USA) using a 60x/1.42 Plan Apo objective and 360/475 nm, 490/528 nm and 555/617 nm filter sets (Chroma 8600v2/89000, Chroma Technology, USA). The images were acquired using a Coolsnap HQ (Photometrics, Tuscan, USA) camera at a resolution of 512x512 pixels per inch with a Z optical spacing of 0.2 mm. Softworx software was used to deconvolute the raw images.

Mechanism of nanoparticle uptake. The mechanism of nanoparticle internalization was studied by measuring the relative cellular uptake of fluorescent nanoparticles in RAW 264.7 macrophages after incubation of cells with a small library of selective inhibitors of different endocytosis mechanisms: cells were treated with each inhibitor before being incubated with the nanoparticles, and afterwards the fluorescence

emission of cell lysates was measured. The relative uptake of nanoparticles was expressed as the ratio of the florescence reading for endocytic inhibitor treated cells to that for control non-treated cells. Macrophages were seeded in 96 well-plate and incubated as described in the previous section. Cells were pre-incubated for 30 minutes with plain DMEM medium containing (inhibitors) cytochalasin D (1 μM), filipin (5 μg/mL), nocodazole (0.1 μg/mL), bafilomycin A1 (200 nM), chlorpromazine (65 μg/mL), sucrose (0.45 M) or sodium azide (10 mM), or for 1 hour with plain DMEM medium containing (inhibitors) EIPA (100 μM) or anti-CD44 antibody [KM81] (20 μg/mL). The medium was then discarded and the cells were gently washed with PBS, and further incubated for 2 hours with full phenol red-free DMEM containing nanoparticles at a final concentration of 250 μg/mL. The cells were then washed with ice-cold PBS and lysed with 100 μL of 0.5% Triton X-100 in 0.2 M NaOH for 15 min at room temperature. Fluorescence readings and BCA assay were carried out as described previously.

3.3 Results and discussion

3.3.1 Nanoparticle characterisation

Effect of chitosan molecular weight (method A)

1) CS-TPP (uncoated) nanoparticles. Nanoparticle dimension increased with increasing chitosan molecular weight (Table 3- 2, top); this effect is ascribed to a less effective cross-linking action of TPP (gel point reached at a lower TPP content) for larger chitosan macromolecules, thus yielding larger but more porous particles for the same chitosan content. This phenomenon has already been shown for chitosan/TPP microparticles, where the TPP content decreases with increasing chitosan molecular weight [25].

2) CS-TPP//HA (HA-coated) nanoparticles. Upon adsorption of HA, all nanoparticles showed a similar dimension and charge, independently on chitosan molecular weight (Table 3- 2, middle); in relation to their parent particles, this corresponded to a significant size increase for CS(25), to a negligible change for CS(325) and to a slight decrease for CS(684). We ascribe this effect to the effect of chitosan molecular weight on the nanoparticle structure: HA would hardly penetrate into compact particles, and indeed CS(25)-TPP//HA showed a crown of loosely bound HA, which is ultimately responsible of the increase in size (Figure 3- 1, left); on the other hand more porous particles such as CS(684)-TPP//HA may better accommodate the anionic polysaccharide in their internal structure, yielding no apparent external crown and a more cross-linked and hence shrunken core (Figure 3- 1, right); (see Chapter Two for more a more comprehensive analysis of particle morphology). However, although present in a different morphology, HA will dictate both surface composition and charge in all cases.

3) CS-TPP//Alg (alginate-coated) nanoparticles. Alginate has twice the charge density of HA and correspondingly should adsorb more rapidly and more efficiently on the cationic CS-TPP nanoparticles. In our experiments, this corresponded to a significantly higher surface charge of the coated particles, but also to a much larger size (Table 3- 2, bottom). The latter finding is most likely due to agglomeration during coating, as a consequence of the increased attraction between partially coated particles.
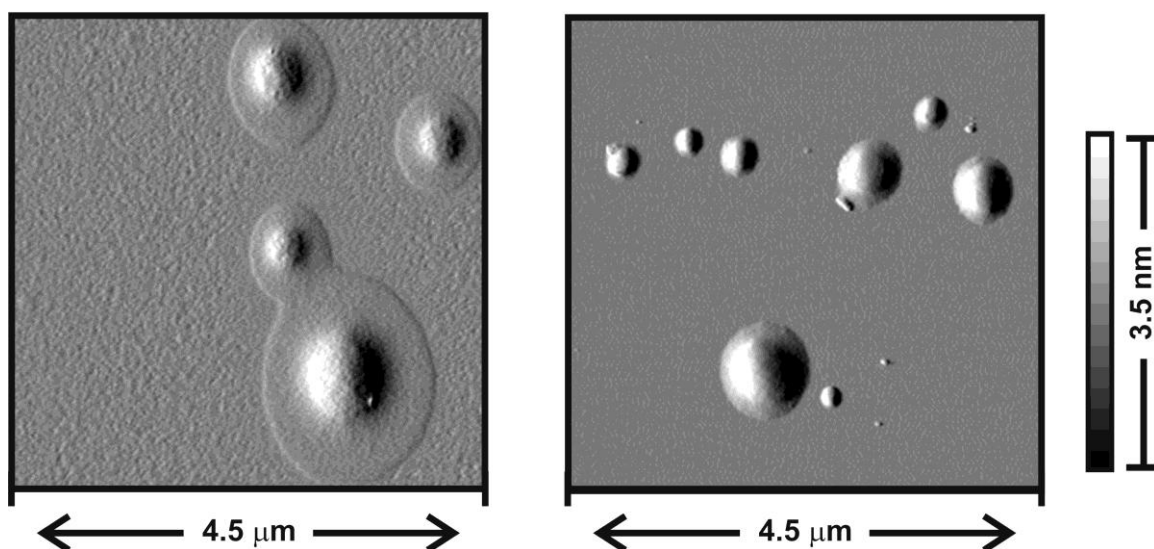
Figure 3- 1 Deflection images of CS(25)-TPP//HA (left) and CS(684)-TPP//HA (right) nanoparticles obtained via contact mode AFM. The two kinds of nanoparticles show a similar flattened morphology on a mica substrate, but those containing lower molecular weight chitosan exhibit an additional, < 2 nm thick crown that we interpret as loosely bound HA. Please note that deflection images do not describe the actually contour of an object but rather the slope of the sample surface; however, they are considerably more sensitive to the fine details than height images and were therefore chosen for the purpose of this visualization; the corresponding height images can be found in Supplementary Information, Figure 3-S 1.

Effect of preparative method (method A vs. method B)

We have compared the two preparative methods using CS(325). In a brief summary, the key differences are as follows: method A − pH = 5 for both chitosan and TPP (charge = -3), the two solutions are rapidly mixed because one is injected into the other. Method B − chitosan at pH = 4 (more positively charged) and TPP at pH = 6.5-7 (charge ≈ -4); one solution (TPP) is added dropwise into the other, which may result in a kinetically controlled process; no dialysis. The conditions of method A are supposed to provide smaller and possibly more compact nanoparticles because of slower complexation (reduced charge density in both partners) but better mixing; those of method B were designed to provide a more rapid complexation, possibly leading to larger and more porous objects, and an easier aseptic process.

Indeed, the CS-TPP nanoparticles produced through method B were considerably larger and with a broader size distribution than those obtained through method A (Table 3- 2). On the other hand, they considerably shrunk upon HA coating and produced smaller and less negatively charged objects than their method A counterparts; this effect is possibly a consequence of the higher porosity of method B

particles, which would allow polyanions to better diffuse into their bulk, further cross-linking and thus shrinking them. However, we cannot exclude an osmotically-driven shrinkage due to the presence of excess (free) polyanions in the medium, since particles prepared through method B are not purified via dialysis.

Finally, it is noteworthy that also for method B nanoparticles the use of the more negatively charged alginate vs. that of HA likely caused nanoparticle agglomeration.

Table 3- 2 Physical characteristics[a] of nanoparticles as a function of chitosan molecular weight (25, 325 and 684 kDa), coating material (HA / alginate) and preparative method (method A / method B).

Chitosan MW (kDa) / preparative method	CS25/method A	CS325/method A	CS325/method B [b]	CS684/method A
	CS-TPP			
Z-average size (nm)	144 ± 28	263 ± 38	487 ± 52	330 ± 47
PDI [c]	0.27 ± 0.01	0.25 ± 0.02	0.44 ± 0.02	0.30 ± 0.01
ζ potential (mV)	+37 ± 4	+41 ± 3	+47 ± 2	+41 ± 6
	CS-TPP//HA			
Z-average size (nm)	317 ± 5	303 ± 59	268 ± 43	292 ± 7
PDI [c]	0.27 ± 0.01	0.28 ± 0.02	0.20 ± 0.02	0.25 ± 0.03
ζ potential (mV)	-52 ± 6	-58 ± 2	-39 ± 1	-53 ± 4
	CS-TPP//Alg			
Z-average size (nm)	696 ± 84	730 ± 95	499 ± 21	671 ± 70
PDI [c]	0.33 ± 0.09	0.30 ± 0.01	0.34 ± 0.11	0.31 ± 0.01
ζ potential (mV)	-76 ± 3	-78 ± 8	-56 ± 6	-72 ± 2

[a] Measurements performed on 250 μg/mL nanoparticle dispersions in deionised water.

[b] Using method B, the CS-TPP nanoparticles were prepared at pH = 4 in deionised water and the resulting, non-dialysed dispersions were measured at that pH. The CS-TPP//HA and Alg nanoparticles were prepared at pH = 7.2 in deionised water and the resulting, non-dialysed dispersions were measured at that pH.

[c] PDI: polydispersity index. It is calculated in a scale 0 (monodisperse distribution) to 1 (very broad distribution).

Effect of medium

In cell culture medium (DMEM supplemented with 10% FBS), all coated nanoparticles considerably shrunk. This effect is well-known [21] and stems from a reduced nanoparticle swelling due to the increased external osmotic pressure.

For method A the size reduction (compare top and bottom graphs in Figure 3- 2) was most significant for alginate-coated nanoparticles, whose agglomerated structure would allow much shrinkage to occur between individual particles.
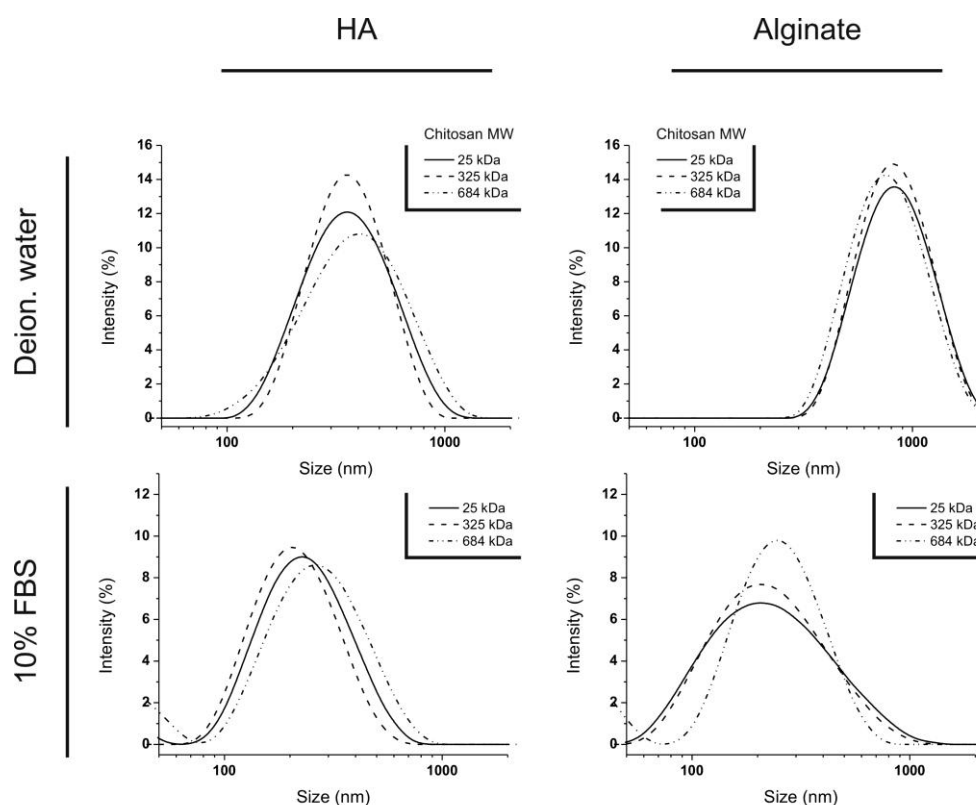
Figure 3- 2 Size distribution of CS-TPP//HA and CS-TPP//Alg nanoparticles prepared using method A and dispersed in deionised water or in cell culture medium (DMEM with 10% v/v FBS). Nanoparticle concentration: 250 µg/mL. Please note that the increase in scattering intensity below 70 nm is due to FBS proteins.

However, all method A nanoparticles showed a comparable final size in cell culture medium, with the majority of the distribution comprised between 100 and 400 nm.

On the other hand, method B nanoparticles shrunk to significantly lower values (Figure 3- 3; in no case the contribution of < 100 nm nanoparticles is negligible), which would confirm them to have a looser, more porous internal structure. For any comparison of their effects on cells, it is therefore important to note that method B nanoparticles may differ because of morphological, structural but also dimensional factors.
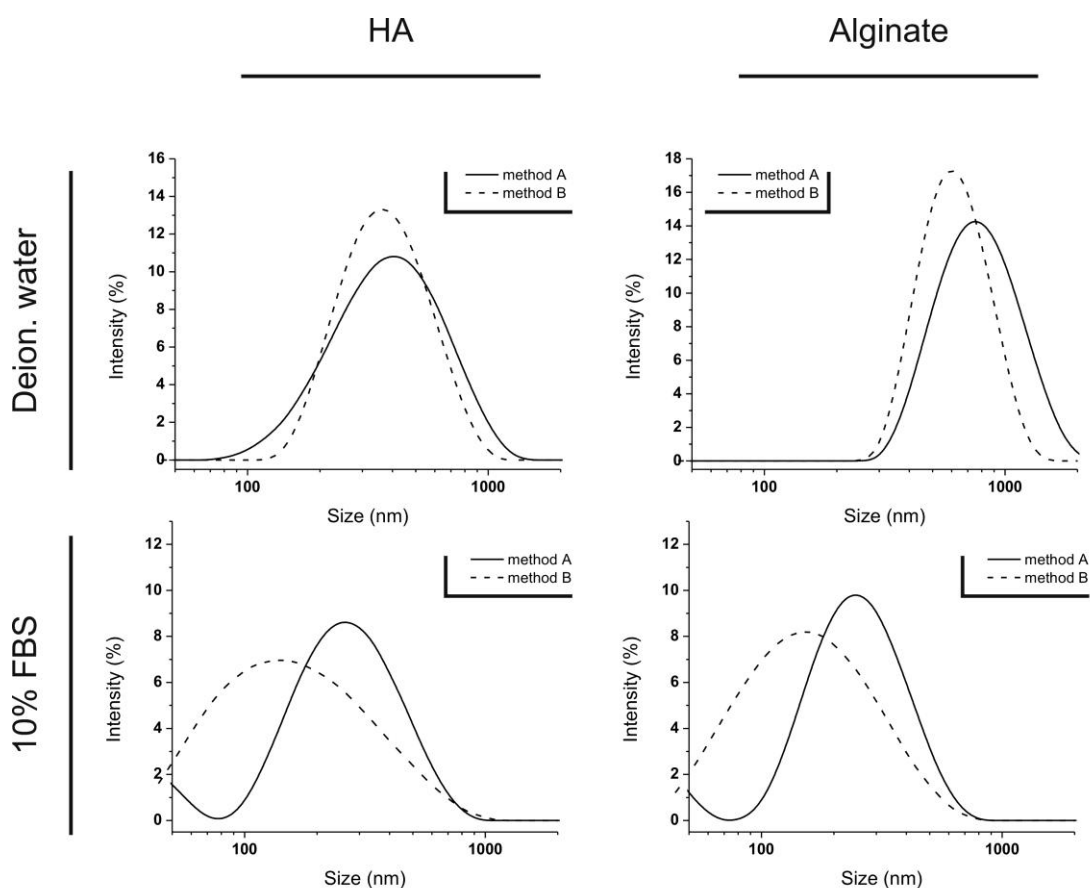
Figure 3- 3 Size distribution of CS-TPP//HA and CS-TPP//Alg nanoparticles (CS385) dispersed in deionised water or culture medium (DMEM with 10% v/v FBS). Nanoparticle concentration: 250 µg/mL. Please note that the increase in scattering intensity below 70 nm is due to FBS proteins.

3.3.2 Cellular interactions

Effects on macrophage metabolic activity (cytotoxicity)

We have studied the effect of nanoparticles on the activity of RAW 264.7 macrophages, a cell line with high sensitivity to potentially toxic chemicals [26, 27], as a function of nanoparticle concentration, time of exposure, chitosan molecular weight, nature of the anionic polysaccharide and preparative method. This analysis was performed by measuring the macrophage mitochondrial reductase activity (MTS assay) normalised by the cell protein content (BCA assay), thus providing an assessment of the average metabolic activity per cell as a function of the nanoparticle exposure (Figure 3- 4).

First, no significant difference was recorded for any method A nanoparticles, independently from chitosan molecular weight and from the nature of the coating

(either HA or alginate): the macrophages showed no significant reduction in metabolic activity (viability) upon exposure to nanoparticles for concentrations up to 750 µg/mL and for times up to 24 hours (Figure 3- 4, A-F). The absence of a chitosan molecular weight dependency is not surprising, since this result has also been recorded for uncoated nanoparticles [28].

Since uncoated chitosan-TPP nanoparticles were reported to significantly reduce the viability of the less sensitive J774 macrophages at 300 µg/mL (24 hours) [21], the negligible toxicity of the coated particles suggests that for all chitosan molecular weights, both anionic polysaccharides effectively shielded the underlying chitosan core.

On the other hand, nanoparticles produced with method B showed a rather high toxicity, which depended both on the dose and on the exposure time (Figure 3- 4, G-H); at 24 hours HA- and Alg-coated nanoparticles yielding IC50 values of 270 µg/mL and 480 µg/mL, respectively. Method B particles showed larger shrinkage in media and a considerably lower (less negative) ζ-potential; these points would indicate larger porosity and lower exposure of the anionic polysaccharides and/or possible exposure of chitosan, which could be the cause of the increased toxicity. It is noteworthy that HA-coated nanoparticles caused a stronger reduction in cell viability than the alginate-coated ones, which could possibly be due to a more efficient internalisation.

Kinetics of nanoparticle uptake

The uptake of nanoparticles was evaluated by measuring the fluorescence of cell lysates (normalised against the protein content) as a function of nanoparticle concentration, time of exposure, chitosan molecular weight, nature of the anionic polysaccharide and preparative method (Figure 3- 5). It is noteworthy that this analysis does not allow discrimination between intracellular and surface-bound materials. In all cases, the uptake increased with incubation time and reached a plateau after 8 hours, as previously recorded for HA-coated CS-TPP nanoparticles using J774.2 macrophages [21]; please note that in this study we have used the more active RAW 264.7 macrophages, which show a considerably higher nanoparticle uptake (hundreds vs. tens of µg/mg of protein).
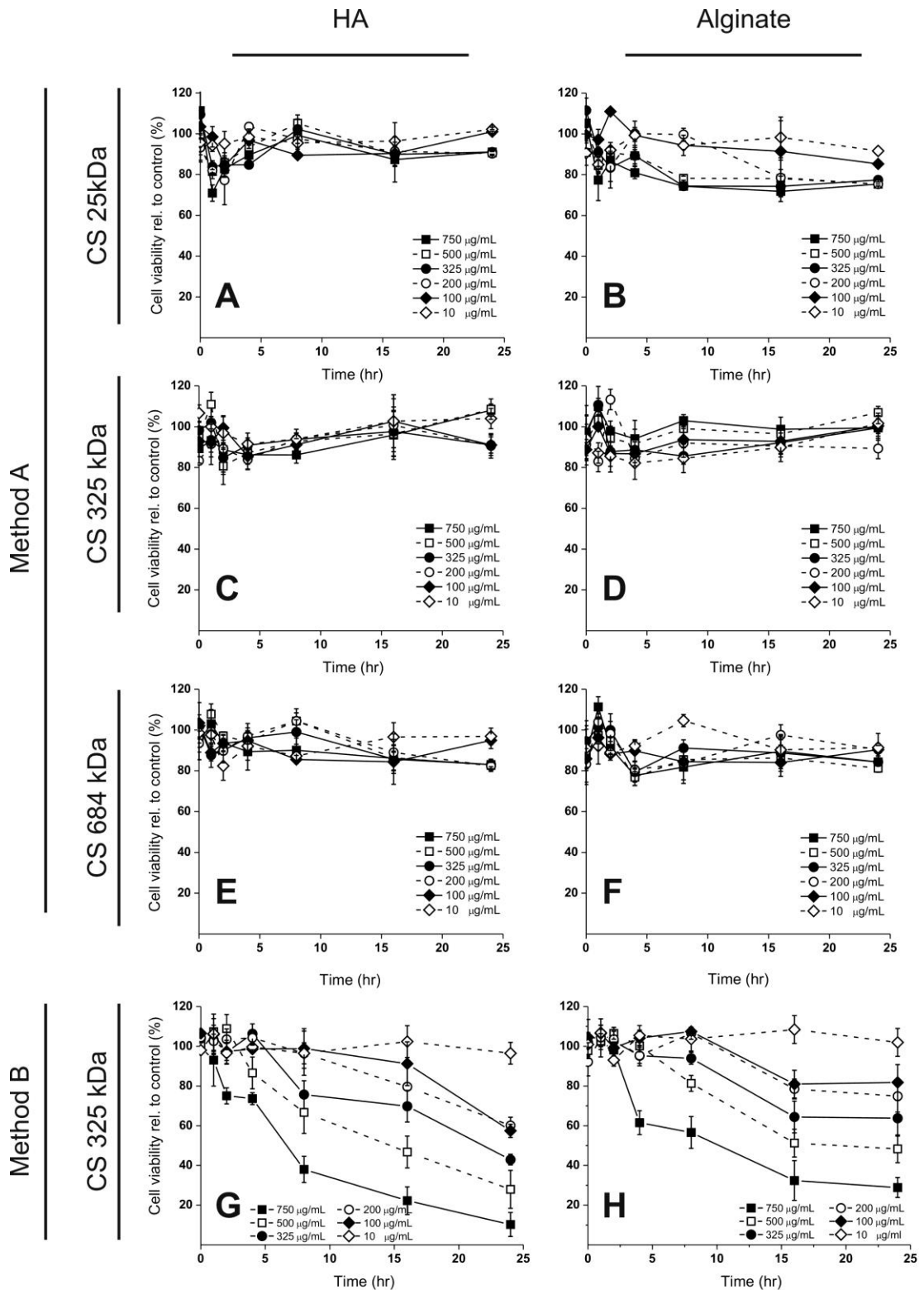
Figure 3- 4 Average cell viability (MTS; mitochondrial activity normalised against protein content) of RAW 264.7 macrophages incubated with CS-TPP//HA and CS-TPP//Alg nanoparticles as a function of time of exposure, chitosan molecular weight, nature of the anionic polysaccharide and nanoparticle preparative method. Data (n = 3) are expressed relative to control experiments.

The presence of a plateau suggests an uptake based on a saturable cell receptor, which for HA-based systems has been hypothesised to be the slowly represented CD44 [13]. After binding, CD44 is internalised and then degraded with its ligands; it generally takes 24-48 hours for the cell to represent it again, thus during this time window the capacity of CD44-mediated uptake will considerably diminish [13, 21]. For alginate-coated nanoparticles, we can only speculate the involvement of a similarly saturatable scavenging receptor.

We have first focused on the analysis of the uptake at saturation.

A) The plateau values increased with increasing nanoparticle concentration, although slowly (a 25-fold increase in concentration corresponded to a 1.5 to 4.5-fold increase in uptake). This dependency suggests the occurrence of a variable mode of binding: a higher particle concentration may lead to a lower number of clustered receptors per particle and thus a larger uptake per cell (the number of receptors per cell being assumed constant).

B) HA-coated nanoparticles always showed 20-70% higher saturation values than alginate-coated ones; this suggests a somewhat higher efficiency for the HA receptor than the putative alginate receptor.

C) The highest saturation values were recorded for high molecular weight (684 kDa) chitosan nanoparticles (compare Figure 3- 5E to F with A to B). This effect is possibly related to the deeper penetration of the polyanions in these particles, which would reduce their accessibility and therefore determine a lower number of interaction sites per particle, that is, a larger number of particles per cell is allowed; however, we cannot completely exclude some direct exposure of chitosan, which can be internalised through the mannose receptor in macrophages [29], as well as in other cell types [30].

D) The plateau uptake of method B nanoparticles (Figure 3- 5G and H) was particularly low, which could be due to the presence of free HA or alginate competing with nanoparticles for the same cell receptors. However, even if the internalisation experiments were conducted under conditions of nanoparticle concentrations/exposure time compatible with untouched viability, we cannot completely exclude effects due to reduction of macrophage metabolic activity.
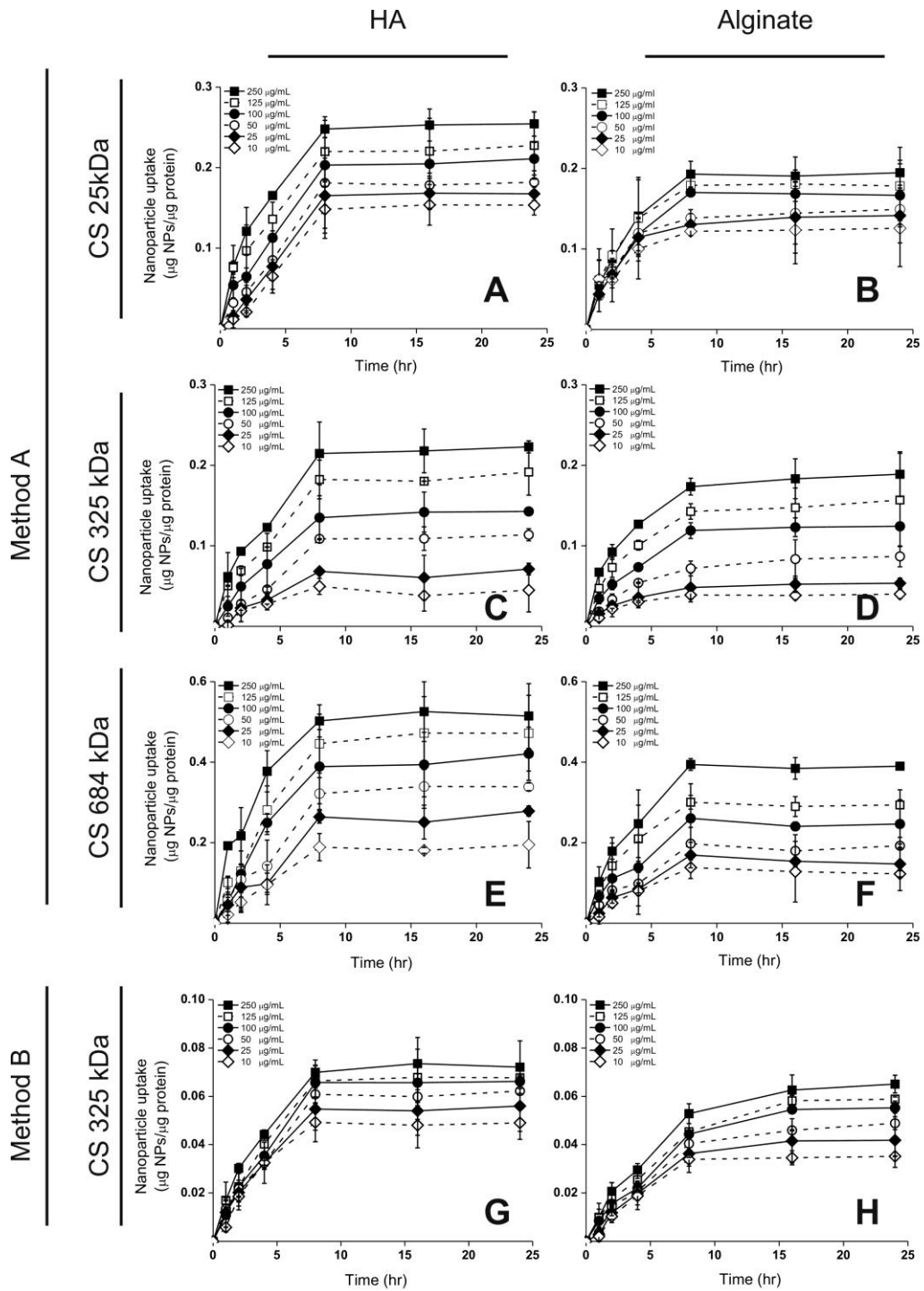
Figure 3- 5 Uptake of CS-TPP//HA (A, C, E and G) and CS-TPP//Alg (B, D, F and H) nanoparticles by RAW 264.7 macrophages as a function of time, nanoparticle, chitosan molecular weight and preparative method (compare method A and B for CS325). n = 3. The uptake was measured as the fluorescence of cell lysates (using a calibration of nanoparticles in cell lysates) and was normalised against the amount of total protein content: the data therefore provide an average amount of internalised material "per cell", assuming the cellular protein content to be roughly constant. Please note that method A CS684 nanoparticles exhibited the highest uptake and method B C325 ones the lowest, and correspondingly the vertical scales are not the same as for the other nanoparticle types.

In order to gather additional quantitative information on the binding kinetics, we have studied how nanoparticle uptake at a given time depended on nanoparticle concentration; the shape of the corresponding curves was strongly influenced by the chitosan molecular weight (Figure 3- 6, left) and by the preparative method (Figure 3- 6, right).
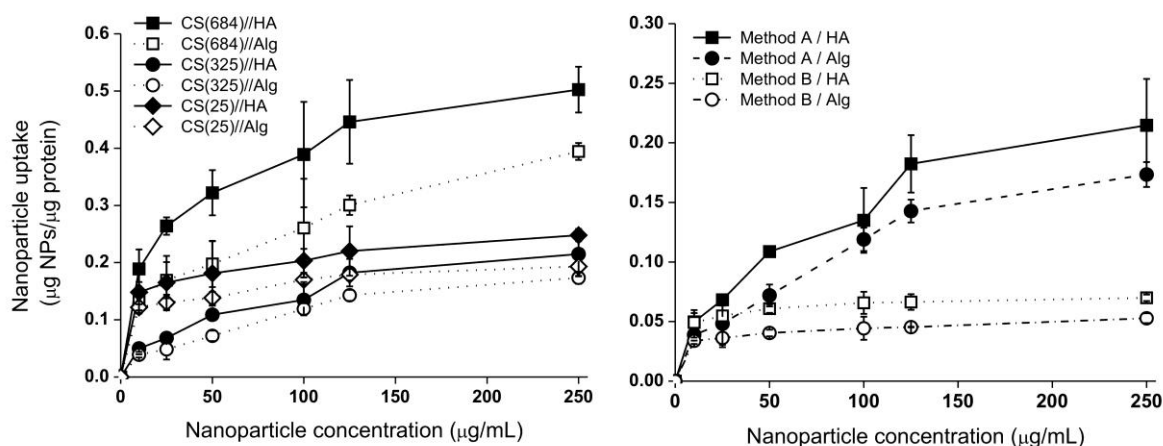
Figure 3- 6 Uptake of chitosan nanoparticles in RAW 264.7 macrophages after 8 hours incubation as a function of nanoparticle concentration, chitosan molecular weight (left) and method of preparation (right).

The uptake after 2 and 8 hours were respectively used to calculate an initial and an overall uptake rate, whose concentration dependency was fitted using a Michaelis-Menten model [19, 25]. This treatment provides an asymptotic internalisation rate at high particle concentration (V_{max}) and a value inversely related to the average nanoparticle affinity for macrophages (K_m) (see Supplementary Information, Figure 3-SI 2 and Figure 3-SI 3). Despite its probably excessive simplicity, this model has been widely applied to study a range of receptor-mediated processes, e.g. the internalisation of proteins [31, 32] or bile salt/drug complexes [33].

Either obtained for the initial phase (0-2 hours) or for the overall kinetics (0-8 hours) the results are substantially analogous (Table 3- 3) and indicate three trends:

A) HA-coated particles showed a 10-50% larger V_{max} and a 20-80% higher affinity (lower K_m) than alginate-coated ones. The difference in V_{max} is probably due to the availability of a different number of receptors for the two polysaccharides. The difference in affinity can be due to a different clustering behaviour of HA and alginate receptors: the latter ones may be less prone to cluster around the same

nanoparticle, decreasing the scavenging efficiency (affinity) at low particle concentration.

Table 3- 3 Kinetic parameters (Michaelis-Menten model) for the uptake of CS-TPP//HA and CS-TPP//Alg nanoparticles.

Preparative method	Nanoparticles	Michaelis-Menten fitting at 2 hours		Michaelis-Menten fitting at 8 hours	
		V_{max}	K_m	V_{max}	K_m
		(μg/mg·h)	(μg/mL)	(μg/mg·h)	(μg/mL)
A	CS(684)-TPP//HA	114 ± 21	57 ± 30	65 ± 4	25 ± 5
	CS(684)-TPP//Alg	110 ± 15	72 ± 25	51.5 ± 5	33 ± 11
	CS(325)-TPP//HA	84 ± 20	204 ± 84	35 ± 4	76 ± 20
	CS(325)-TPP//Alg	70 ± 14	136 ± 53	25 ± 3.4	84 ± 27
	CS(25)-TPP//HA	94 ± 17	49 ± 13	27 ± 0.5	4.5 ± 0.6
	CS(25)-TPP//Alg	42 ± 3	5 ± 2	21 ± 1	5.6 ± 2
B	CS(325)-TPP//HA	13 ± 1	5 ± 2.7	8.6 ± 0.2	4.7 ± 1
	CS(325)-TPP//Alg	9.7 ± 1	13 ± 4.2	6.4 ± 0.2	8.8 ± 2

B) The dependency of uptake kinetics on chitosan molecular weight can be explained in a similar fashion, with the accessibility of HA or alginate being reduced in high molecular weight chitosan particles and therefore allowing for more internalisation points (higher V_{max}) with lower affinity (higher K_m). An explanation for the much reduced affinity of CS(325)-TPP coated nanoparticles can only be tentative and invoke a tighter binding of the anionic polysaccharides: CS325 has the highest content of amino groups that may also increase the local density of the cationic groups.

C) Method B nanoparticles were internalised with a slower kinetics (3-5 time smaller V_{max}) but much higher affinity (10-40 times lower K_m) than those with identical composition obtained with method A. As previously mentioned, their uptake kinetics can be heavily influenced by the competition with excess of (non-bound) polyanions in solution, which may allow internalisation only of particles with affinity higher than that of free HA/alginate; however, the considerably smaller diameter of most particles (Figure 3- 3, bottom graphs) may also facilitate receptor clustering leading to higher affinity.

Finally, it is worth mentioning that the bio-nano interface (i.e. protein coronas around nanoparticles) could be affected by different HA arrangement which may result in distinct uptake kinetics [34].

3.3.3 Mechanism of internalisation

As recently reviewed [35], the use of selective endocytic inhibitors can be applied to assess the mechanism of internalization of nanomaterials. Here, we have quantitatively assessed the effect of inhibitors by first exposing RAW 264.7 macrophages to them and then measuring the fluorescence of cell lysates after 2 hours incubation with the nanoparticles (Figure 3- 7).

It is noteworthy that chitosan molecular weight and method of preparation did not appear to affect the mechanism of internalisation, which on the contrary seemed to depend on the chemistry of the adsorbed polyanion.
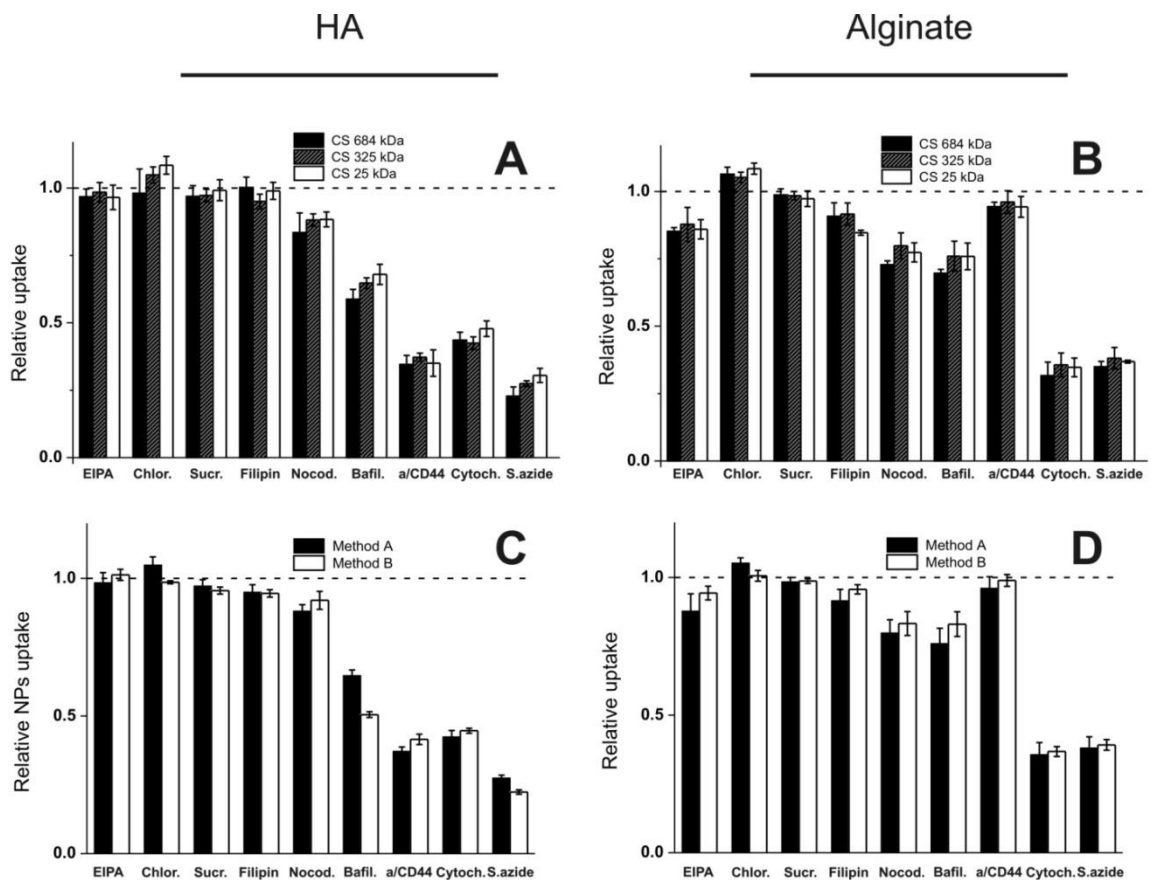
Figure 3- 7 Effect of endocytosis inhibitors on the 2 hours uptake of HA- and alginate-coated CS-TPP nanoparticles in RAW 264.7 macrophages as a function of chitosan molecular weight (A and B) and method of preparation (C and D). The uptake was measured as the fluorescence of cell lysates (using a calibration of nanoparticles in cell lysates); it was then normalised to the amount of total cellular protein content and expressed in relation to control experiments performed without inhibitors. n = 3.

- Sodium azide, cytochalasin D, nocodazole and bafilomycin A1 were used as positive controls: by interfering respectively with all energy dependent processes

[36], F-actin polymerization microtubule formation/active vesicular transport [37, 38] and endosomal acidification/receptor recycling [39]. They are general inhibitors of all or most forms of endocytosis and intracellular trafficking. Sodium azide and cytochalasin D very significantly reduced the internalisation of all kinds of particles (20-40% values of the control), showing the uptake to be an active, endocytic process. The lower influence of nocodazol (10-15% and 15-23% reduction in uptake for HA-coated and Alg-coated nanoparticles, respectively) and bafilomycin A1 (35-50% and 20-30% reduction in uptake for HA-coated and Alg-coated nanoparticles respectively) is probably ascribable to the relatively short time of the test, which allows only for a limited extent of intracellular trafficking; however, their clear inhibitory effect indicates that all particles are likely trafficked in endosomes (nocodazol) and that their endocytosis is probably a receptor-mediated process jammed by inhibition of acidification (bafilomycin). Indeed, fluorescence microscopy showed a significant co-localisation of the nanoparticles with late endosomes/lysosomes (Figure 3- 8). It is noteworthy that the fluorescence associated to chitosan typically covered larger areas around those associated to Lysotracker fluorescence (see the red halos around the yellow dots in the merged pictures of Figure 3- 8), which is a sign of lysosomal escape.

- Chlorpromazine and hypertonic sucrose (0.45 M) interfere with the formation of clathrin-coated pits [40, 41] and are therefore widely considered as inhibitors of the clathrin-mediated endocytosis. In no case, they appeared to reduce uptake, suggesting, therefore, no involvement of clathrin in the internalisation process. It is worth pointing out that this may be a cell-specific process. For example, RAW 264.7 macrophages have shown clathrin-dependent internalisation of nanomaterials such as superparamagnetic iron oxide nanoparticles [42], while other endo/phagocytic processes are not affected by clathrin inhibition [43]. On the other hand, in a previous study by our group, J774.2 macrophages showed a 20-30% reduction of HA-coated CS(477)-TPP nanoparticles internalisation with clathrin inhibition via hypertonic sucrose or potassium-free buffer [21], a difference that we are inclined to ascribe to the different endocytic behaviour of the two cell lines.
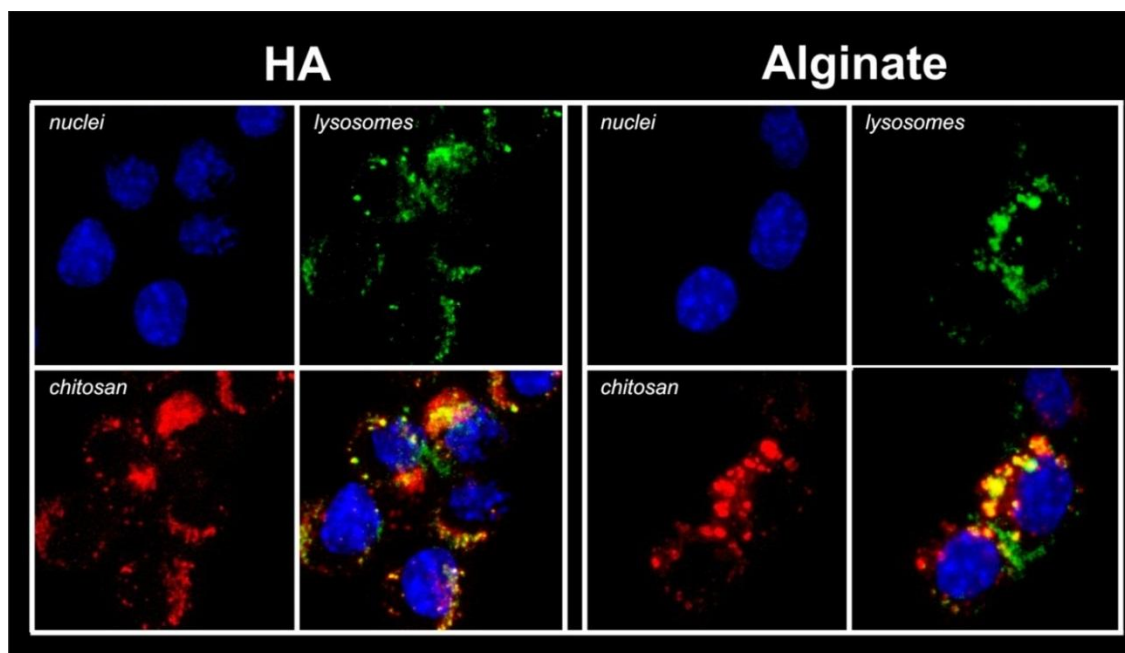
Figure 3- 8 Intracellular localisation of CS(325)-TPP//HA and CS(325)-TPP//Alg nanoparticles (method A) in RAW 264.7 macrophages after a 4 hours incubation. Blue: nuclei (DAPI); Green: late endosomes and lysosomes (Lysotracker Green); Red: chitosan (rhodamine). Please note that trypan blue was used to quench the fluorescence of surface-bound nanoparticles.

- Pre-incubation with 5-(N-ethyl-N-isopropyl)amiloride (EIPA), which suppresses endocytosis via macropinocytosis [13, 44], did not affect the internalisation of HA-coated nanoparticles, while resulted in a 10-20% decrease in alginate-coated ones, with no statistically significant difference attributable to chitosan molecular weight or method of preparation. Due to this negligible or relatively little effect, macropinocytosis was concluded not to be a major internalisation route for any of the nanoparticle formulations.

- Filipin is a cholesterol-sequestrant that inhibits lipid raft-dependent internalisation processes such as caveolae-mediated endocytosis [41, 45]. Filipin had no effect on the internalisation of HA-coated nanoparticles and caused a rather slight decrease in alginate-coated nanoparticles (alginate-coated nanoparticles uptake was reduced by 16% and 10% for 25 and 684 kDa chitosan, respectively), which possibly suggests some involvement of lipid raft-mediated endocytosis in the uptake of alginate-coated nanoparticles.

- Finally, the use of a mouse anti-CD44 antibody [KM81] produced a 65% reduction in the uptake of HA-coated nanoparticles while only marginally affected (-5%) the

internalisation of alginate-coated ones. This result finally proved that the internalisation of the HA-coated particles is a CD44-mediated process.

From the above analysis it appears that HA-coated nanoparticles were internalised in RAW 264.7 macrophages through a CD44-mediated process leading to acidified late endosomes. The precise nature of the internalisation mechanism is not completely clarified and shows differences from that in J774 macrophages, which was at least partially clathrin-dependent [21].

3.4 Conclusions

In this study, we believe to have demonstrated that:

1) the internalisation of HA-coated nanoparticles is a CD44-mediated process; their similar kinetic profile suggests that the uptake of alginate-coated nanoparticles is also a process mediated by a saturatable (scavenging) receptor.

2) an identical ligand, e.g. HA with the same molecular weight, can be presented in a different arrangement on the nanoparticle surface, due to morphological differences arising, for example, from the method of preparation, or from the use of chitosan with different molecular weights. These differences do not appear to affect the nature of the uptake, which for HA-coated nanoparticles appears to be still based on CD44 complexation. On the other hand, the different ligand presentation seems to have major effects on the mode of interactions affecting affinity and speed of uptake and also cytotoxicity. We believe this to be a consequence of the limited number and of the slow re-presentation of the internalisation receptors; under these conditions, a lower number of receptors would cluster around nanoparticles with poorly presented HA resulting in lower affinity but higher overall number of bound particles.

3.5 References

1.   Ghosh, S.C., S.N. Alpay, and J. Klostergaard, *CD44: a validated target for improved delivery of cancer therapeutics.* Expert Opinion on Therapeutic Targets, 2012. **16**(7): p. 635-650.
2.   Negi, L.M., et al., *Role of CD44 in tumour progression and strategies for targeting.* Journal of Drug Targeting, 2012. **20**(7): p. 561-573.
3.   Coradini, D., et al., *Hyaluronic acid as drug delivery for sodium butyrate: Improvement of the anti-proliferative activity on a breast-cancer cell line.* International Journal of Cancer, 1999. **81**(3): p. 411-416.
4.   Auzenne, E., et al., *Hyaluronic acid-paclitaxel: Antitumor efficacy against CD44(+) human ovarian carcinoma xenografts.* Neoplasia, 2007. **9**(6): p. 479-486.
5.   Choi, K.Y., et al., *Self-assembled hyaluronic acid nanoparticles for active tumor targeting.* Biomaterials, 2010. **31**(1): p. 106-114.
6.   Lee, H., C.-H. Ahn, and T.G. Park, *Poly lactic-co-(glycolic acid) -Grafted Hyaluronic Acid Copolymer Micelle Nanoparticles for Target-Specific Delivery of Doxorubicin.* Macromolecular Bioscience, 2009. **9**(4): p. 336-342.
7.   Lee, H., et al., *Target-specific intracellular delivery of siRNA using degradable hyaluronic acid nanogels.* Journal of Controlled Release, 2007. **119**(2): p. 245-252.
8.   Choi, K.Y., et al., *PEGylation of hyaluronic acid nanoparticles improves tumor targetability in vivo.* Biomaterials, 2011. **32**(7): p. 1880-1889.
9.   Choi, K.Y., et al., *Hyaluronic acid-based nanocarriers for intracellular targeting: Interfacial interactions with proteins in cancer.* Colloids and Surfaces B-Biointerfaces, 2012. **99**: p. 82-94.
10.   Ossipov, D.A., *Nanostructured hyaluronic acid-based materials for active delivery to cancer.* Expert Opinion on Drug Delivery, 2010. **7**(6): p. 681-703.
11.   Hyung, W., et al., *Novel hyaluronic acid (HA) coated drug carriers (HCDCs) for human breast cancer treatment.* Biotechnology and Bioengineering, 2008. **99**(2): p. 442-454.
12.   Coradini, D., et al., *Inhibition of hepatocellular carcinomas in vitro and hepatic metastases in vivo in mice by the histone deacetylase inhibitor HA-But.* Clinical Cancer Research, 2004. **10**(14): p. 4822-4830.
13.   Ouasti, S., et al., *The CD44/integrins interplay and the significance of receptor binding and re-presentation in the uptake of RGD-functionalized hyaluronic acid.* Biomaterials, 2012. **33**(4): p. 1120-1134.
14.   Pure, E. and C.A. Cuff, *A crucial role for CD44 in inflammation.* Trends in Molecular Medicine, 2001. **7**(5): p. 213-221.
15.   Teder, P., et al., *Resolution of lung inflammation by CD44.* Science, 2002. **296**(5565): p. 155-158.
16.   Wolny, P.M., et al., *Analysis of CD44-Hyaluronan Interactions in an Artificial Membrane System Insights into the distinct binding properties of high and low molecular weight hyaluronan.* Journal of Biological Chemistry, 2010. **285**(39): p. 30170-30180.
17.   de la Motte, C.A., et al., *Mononuclear leukocytes bind to specific hyaluronan structures on colon mucosal smooth muscle cells treated with polyinosinic*

acid: Polycytidylic acid - Inter-alpha-trypsin inhibitor is crucial to structure and function. American Journal of Pathology, 2003. **163**(1): p. 121-133.

18.   Jokela, T.A., et al., *Induction of hyaluronan cables and monocyte adherence in epidermal keratinocytes.* Connective Tissue Research, 2008. **49**(3-4): p. 115-119.

19.   Lesley, J., et al., *TSG-6 modulates the interaction between hyaluronan and cell surface CD44.* Journal of Biological Chemistry, 2004. **279**(24): p. 25745-25754.

20.   Laroui, H., et al., *Hyaluronate-covered nanoparticles for the therapeutic targeting of cartilage.* Biomacromolecules, 2007. **8**(12): p. 3879-3885.

21.   Zaki, N.M., A. Nasti, and N. Tirelli, *Nanocarriers for Cytoplasmic Delivery: Cellular Uptake and Intracellular Fate of Chitosan and Hyaluronic Acid-Coated Chitosan Nanoparticles in a Phagocytic Cell Model.* Macromolecular Bioscience, 2011. **11**(12): p. 1747-1760.

22.   Nasti, A., et al., *Chitosan/TPP and Chitosan/TPP-hyaluronic Acid Nanoparticles: Systematic Optimisation of the Preparative Process and Preliminary Biological Evaluation.* Pharmaceutical Research, 2009. **26**(8): p. 1918-1930.

23.   Kasaai, M.R., J. Arul, and C. Charlet, *Intrinsic viscosity-molecular weight relationship for chitosan.* Journal of Polymer Science Part B-Polymer Physics, 2000. **38**(19): p. 2591-2598.

24.   Kaeuper, P., C. Laue, and P. Kauper, *Hydrophilic particles, useful in a composition e.g. pharmaceutical composition and for transport and the concentration of biologically active substances in biological system, comprises chitosan and anionic polysaccharide*, MEDIPOL SA (MEDI-Non-standard) KAUPER P (KAUP-Individual) LAUE C (LAUE-Individual). p. 1968613-A1:.

25.   Ungphaiboon, S., et al., *Materials for microencapsulation: what toroidal particles ("doughnuts") can do better than spherical beads.* Soft Matter, 2010. **6**(17): p. 4070-4083.

26.   Kagan, V.E., et al., *Direct and indirect effects of single walled carbon nanotubes on RAW 264.7 macrophages: Role of iron.* Toxicology Letters, 2006. **165**(1): p. 88-100.

27.   Xia, T., et al., *Comparison of the Mechanism of Toxicity of Zinc Oxide and Cerium Oxide Nanoparticles Based on Dissolution and Oxidative Stress Properties.* Acs Nano, 2008. **2**(10): p. 2121-2134.

28.   Huang, M., E. Khor, and L.Y. Lim, *Uptake and cytotoxicity of chitosan molecules and nanoparticles: Effects of molecular weight and degree of deacetylation.* Pharmaceutical Research, 2004. **21**(2): p. 344-353.

29.   Han, Y.P., et al., *Role of mannose receptor in oligochitosan-mediated stimulation of macrophage function.* International Immunopharmacology, 2005. **5**(10): p. 1533-1542.

30.   Douglas, K.L., C.A. Piccirillo, and M. Tabrizian, *Cell line-dependent internalization pathways and intracellular trafficking determine transfection efficiency of nanoparticle vectors.* European Journal of Pharmaceutics and Biopharmaceutics, 2008. **68**(3): p. 676-687.

31.   Schwartz, A.L., S.E. Fridovich, and H.F. Lodish, *Kinetics of internalization and recycling of the asialoglycoprotein receptor in a hepatoma-cell line.* Journal of Biological Chemistry, 1982. **257**(8): p. 4230-4237.

32. Krippendorff, B.F., et al., *Nonlinear pharmacokinetics of therapeutic proteins resulting from receptor mediated endocytosis.* Journal of Pharmacokinetics and Pharmacodynamics, 2009. **36**(3): p. 239-260.

33. Ballatori, N., et al., *Carrier-mediated uptake of lucifer yellow in skate and rat hepatocytes: a fluid-phase marker revisited.* American Journal of Physiology-Gastrointestinal and Liver Physiology, 1999. **277**(4): p. G896-G904.

34. Mahon, E., et al., *Designing the nanoparticle-biomolecule interface for "targeting and therapeutic delivery".* Journal of Controlled Release, 2012. **161**(2): p. 164-174.

35. Zaki, N.M. and N. Tirelli, *Gateways for the intracellular access of nanocarriers: a review of receptor-mediated endocytosis mechanisms and of strategies in receptor targeting.* Expert Opinion on Drug Delivery, 2010. **7**(8): p. 895-913.

36. Behrens, I., et al., *Comparative uptake studies of bioadhesive and non-bioadhesive nanoparticles in human intestinal cell lines and rats: The effect of mucus on particle adsorption and transport.* Pharmaceutical Research, 2002. **19**(8): p. 1185-1193.

37. Goncalves, C., et al., *Macropinocytosis of polyplexes and recycling of plasmid via the clathrin-dependent pathway impair the transfection efficiency of human hepatocarcinoma cells.* Molecular Therapy, 2004. **10**(2): p. 373-385.

38. van der Aa, M., et al., *Cellular uptake of cationic polymer-DNA complexes via caveolae plays a pivotal role in gene transfection in COS-7 cells.* Pharmaceutical Research, 2007. **24**(8): p. 1590-1598.

39. Issa, M.M., et al., *Targeted gene delivery with trisaccharide-substituted chitosan oligomers in vitro and after lung administration in vivo.* Journal of Controlled Release, 2006. **115**(1): p. 103-112.

40. Gotte, M., D.D.S. Feugaing, and H. Kresse, *Biglycan is internalized via a chlorpromazine-sensitive route.* Cellular & Molecular Biology Letters, 2004. **9**(3): p. 475-481.

41. Qaddoumi, M.G., et al., *Clathrin and caveolin-1 expression in primary pigmented rabbit conjunctival epithelial cells: Role in PLGA nanoparticle endocytosis.* Molecular Vision, 2003. **9**(68-69): p. 559-568.

42. Yang, C.Y., et al., *Mechanism of Cellular Uptake and Impact of Ferucarbotran on Macrophage Physiology.* Plos One, 2011. **6**(9).

43. Tse, S.M.L., et al., *Differential role of actin, clathrin, and dynamin in Fc gamma receptor-mediated endocytosis and phagocytosis.* Journal of Biological Chemistry, 2003. **278**(5): p. 3331-3338.

44. Nakase, I., et al., *Cellular uptake of arginine-rich peptides: Roles for macropinocytosis and actin rearrangement.* Molecular Therapy, 2004. **10**(6): p. 1011-1022.

45. Rejman, J., A. Bragonzi, and M. Conese, *Role of clathrin- and caveolae-mediated endocytosis in gene transfer mediated by lipo- and polyplexes.* Molecular Therapy, 2005. **12**(3): p. 468-474.

3.6 Supplementary information

3.6.1 Preparation of 2 X full phenol red-free DMEM medium

8.3 g of phenol red-free DMEM powder were dissolved in 450 mL of sterile water. 1 g of D-glucose, 3.7 g of sodium bicarbonate, 0.11 g of sodium pyruvate and 0.58 g of L-glutamine were then added to the solution. The pH was adjusted to 7.4 and sterile water was used to make up the volume to 500 mL. The solution was sterile filtered using a vacuum pump filter of 0.22 μm and then supplemented with 20% heat-inactivated foetal bovine serum (FBS), 4×10^{-3} M glutamine, 200 U·mL^{-1} penicillin and 200 U·mL^{-1} streptomycin.

3.6.2 Preparation of nanoparticles in 2 X full phenol red-free DMEM medium

Nanoparticles prepared with method A were concentrated to 3 mg/mL, in an ultrafiltration chamber (Amicon system), MWCO of 300 kDa. Proper volumes of the stock suspension were then added to sterile deionised water and then to 2 X full medium (in a 1:1 v/v ratio) in order to obtain 750, 500, 325, 200, 100, 10, 1 and 0 μg/mL of nanoparticles in full phenol red-free DMEM medium.

The initial concentration of nanoparticles prepared with method B was 750 μg/mL. Nanoparticle suspension was diluted with sterile water and added to 2 X full DMEM in a 1:1 v/v ratio to obtain concentrations of 325, 200, 100, 10, 1 and 0 μg/mL. Concentrations of 750 and 500 μg/mL in phenol red-free DMEM were prepared by dissolving powder DMEM, D-glucose, sodium bicarbonate, sodium pyruvate and L-glutamine in the nanoparticle suspensions.
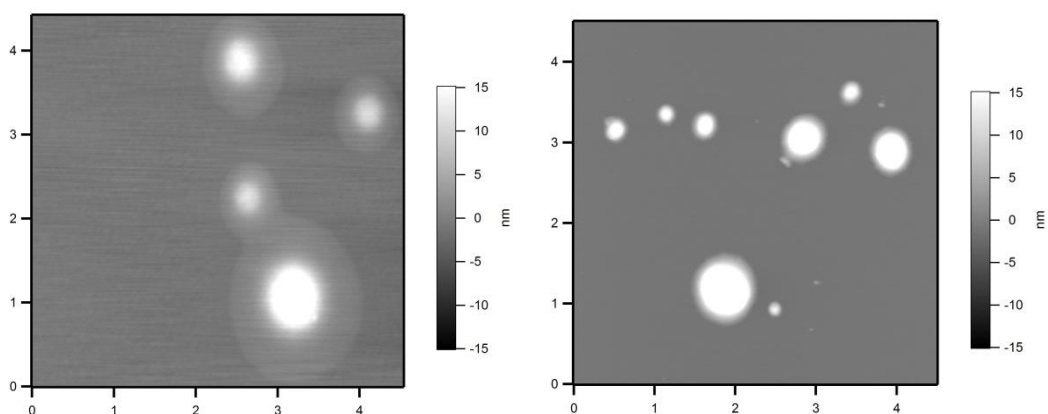
Figure 3-SI 1 Height images recorded for the same samples as in Figure 3- 1: CS(25)-TPP//HA (left) and CS(684)-TPP//HA (right).

Table 3-SI 1 Physical characteristics of nanoparticles prepared with different chitosan molecular weights and different coating materials. Table represents the characteristics of nanoparticle formulations prepared with method A at final concentration of 250 μg/mL in culture medium (10% v/v FBS in DMEM) in an average of 3 different samples (± SD).

	CS-TPP//HA		CS-TPP//Alg	
Chitosan MW (kDa)	(25)	(684)	(25)	(684)
Z-average size (nm)	73 ± 6	70 ± 5	73 ± 17	74 ± 12
ζ potential (mV)	-17 ± 3	-20 ± 1	-11 ± 9	-19 ± 4

Table 3-SI 2 Physical characteristics of nanoparticles prepared with different methods and different coating materials. Table represents the characteristics of nanoparticles prepared with CS(325) at final concentration of 250 μg/mL in culture medium (10% v/v FBS in DMEM) in an average of 3 different samples (± SD).

	CS-TPP//HA		CS-TPP//Alg	
Method	A	B	A	B
$d_{H,Z}$ [nm]	84 ± 11	95 ± 1	95 ± 7	104 ± 3
ζ potential [mV]	-18 ± 1	-13 ± 1	-23 ± 1	-15 ± 1
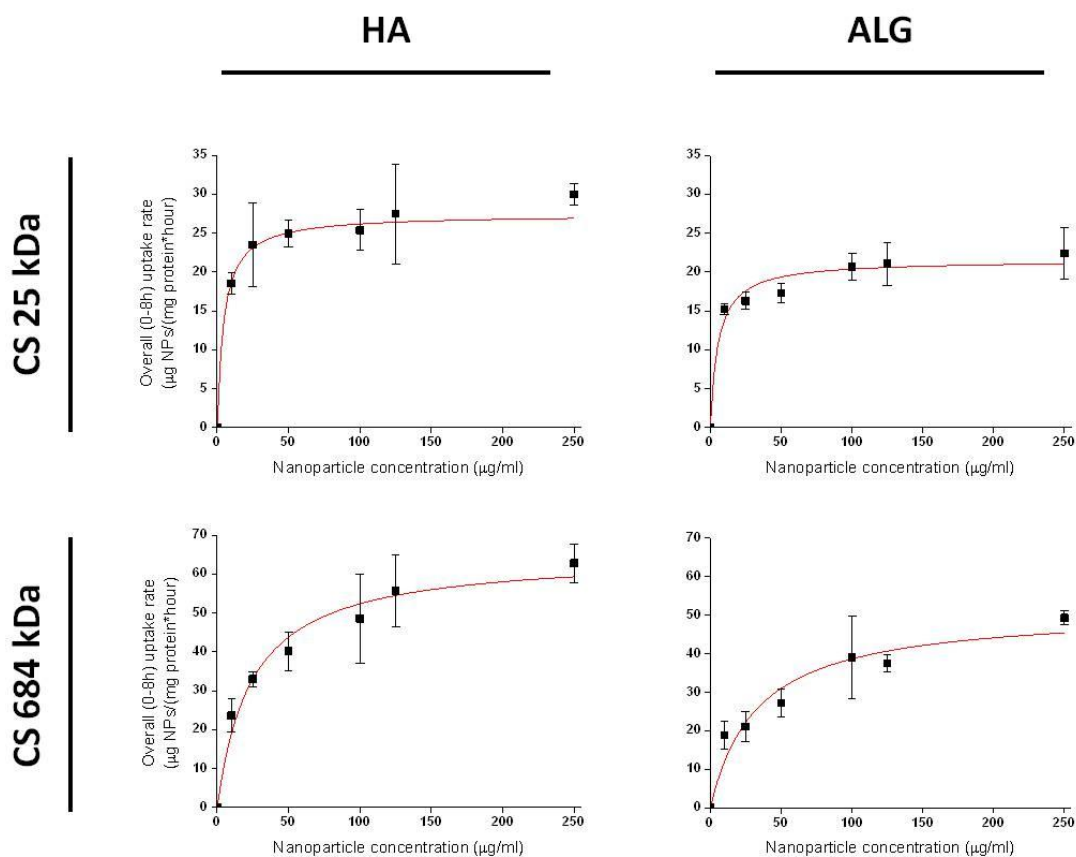
Figure 3-SI 2 Overall uptake rate of HA- or Alg-coated CS-TPP method A nanoparticles in RAW 264.7 macrophages as a function of nanoparticle concentration and chitosan molecular weight. The result of Michaelis-Menten fitting are presented as a red curve.
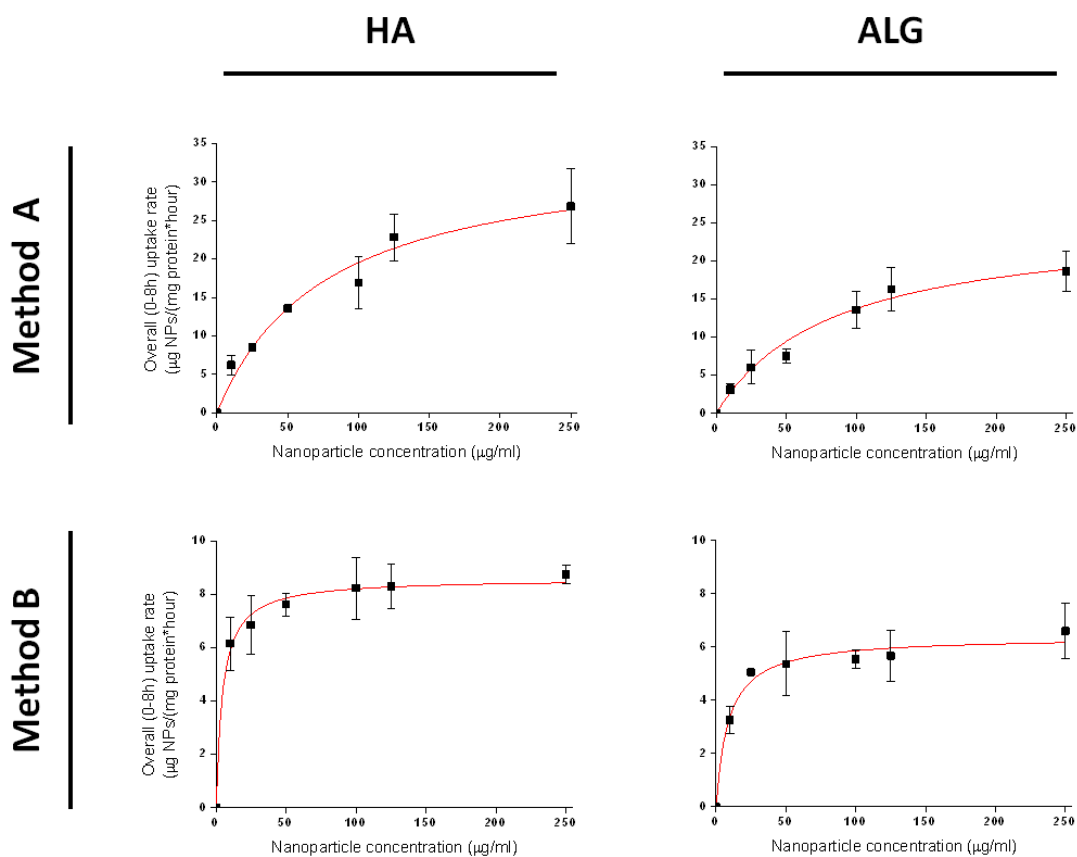
Figure 3-SI 3 Overall uptake rate of HA- or Alg-coated CS-TPP method A nanoparticles in RAW 264.7 macrophages as a function of nanoparticle concentration and method of preparation (for CS325). The results of Michaelis-Menten fitting are presented as a red curve.

Chapter Four

Use of HA-coated nanoparticles for CD44-mediated therapies

Abstract

CD44, the main HA receptor, is overexpressed in several pathological conditions, including many inflammatory diseases. Therefore, CD44-dependent therapeutic approaches would be of great interest. In the current study, we investigated the feasibility of such approach using HA-coated chitosan-TPP nanoparticles.

Nanoparticles were prepared from chitosan with different MWs with or without a nucleic acid payload to compare the physico-chemical characteristics and the nucleic acid encapsulation efficiency. In general, the nanoparticles allowed for the successful entrapment and delivery of both siRNA and pDNA. The transfection efficiency was studied using cells characterised by a significantly different CD44 expression, showing the possibility to perform a CD44-mediated targeted delivery. Further, transfection seemed to be significantly dependent on chitosan MW, possibly because of more efficient endosomal disruption and de-complexation when low MW chitosan was used.

Finally, HA-coated nanoparticles devoid of any payload showed an inherent anti-inflammatory character. This effect was unmatched by soluble HA of different MWs at analogous concentration to HA adsorbed on the surface of nanoparticles.

4.1 Introduction

The delivery of nucleic acid constructs to specific cell populations in the body aims to modulate the expression of a gene encoding a target protein, either by stimulating it or by knocking it down and thus resolving a pathological situation [1]. The vectors used for the majority of gene therapy studies are genetically modified viruses [2]. However, the risk of mutagenic and immunogenic responses was a major concern. Therefore, the development of safe and effective vectors for non-viral gene delivery is of a great interest [3]. The majority of non-viral vectors developed to date make use of cationic lipids, such as lipofectamine, and polymers, such as polyethyleneimine (PEI). Among the latter class, chitosan has been rather widely used for the delivery of plasmid DNA (pDNA), siRNA and oligonucleotides due to its low immunogenicity, relatively low toxicity and excellent biocompatibility [4-7]. The relatively high positive charge of its polymeric backbone allows chitosan to form nano-sized complexes with oppositely charged nucleic acids, which protect the latter from endogenous nucleases [8], enhance its cellular uptake via binding to negatively charged cellular membranes [8] and allow its escape from the digestive endo-lysosomal compartments due to the so called "the proton sponge effect" [9]. However, high positive charge density is associated with high cytotoxicity [10, 11], unselective uptake and also aggregation with serum proteins [12]. Therefore, surface modification of cationic carriers with anionic macromolecules, such as glycosaminoglycans (GAGs) and in particular hyaluronic acid (HA) and heparin/heparan sulfate have been used to overcome this problem [13-15]. Furthermore, nucleic acid carriers have been decorated with targeting ligands to reduce the unspecificity in biodistribution and cellular uptake of cationic carriers [5]. For example, chitosan-based nucleic acid carriers have been modified to facilitate the receptor-mediated endocytosis [5] by introducing ligands such as folate [16], transferrin [17], mannose [18] and galactose [19].

In this study we have aimed to investigate the use of HA as a possible targeting ligand. Receptors for HA, and in particular the most common one, CD44, are significantly expressed in certain cellular populations such as activated inflammatory cells [20, 21] or certain types of tumour cells [22, 23]. HA has been used to enhance

the uptake of chitosan/HA nanocarriers by receptor-mediated endocytosis [24-26], but the details of the mechanism and the targeting possibilities remain unknown.

We are specifically interested in targeting of inflammatory pathologies. Inflammation, a mechanism of innate immunity, is a complex and much regulated biological response, which involves a sequence of events propagated upon extrinsic or intrinsic stimuli such as pathogens, damaged cells, or irritants [27, 28]. One of the most important cell types of the innate immune system are macrophages [29]. Among their main functions, one should mention phagocytosis (engulfing and digesting cellular debris and foreign bodies), release of reactive oxygen species and production of a variety of inflammatory cytokines and chemokines [29]. Therefore, nanocarriers targeting macrophages and their products may open new avenues for treating inflammatory diseases. Macrophages, in particular, are known to express CD44 [30] and in this study we have selected RAW 264.7 macrophages as a main cellular model, since they are often used as a sensitive model to study inflammatory activation in response to a variety of stimuli ranging from e.g. reperfusion injury [31], stimulation of Toll-Like Receptors [32], ingestion of bacterial (plasmid) DNA [33], exposure to particulates [34].

In particular, we have first compared the cellular interactions and the transfection efficiency of HA-coated chitosan nanoparticles in relation to cells characterised by a significantly different expression of CD44: A) RAW 264.7 macrophages, which display large amounts of CD44 and employ it as a major internalisation ligand [35], as we have demonstrated on our HA-coated chitosan nanoparticles (see Chapter Three). B) Kelly neuroblastoma cells, which are devoid of this receptor [36, 37]. C) K562 chronic myelogenous leukemia cells, where CD44 appears to be generally poorly expressed [38], and in some cases it has even been reported absent [39], or easily downregulated e.g. during the acquisition of a chemoresistant character [40].

We have also investigated the possibility for the HA-coated nanoparticles to exert a direct pharmacological effect, due to the presentation of HA and its binding to cell surface receptors such as CD44; indeed HA has a significant role in inflammation, which depends on its molecular weight [41]. High molecular weight HA is known to produce anti-inflammatory effects, which are at least partially dependent on its binding to leukocyte receptors such as CD44; for example, HA reduces cytokine production by synoviocytes and the effect is abrogated by blocking CD44 [42]. It has

also been suggested that HA-based clustered structures can be created as a protective mechanism during inflammatory reactions, in order to keep leukocytes in non- or less-activated state [43]. We have therefore investigated the possible anti-inflammatory effects of HA-coated nanoparticles, always using RAW 264.7 macrophages as a model cell line.

4.2 Materials and methods

4.2.1   Materials

Chemicals. Middle viscous chitosan (CS, average viscosimetric molecular weight $\overline{M_v}$ = 684 kDa) and degree of deacetylation 85 %) was purchased from Sigma-Aldrich (Gillingham, UK). Chitosan with $\overline{M_v}$ of 25 kDa was obtained by oxidative degradation of middle viscous chitosan (1% wt. in 0.1 M HCl / 3 mM sodium nitrite). Chitosan samples were purified in-house prior to use as previously described. Hyaluronic acid (HA) $\overline{M_v}$ of 60, 360 and 1000 kDa was provided by Medipol (Medipol SA., Ecublens, Switzerland). 1 M hydrochloric acid (HCl), 1 M sodium hydroxide (NaOH), sodium triphosphate pentabasic (TPP), DNase I and chitosanase from *Streptomyces griseus* were obtained from Sigma-Aldrich (Gillingham, UK); 10 mM phosphate buffered saline (PBS) was prepared from appropriate tablets (Oxoid, Basingtoke, UK); glacial acetic acid and sodium acetate were purchased from VWR BDH Chemicals (Poole, UK). GelRed® and PicoGreen® reagent were from Biotium (CA, USA) and Molecular Probes (OR, USA) respectively.

Nucleic acids. pGL3–control Luciferase reporter vector (Promega, Madison, WN) was amplified in *Escherichia coli* DHT5α, Briefly, cells were transformed with pGL3 by heat shock in a 42 °C water bath for 90 seconds. For bacterial culture, LB Agar (Sigma-Aldrich, St. Louis, MO) was dissolved in deionised water and autoclaved. Transformed bacteria were then streaked on solid agar plate and incubated at 37 °C overnight for growth of colonies. A single colony was picked using a sterile inoculation loop and transferred to LB medium containing 10 μg/mL ampicillin (for selection of pGL3 transformed *E. coli*). The *E. coli* were cultured for 12-16 h at 37 °C and plasmid DNA was extracted and purified using EndoFree Plasmid Maxi Kit according to the manufacturer's instructions (Qiagen, CA, USA). The quantity and quality of the purified pDNA was assessed spectrophotometrically at 260 and 280 nm (NanoDrop 1000 Spectrophotometer). Anti-Luc siRNA (Targets the pGL3 control plasmid) (siLUC, sense: 5'-CUUACGCUGAGUACUUCGAdTdT-3'; antisense: 3'-dTdTGAAUGCGACUCAUGAAGCU-5', Dharmacon Inc., Chicago, IL).

The siRNA sequence directed against the mouse TNF-α gene was designed and chemically synthesized by GenePharma (Shanghai, China). Search of the genome database (BLAST search) was carried out to ensure that this sequence would not target other mouse genes. (siTNF sense: 5′-GGUUGCCUCUGUCUCAGAATT-3′; antisense: 5′-UUCUGAG ACAGAGGCAACCTG-3′).

Cell culture. RAW 264.7 macrophages, K562 human leukaemia and Kelly nueroblastoma (ECACC, UK), Dulbecco's Modified Eagle Medium (DMEM), the quantipro BCA assay kit, TritonX-100, antibiotic-antimycotic solution, lypopolysaccharides (LPS) from *E. coli* O26:B6 were bought from Sigma (Sigma-Aldrich, UK). Foetal bovine serum (FBS) was purchased from Invitrogen (Paisley, UK). CellTiter 96® AQ$_{ueous}$ one solution cell proliferation assay (MTS) kit, Griess reagent system and luciferase assay system were bought from Promega (Madison, WN, USA). BD OptEIA^{TM} mouse TNF (Mono/Mono) ELISA set and OptEIA^{TM} mouse IL-1β ELISA, BD OptEIA^{TM} reagent set A and BD OptEIA^{TM} reagent set B were obtained from BD Biosciences (Oxford,UK).

4.2.2   Nanoparticle preparation and characterisation

Uncoated nanoparticles. A 0.069 % wt. chitosan solution was prepared by dissolving purified chitosan in 4.6 mM HCl and the pH was adjusted to 5 by the addition of appropriate volumes of NaOH 0.1 M. The solution was kept under magnetic stirring overnight and sonicated for 40 min prior to use. A 0.1 % wt. TPP solution in deionised water was brought to pH = 5 using HCl 0.1 M. Both solutions were filtered through a 0.22 μm pore size filter. 214 μL of the TPP solution were added to the chitosan solution for a final total volume of 3 mL and a 9:1 TPP / chitosan mass ratio (concentrations of chitosan and TPP respectively 0.064 and 0.0071% wt.). Loaded nanoparticles were produced by solubilising pDNA or siRNA in the TPP solution, typically in an amount corresponding to 2% wt. of chitosan (2 mg of pDNA or siRNA/100 mg of chitosan). The complexation was carried under magnetic agitation (750 rpm), for 30 min at 25 °C. The final dispersion was sonicated for 40 minutes, left undisturbed for additional 16 h and finally dialysed against deionised water (MWCO 1,000 kDa).

HA-coated nanoparticles. Chitosan-TPP nanoparticles were dispersed at a concentration of 0.025 % wt. in a 100 mM acetic acid/acetate buffer at pH = 5. The

dispersions were then slowly added under vigorous stirring (30 min, 1,200 rpm) to an equal amount of acetate buffer of equal strength, containing hyaluronic acid (360 kDa) at a concentration of 1.5 mg/mL. The dispersions were then dialysed against deionised water (MWCO 1,000 kDa). Equal volumes of HA-coated and non coated nanoparticles in deionised water were freeze dried and then weighted; the dry weight for HA-coated was roughly double that of the uncoated ones, indicating a that the HA weight fraction is approximately 0.5.

Dynamic light scattering (DLS). Hydrodynamic diameter (Z-average size), size polydispersity (PDI) and ζ potential measurements were always performed on three independent samples at a temperature of 25 °C using a Zetasizer Nano ZS instrument (Model ZEN3600, Malvern Instruments Ltd., UK) equipped with a solid state HeNe laser (λ=633 nm) at a scattering angle of 173°.

Encapsulation efficiency. The encapsulation efficiency of the pDNA or siRNA was assessed by recovering non-encapsulated nucleic acids from the supernatant collected upon centrifugation (13,000 rpm for 60 minutes) of non-dialysed nanoparticles after preparation.

The encapsulation was qualitatively evaluated using a gel electrophoresis assay (gel retardation in 1% or 2% Gel-Red®-containing agarose, respectively for pDNA and siRNA; 50 V, 120 min, Sub-Cell GT 96/192; Bio-Rad Laboratories Ltd., UK). A quantitative assessment of encapsulation was provided by fluorimetry (Synergy2 Biotek plate reader using Gen5 software) using the PicoGreen® reagent according to manufacturer instructions; the supernatant of non-loaded nanoparticles was employed as a baseline correction. The encapsulation efficiency (EE) was calculated as *EE = (A-B)/A×100*, where *A* is the total amount of nucleic acid used and B is the amount recovered in the supernatant.

Endonuclease protection assay. 400 μL of deionised water containing 5 μg of pDNA (naked or encapsulated in HA-coated nanoparticles) were incubated with 100 μL of DNase I (1 unit of DNase I per 1 μg of pDNA) in the supplied reaction buffer and the reaction was conducted for 10 minutes at 37 °C. The reaction was terminated by the addition of 50 μL of 50 mM EDTA. The samples were then incubated for 4 h with 0.7 U chitosanase per mg of nanoparticle and analysed by gel electrophoresis (1% agarose).

4.2.3 Cellular studies

Nanoparticles in full medium were prepared by the addition of equal volumes of nanoparticle dispersions to 2X full medium (DMEM supplemented with 20% heat-inactivated foetal bovine serum (FBS), 4×10^{-3} M glutamine, 200 U. mL $^{-1}$ penicillin and 200 U. mL $^{-1}$ streptomycin).

Cell viability. RAW 264.7 macrophages were seeded (10,000 cells/well) in a 96-well plate, cultured in DMEM medium containing 10% FBS, 1% antibiotic/antimitotic solution, and 1% L-glutamate (full medium) and incubated for 24 hours under standard sterile conditions for cell culture (5% CO_2, 37 °C). Nanoparticles dispersions were concentrated to 3 mg/mL, in an ultrafiltration chamber (Amicon system), MWCO of 300 kDa and appropriate dilutions were prepared in full medium. 200 µL of these dispersions were added in each well and the cells were incubated for further 24 hours. At the completion of the incubation, the cells were washed and incubated further for two hours in plain medium containing 5% v/v MTS. The cytotoxicity was measured colorimetrically using the conversion of MTS to a colored formazan, which is soluble in the culture medium. The quantity of formazan produced was evaluated from its absorbance at 490 nm using a Synergy2 Biotek plate reader using Gen5 software. Since MTS absorbance is proportional to both the number and the metabolic activity of the living cells in culture, the absorbance readings were normalised against the total protein content obtained via the Quantipro BCA assay kit. Briefly, the cells were washed with PBS, and incubated for 15 min, in 100 mL cell lysis buffer (0.5%triton X-100 in 0.2 M NaOH), to which 100 mL of Quantipro solution (prepared following the instructions of the manufacturer) was added. The absorbance at 562 nm was finally recorded after 2 hours incubation at 37 °C.

pDNA transfection. RAW 264.7 macrophages, K562 human leukaemia and Kelly nueroblastoma were seeded into 6-well plates at a density of 2×10^5 cells per well and incubated overnight to about 50-70% confluency in 2 mL of DMEM containing 10 % (v/v) FBS under standard sterile conditions for cell culture (5% CO_2, 37 °C). The culture medium was discarded and cells were washed with PBS. 4µg of pGL3 alone or encapsulated in nanoparticles in full medium were added to each well. After 24 hours, the medium was discarded and replaced by 2 mL of fresh DMEM containing 10% (v/v) FBS and incubated for additional 24 hours. The culture

medium was then discarded and cells were washed with PBS. 4 μg of pGL3 complexed with lipofectamine was used as a positive control according to manufacturer instructions. Briefly, 8 μL of lipofectamine 2000 was diluted in 50 μL of serum free DMEM and added to 50 μL of serum free DMEM containing 4 μg pGL3 and kept for 20 minutes before added to the wells. The transfected cells were lysed with Cell culture lysis reagent obtained from Promega. The luciferase activity was measured using the luciferase assay kit and normalized to the total protein content of cell lysate quantified using the Quantipro BCA assay kit as described above.

Silencing experiments. RAW 264.7 macrophages were seeded into 24-well plates at a density of 0.5×10^5 cells/well and incubated at 37 $^{\circ}$C for 24 h. Cells were pre-transfected with 0.5 mL of DMEM containing 1 μg of pGL3 vector using a lipofectamine reagent as described in the previous section. After incubation for 2 hours and subsequent washing with PBS, 200 nM anti-Luc siRNA in full medium alone or encapsulated in HA-coated nanoparticles, were added to each well. After 24 h, the medium was discarded and replaced by 2 mL of fresh DMEM containing 10% (v/v) FBS and incubated for additional 48 hours. Anti-Luc siRNA/lipofectamine complex was used as a positive control. The transfected cells were lysed with cell culture lysis reagent (Promega). The luciferase activity was measured and normalised to the total protein content of cell lysate as described in the previous section.

Effect of nanoparticles on the production of inflammatory mediators. Macrophages were seeded in 24-well flat-bottomed plates at a density of 1×10^5 cells per well and allowed to adhere overnight in standard conditions for cell culture. The cells were then washed once with PBS and treated with fresh medium containing 1 μg/mL LPS alone, nanoparticles at 250 μg/mL, or LPS and nanoparticles or LPS with HA at 125 μg/mL. Cells with fresh medium without any effectors were used as a negative control. After 24 hours incubation, the supernatant was centrifuged at 13,000 rpm for 5 minutes and the presence of inflammatory mediators quantified as indicated below:

a) production of nitrite. 50 μL of the supernatant were transferred to 96-well flat bottomed microtiter plate and mixed with Griess reagent (1 % (w/v) sulfanilamide in 5% (v/v) phosphoric acid and 0.1% (w/v) naphthylethylenediamide–HCl), according

to manufacturer instructions and the absorbance was measured at 550 nm. Nitrite concentrations were calculated from standard curve generated using serial dilutions of sodium nitrite in fresh culture medium. The protein content of each well was evaluated as described previously.

b) production of TNF-α and IL-1β. The amount of TNF-α and IL-1β in culture medium was determined by BD OptEIA^{TM} mouse TNF (Mono/Mono) ELISA set and OptEIA^{TM} mouse IL-1β ELISA set respectively according to manufacturer instructions. TNF-α and IL-1β levels were normalized to the protein content in each well as previously described.

4.3 Results and discussion

4.3.1 Properties and biocompatibility of (loaded) HA-coated nanoparticles

Chitosan-TPP nanoparticles were prepared by ionotropic gelation in water and subsequently coated with HA, both operations being conducted at pH = 5. Size and ζ potential of uncoated and coated nanoparticles are reported in Table 4- 1. For both chitosan molecular weights the coating process reversed the nanoparticle charge from cationic to anionic; it also caused a significant increase in nanoparticle dimensions for 25 kDa chitosan nanoparticles, but not for 684 kDa ones (Figure 4- 1): the different penetration of HA in the nanoparticle cores led to the formation of an HA corona around the low MW chitosan nanoparticles (Chapter Two). At least up to a concentration of 1 mg/mL the HA-coated nanoparticles had negligible effects on the viability (mitochondrial activity normalised against the cell protein content) of CD44-displaying 264.7 RAW macrophages and CD44-devoid neuroblastoma cells, Figure 4- 2. It is also noteworthy that the possible interactions with CD44 did not cause significant inflammatory activation in RAW macrophages: using a nanoparticle concentration of 250 µg/mL, for both 25 and 684 kDa chitosan-containing nanoparticles we have observed small or negligible production of inflammatory cytokines (TNF-α, IL-1β) and NO (measured as nitrite), typically 50-100 smaller than those caused by 1 µg/mL LPS (Figure 4- 3).

Table 4- 1 Physical characteristics of uncoated and HA-coated nanoparticles prepared with 25 and 684 kDa chitosan, with or without a 2 % wt. (in relation to chitosan) loading of pDNA or siRNA

	Unloaded nanoparticles		pDNA loading		siRNA loading	
Chitosan MW(kDa)	25	684	25	684	25	684
CS-TPP						
Z-average size (nm)	149 ± 29	297 ± 17	132 ± 6	350 ± 44	121 ± 16	270 ± 21
PDI	0.25 ± 0.02	0.29 ± 0.01	0.13 ± 0.03	0.30 ± 0.03	0.25 ± 0.09	0.34 ± 0.04
ζ potential (mV)	+38 ± 6	+44 ± 7	+35 ± 4	+40 ± 3	+37 ± 1	+44 ± 1
Encaps. eff. (%wt.)	=	=	95 ± 2	78 ± 3	93 ± 1	94 ± 1
CS-TPP//HA						
Z-average size (nm)	336 ± 43	300 ± 32	327 ± 20	315 ± 7	318 ± 70	315 ± 61
PDI	0.24 ± 0.06	0.28 ± 0.06	0.24 ± 0.02	0.29 ± 0.04	0.22 ± 0.04	0.22 ± 0.03
ζ potential (mV)	-46 ± 3	-45 ± 3	-43 ± 2	-43 ± 4	-45 ± 4	-42 ± 4

Plasmid DNA and siRNA (both in a 2%wt. ratio in relation to chitosan) were loaded in chitosan-TPP nanoparticles during their formation. The encapsulation efficiency was quantitative in most cases, as previous recorded for salmon sperm DNA (Chapter Two); a slightly reduced encapsulation (78%) was recorded for plasmid DNA in 684 kDa chitosan nanoparticles; this is probably due to a lower binding strength between the two polyelectrolytes: they are respectively the largest polyanion and polycation, and the number of interaction sites per molecule decreases by increasing the dimension of a polymer coil.
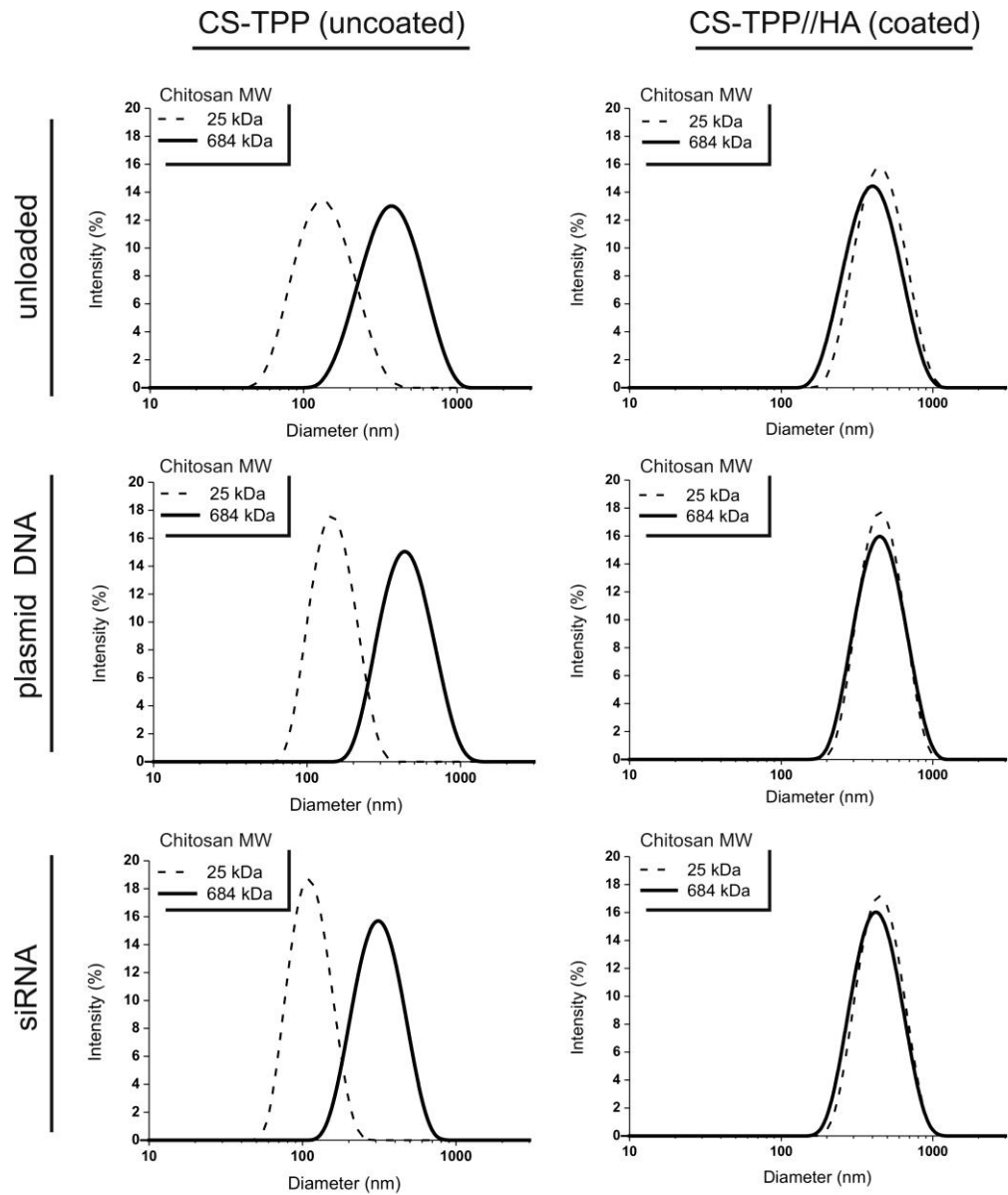
Figure 4- 1 Size distribution of nanoparticles (250 μg/mL, deionised water) prepared from chitosan with different molecular weight as a function of coating and loading with plasmid DNA and siRNA.
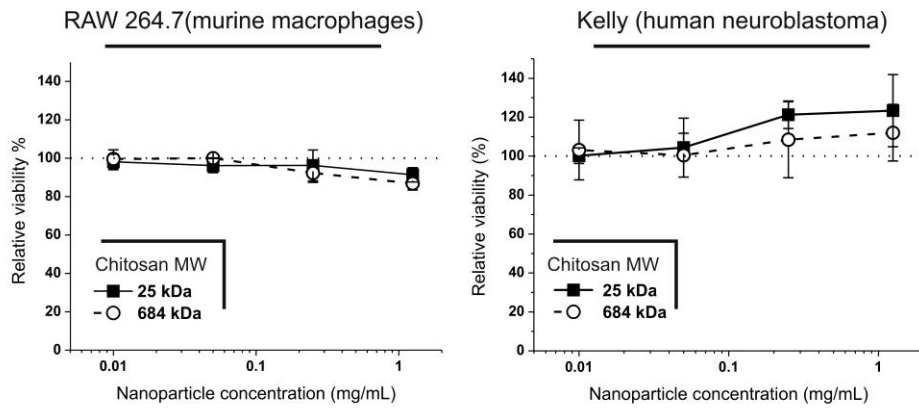
Figure 4- 2 Viability of two model cell lines, one expressing CD44 (RAW 264.7, left) and one substantially devoid of this receptor (Kelly, right), as a function of the concentration of chitosan-TPP/HA nanoparticles.
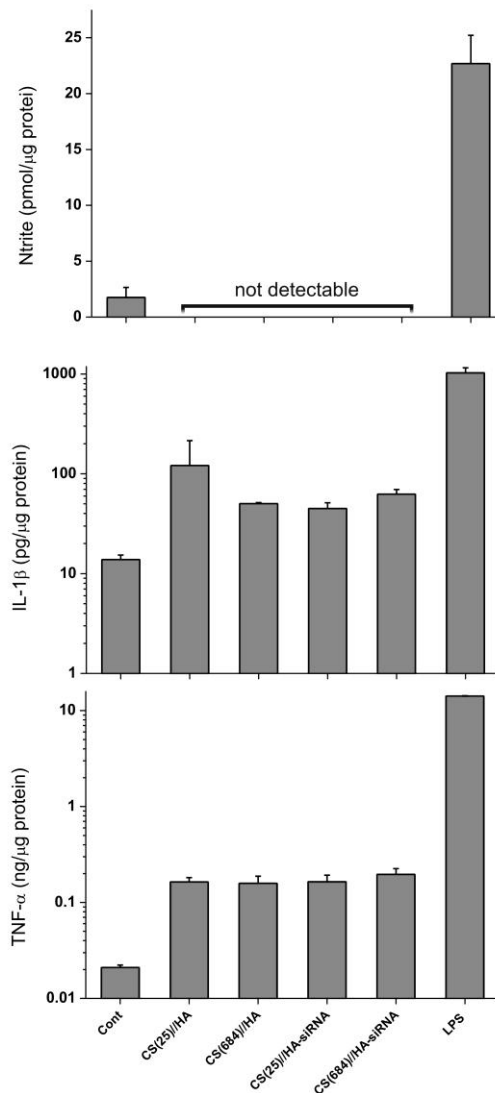
Figure 4- 3 Concentration of nitrite, TNF-α and IL-1β as a result of the 24 hours exposure of RAW 264.7 macrophages to 250 μg/mL CS-TPP//HA nanoparticles. The concentration of siTNF encapsulated in the nanoparticles was 200 nM/well. LPS at 1 μg/mL and plain medium were used as positive and negative control respectively.

The high efficiency of nucleic acid entrapment was also confirmed by the absence of significant amounts of free nucleic acids in gel retardation assays (Figure 4- 4, left). The presence of loaded nucleic acids did not significantly affect size and charge of the nanoparticles, nor the outcome of the coating process (Table 4- 1 and Figure 4- 1), nor the substantial absence of macrophage activation (Figure 4- 3).

A key factor for a successful gene delivery is the ability of the delivery system to protect the payload from enzymatic degradation. For example, more than 95% of naked plasmid injected intramuscularly is degraded in the muscle tissue within 90 minutes post-administration, hindering its possible therapeutic benefits [44]. Using DNase I as a model enzyme to degrade pDNA and then chitosanase to degrade the host matrix, in preliminary experiments we have not observed any significant release of intact DNA or decrease of the nanoparticle-associated fluorescence, suggesting the resistance of the loaded nanoparticles and of their payload to both enzymes (Figure 4- 4, right).
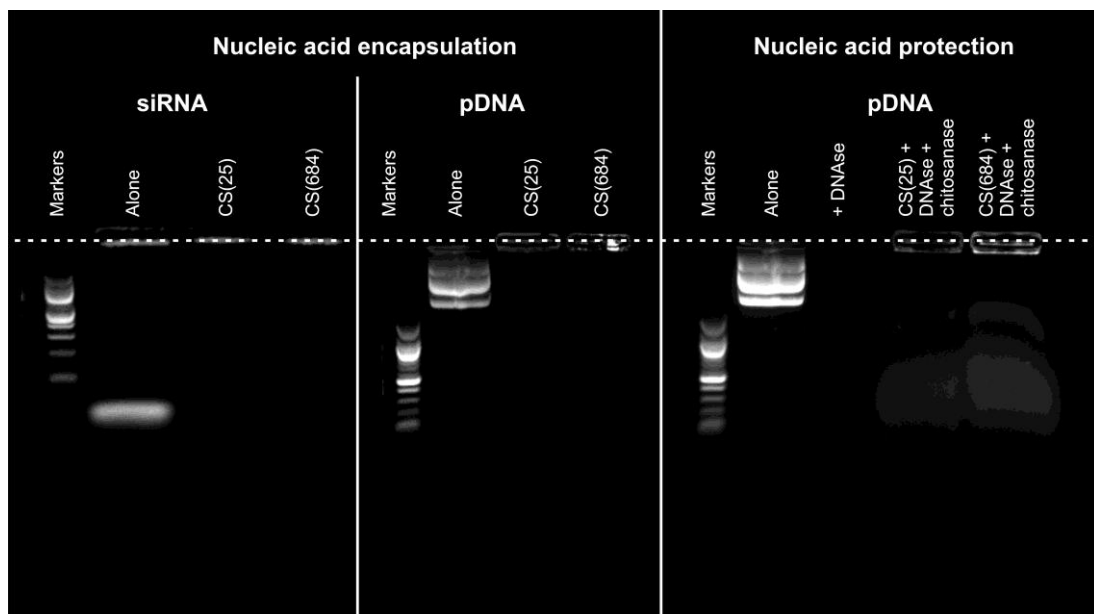
Figure 4- 4 *Left:* gel retardation assays for siRNA and plasmid DNA in a free form or encapsulated in chitosan-TPP//HA nanoparticles. Due to its cationic nature (repelled by chitosan), the GelRed fluorophore cannot efficiently stain loaded nucleic acids, hence the fluorescence associated to the nanoparticles has a low intensity and in particular it is barely visible for siRNA. *Right:* gel retardation assays for plasmid DNA in a free form or encapsulated in chitosan-TPP//HA nanoparticles when exposed to DNAse I; the nanoparticles were then incubated with chitosanase, which is known to facilitate pDNA recovery. Only traces of DNA were released, in possibly higher amount for the nanoparticles containing 684 kDa chitosan, which are known to be more susceptible to chitosanase degradation. Please note that, due to the high activity of DNAse I, free pDNA is rapidly degraded to monomeric units and is no longer stained by GelRed.

4.3.2 CD44-mediated therapies

Two sets of preliminary experiments were conducted with the common aim to demonstrate the feasibility of CD44-dependent therapeutic approaches.

CD44-mediated nucleic acid delivery. We have first examined the possibility of delivering a large nucleic acid payload, i.e. a luciferase-encoding plasmid DNA (pGL3). We have employed three cell lines: first, they have different CD44 expression in the order RAW >> K562 > Kelly; second, as neuroblastoma cells are notoriously difficult to transfect even with lipofectamine [45], Kelly cells can be used as an internal double negative control. The results are summarised in, Figure 4-5, left.
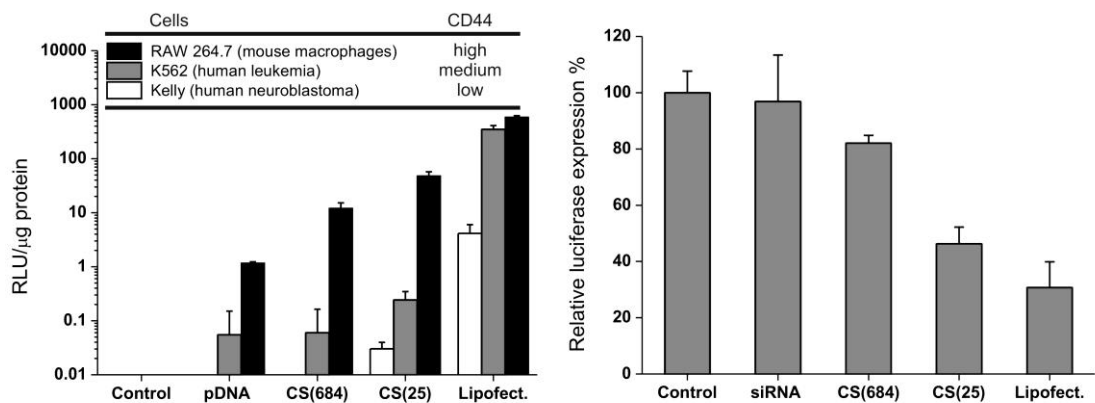
Figure 4- 5 *Left:* comparison of gene transfection efficiencies in 264.7 RAW macrophages, Kelly neuroblastoma cells and K562 leukemia cells. Cells were transfected with 4 µg pGL3 either naked or encapsulated in chitosan-TPP//HA nanoparticles (please note that in the graph the nanoparticles are identified only with the chitosan molecular weight; loading: 2%wt. in relation to chitosan). Cells were incubated with medium only or 4 µg pGL3 complexed with lipofectamine 2000 were used as a negative and a positive control, respectively. The results are expressed as relative light units (RLUs) normalized to total protein content of each well. *Right:* Nanoparticle-mediated RNA interference in 264.7 RAW macrophages. Cells were transfected with 1 µg pGL3 complexed with Lipofectamine 2000 and luciferase expression was interfered by 200nM Anti-Luc siRNA/well either naked or encapsulated in nanoparticles (loading: 2%wt. in relation to chitosan). Cells incubated with medium only or Anti-Luc siRNA complexed with lipofectamine 2000 were used as a negative and a positive control respectively. Luciferase expression was recorded as relative light units (RLUs) normalized to total protein content of each well. The results are expressed as the percentage of luciferase expression relative to control.

Lipofectamine provided the highest luciferase luminescence with all cells lines, which is primarily to ascribe to the rapid endocytic uptake of its lipoplexes, whereas HA-coated nanoparticles are internalised via a slower and saturatable mechanism (see Chapter Three). As expected, Kelly cells' transfection efficiency was at least two orders of magnitude lower than that of K562 and RAW cells also using lipofectamine, therefore confirming the reliability of the results.

Two main points are noteworthy:

A) lipofectamine transfected RAW macrophages and K562 cells equally well, while a >100-fold difference in favour of CD44-displaying macrophages could be seen when using HA-coated nanoparticles. Although more controls are needed, this is a promising indication of the possibility of CD44-mediated targeted nucleic acid therapy.

B) We have previously demonstrated (Chapter Two and Chapter Three) that the use of 25 kDa chitosan causes HA to form an external, thick layer (a corona), and there is evidence that this increases the overall affinity of the nanoparticles to HA receptor(s), but decreases the overall amount of uptaken nanoparticles at saturation; this would reduce the overall transfection efficiency. On the other hand, the bulk composition of the 25 kDa chitosan nanoparticles is probably more labile under acidic (endosomal) conditions: high molecular weight always increases the strength of polyelectrolyte complexation due to cooperative effect, and for 684 kDa chitosan the nanoparticle structure is further stabilised by the infiltration of HA in its bulk; this would determine a higher transfection efficiency for low molecular weight chitosan nanoparticles.

The transfection efficiency was indeed 4-5 times higher for 25 kDa chitosan-based nanoparticles, on both macrophages and Kelly cells; due to the above considerations, we are therefore inclined to ascribe this effect to a more efficient intracellular delivery (endosomal escape and liberation of pDNA).

A similar effect was recorded when RAW macrophages were first transfected with pDNA/lipofectamine to express luciferase and then treated with siRNA-containing vectors to quench this expression (Figure 4- 5, right). 25 kDa chitosan nanoparticles showed a silencing efficiency about 3 times higher than that of the 684 kDa ones, and only marginally worse than lipofectamine. The better relative performance in the release of siRNA (closer to lipofectamine than in the release of pDNA) is probably

again to ascribe to the details of the intracellular delivery phase: complexes of chitosan with the smaller siRNA are easier to disrupt than those with the larger pDNA.

Anti-inflammatory effects of HA-coated nanoparticles. We have investigated whether the different organisation and possibly different crowding and mobility of HA chains on nanoparticles of 25 and 684 kDa chitosan may give rise to significant effects on macrophage inflammatory activation, which was obtained using 1 µg/mL LPS (Figure 4- 6); the choice of this LPS concentration was due to the high inflammatory cytokine induction in the absence of any apparent reduction in cell viability (see Supplementary Information, Figure 4-SI 1). Soluble HA was used as a control, confirming its increasing anti-inflammatory character with increasing molecular weight; for example, at a concentration of 125 µg/mL 1 MDa HA produced a 75% reduction in TNF-α production, a 50% in for IL-1β and a 40% for NO, whereas 60 kDa HA showed negligible effects. On the other hand, using HA-coated nanoparticles at an analogous HA concentration (due to an HA content of about 50% wt., 250 µg/mL nanoparticles correspond to 125 µg/mL of HA), the production of both cytokines and NO was substantially abrogated ($\leq 10\%$), with a slightly higher efficiency for 25 kDa chitosan nanoparticles. The latter is possibly due to the better presentation of HA (HA corona) on the surface of these nanoparticles.

Due to the good transfection efficiency previously recorded for siRNA, additional experiments were performed by loading the nanoparticles with TNF-α silencing siRNA loaded in the nanoparticles or in lipofectamine; chitosan and polyethyleneimine polyplexes have already been employed as carriers for siRNA designed to silence the TNF-α gene [46] and this could in principle allow as synergic anti-inflammatory action. However, no further reduction of the inflammatory mediators was recorded and the results mirrored those of unloaded nanoparticles, again with a slightly higher activity of 25 kDa chitosan-based nanoparticles. It was therefore provisionally concluded that the anti-inflammatory character of the nanoparticles themselves, possibly arising to clustered binding to HA receptors such as CD44, overwhelmed any further action due to siRNA release.
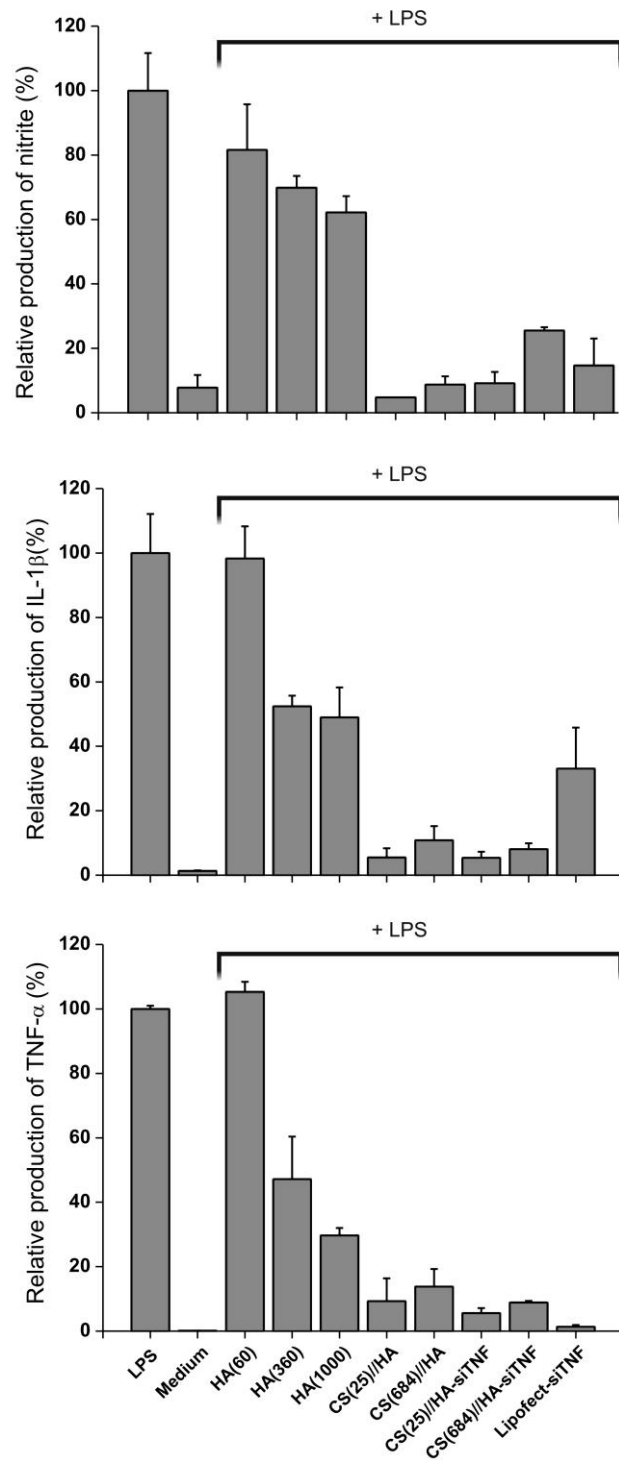
Figure 4- 6 Effect of CS-TPP//HA nanoparticles on the extracelluler level of nitrite, TNF-α and IL-1β in LPS-activated (1 µg/mL) RAW 264.7 macrophages. Cells were exposed to 1 µg/mL LPS for 24 h co-administered with free HA at 125 µg/mL or nanoparticles at 250 µg/mL (roughly corresponding to the same HA concentration). siTNF was encapsulated in nanoparticles and incubated at 200nM/well. LPS and plain medium were respectively used as a positive and negative control.

4.4 Conclusions

The results presented here have mostly a proof-of-principle character, but have clearly indicated the feasibility of the use of HA-coated nanoparticles for CD44 targeting and the usefulness of low molecular weight chitosan for an improved delivery of nucleic acid payloads.

Although a number of additional experiments are required, such as CD44 blocking, time- and dose-dependent behaviour etc., we believe to have also qualitatively shown an unprecedented effect anti-inflammatory of HA-coated nanoparticles devoid of any payload, which significant promise for the development of future therapies.

4.5 References

1. Chernajovsky, Y., D.J. Gould, and O.L. Podhajcer, *Gene therapy for autoimmune diseases: Quo Vadis?* Nature Reviews Immunology, 2004. **4**(10): p. 800-811.

2. Nabel, G.J., et al., *Direct Gene-Transfer with DNA Liposome Complexes in Melanoma - Expression, Biologic Activity, and Lack of Toxicity in Humans.* Proceedings of the National Academy of Sciences of the United States of America, 1993. **90**(23): p. 11307-11311.

3. Glover, D.J., H.J. Lipps, and D.A. Jans, *Towards safe, non-viral therapeutic gene expression in humans.* Nature Reviews Genetics, 2005. **6**(4): p. 299-U29.

4. Liu, X.D., et al., *The influence of polymeric properties on chitosan/siRNA nanoparticle formulation and gene silencing.* Biomaterials, 2007. **28**(6): p. 1280-1288.

5. Mao, S.R., W. Sun, and T. Kissel, *Chitosan-based formulations for delivery of DNA and siRNA.* Advanced Drug Delivery Reviews, 2010. **62**(1): p. 12-27.

6. Gao, S.Y., et al., *Targeting delivery of oligonucleotide and plasmid DNA to hepatocyte via galactosylated chitosan vector.* European Journal of Pharmaceutics and Biopharmaceutics, 2005. **60**(3): p. 327-334.

7. Mansouri, S., et al., *Chitosan-DNA nanoparticles as non-viral vectors in gene therapy: strategies to improve transfection efficacy.* European Journal of Pharmaceutics and Biopharmaceutics, 2004. **57**(1): p. 1-8.

8. Huang, M., et al., *Transfection efficiency of chitosan vectors: Effect of polymer molecular weight and degree of deacetylation.* Journal of Controlled Release, 2005. **106**(3): p. 391-406.

9. Mao, H.Q., et al., *Chitosan-DNA nanoparticles as gene carriers: synthesis, characterization and transfection efficiency.* Journal of Controlled Release, 2001. **70**(3): p. 399-421.

10. Fischer, D., et al., *A novel non-viral vector for DNA delivery based on low molecular weight, branched polyethylenimine: Effect of molecular weight on transfection efficiency and cytotoxicity.* Pharmaceutical Research, 1999. **16**(8): p. 1273-1279.

11. Zaki, N.M., A. Nasti, and N. Tirelli, *Nanocarriers for Cytoplasmic Delivery: Cellular Uptake and Intracellular Fate of Chitosan and Hyaluronic Acid-Coated Chitosan Nanoparticles in a Phagocytic Cell Model.* Macromolecular Bioscience, 2011. **11**(12): p. 1747-1760.

12. Goldman, C.K., et al., *In vitro and in vivo gene delivery mediated by a synthetic polycationic amino polymer.* Nature Biotechnology, 1997. **15**(5): p. 462-466.

13. Xu, P.S., G.K. Quick, and Y. Yeo, *Gene delivery through the use of a hyaluronate-associated intracellularly degradable crosslinked polyethyleneimine.* Biomaterials, 2009. **30**(29): p. 5834-5843.

14. Passirani, C., et al., *Long-circulating nanoparticles bearing heparin or dextran covalently bound to poly(methyl methacrylate).* Pharmaceutical Research, 1998. **15**(7): p. 1046-1050.

15. Nasti, A., et al., *Chitosan/TPP and Chitosan/TPP-hyaluronic Acid Nanoparticles: Systematic Optimisation of the Preparative Process and*

Preliminary Biological Evaluation. Pharmaceutical Research, 2009. **26**(8): p. 1918-1930.

16. Chan, P., et al., *Synthesis and characterization of chitosan-g-poly(ethylene glycol)-folate as a non-viral carrier for tumor-targeted gene delivery.* Biomaterials, 2007. **28**(3): p. 540-549.

17. Zhang, H., et al., *Design of biocompatible chitosan microgels for targeted pH-mediated intracellular release of cancer therapeutics.* Biomacromolecules, 2006. **7**(5): p. 1568-1572.

18. Kim, T.H., et al., *Receptor-mediated gene delivery into antigen presenting cells using mannosylated chitosan/DNA nanoparticles.* Journal of Nanoscience and Nanotechnology, 2006. **6**(9-10): p. 2796-2803.

19. Gao, S.Y., et al., *Galactosylated low molecular weight chitosan as DNA carrier for hepatocyte-targeting.* International Journal of Pharmaceutics, 2003. **255**(1-2): p. 57-68.

20. Katoh, S., et al., *Glycosylation of CD44 negatively regulates its recognition of hyaluronan.* Journal of Experimental Medicine, 1995. **182**(2): p. 419-429.

21. Katoh, S., et al., *Cutting edge: An inducible sialidase regulates the hyaluronic acid binding ability of CD44-bearing human monocytes.* Journal of Immunology, 1999. **162**(9): p. 5058-5061.

22. Ossipov, D.A., *Nanostructured hyaluronic acid-based materials for active delivery to cancer.* Expert Opinion on Drug Delivery, 2010. **7**(6): p. 681-703.

23. Ghosh, S.C., S.N. Alpay, and J. Klostergaard, *CD44: a validated target for improved delivery of cancer therapeutics.* Expert Opinion on Therapeutic Targets, 2012. **16**(7): p. 635-650.

24. Ravina, M., et al., *Hyaluronic Acid/Chitosan-g-Poly(ethylene glycol) Nanoparticles for Gene Therapy: An Application for pDNA and siRNA Delivery.* Pharmaceutical Research, 2010. **27**(12): p. 2544-2555.

25. de la Fuente, M., B. Seijo, and M.J. Alonso, *Novel hyaluronic acid-chitosan nanoparticles for ocular gene therapy.* Investigative Ophthalmology & Visual Science, 2008. **49**(5): p. 2016-2024.

26. Contreras-Ruiz, L., et al., *Intracellular trafficking of hyaluronic acid-chitosan oligomer-based nanoparticles in cultured human ocular surface cells.* Molecular Vision, 2011. **17**(34-35): p. 279-290.

27. Stevenson, R., et al., *Nanoparticles and Inflammation.* Thescientificworldjournal, 2011. **11**: p. 1300-1312.

28. Fujiwara N, K.K., *Macrophages in inflammation.* Curr Drug Targets Inflamm Allergy, 2005. **4**(3): p. 281-286.

29. Glaros, T., M. Larsen, and L.W. Li, *Macrophages and fibroblasts during inflammation, tissue damage and organ injury.* Frontiers in Bioscience, 2009. **14**: p. 3988-3993.

30. Glucksam-Galnoy, Y., T. Zor, and R. Margalit, *Hyaluronan-modified and regular multilamellar liposomes provide sub-cellular targeting to macrophages, without eliciting a pro-inflammatory response.* Journal of Controlled Release, 2012. **160**(2): p. 388-393.

31. Day, Y.J., et al., *Renal ischemia-reperfusion injury and adenosine 2A receptor-mediated tissue protection: role of macrophages.* American Journal of Physiology-Renal Physiology, 2005. **288**(4): p. F722-F731.

32. Andreyev, A.Y., et al., *Subcellular organelle lipidomics in TLR-4-activated macrophages.* Journal of Lipid Research, 2010. **51**(9): p. 2785-2797.

33.   Stacey, K.J., M.J. Sweet, and D.A. Hume, *Macrophages ingest and are activated by bacterial DNA.* Journal of Immunology, 1996. **157**(5): p. 2116-2122.

34.   Xiao, G.G., et al., *Use of proteomics to demonstrate a hierarchical oxidative stress response to diesel exhaust particle chemicals in a macrophage cell line.* Journal of Biological Chemistry, 2003. **278**(50): p. 50781-50790.

35.   Vachon, E., et al., *CD44 is a phagocytic receptor.* Blood, 2006. **107**(10): p. 4149-4158.

36.   Gross, N., K. Balmas, and C.B. Brognara, *Absence of functional CD44 hyaluronan receptor on human NMYC-amplified neuroblastoma cells.* Cancer Research, 1997. **57**(7): p. 1387-1393.

37.   Shtivelman, E. and J.M. Bishop, *expression of cd44 is repressed in neuroblastoma-cells.* Molecular and Cellular Biology, 1991. **11**(11): p. 5446-5453.

38.   Turner, M.L., et al., *Comparative adhesion of human haemopoietic cell lines to extracellular matrix components, bone marrow stromal and endothelial cultures.* British Journal of Haematology, 1998. **100**(1): p. 112-122.

39.   Buscher, K., et al., *The Transmembrane Domains of L-selectin and CD44 Regulate Receptor Cell Surface Positioning and Leukocyte Adhesion under Flow.* Journal of Biological Chemistry, 2010. **285**(18): p. 13490-13497.

40.   Johnsson, A., et al., *Gene expression profiling in chemoresistant variants of three cell lines of different origin.* Anticancer Research, 2005. **25**(4): p. 2661-2668.

41.   Pure, E. and C.A. Cuff, *A crucial role for CD44 in inflammation.* Trends in Molecular Medicine, 2001. **7**(5): p. 213-221.

42.   Wang, C.T., et al., *High molecular weight hyaluronic acid down-regulates the gene expression of osteoarthritis-associated cytokines and enzymes in fibroblast-like synoviocytes from patients with early osteoarthritis.* Osteoarthritis and Cartilage, 2006. **14**(12): p. 1237-1247.

43.   Day, A.J. and C.A. de la Motte, *Hyaluronan cross-linking: a protective mechanism in inflammation?* Trends in Immunology, 2005. **26**(12): p. 637-643.

44.   Faurez, F., et al., *Biosafety of DNA vaccines: New generation of DNA vectors and current knowledge on the fate of plasmids after injection.* Vaccine, 2010. **28**(23): p. 3888-3895.

45.   Koticha, D.K., E.E. McCarthy, and G. Baldini, *Plasma membrane targeting of SNAP-25 increases its local concentration and is necessary for SNARE complex formation and regulated exocytosis.* Journal of Cell Science, 2002. **115**(16): p. 3341-3351.

46.   Laroui, H., et al., *Functional TNF alpha gene silencing mediated by polyethyleneimine/TNF alpha siRNA nanocomplexes in inflamed colon.* Biomaterials, 2011. **32**(4): p. 1218-1228.
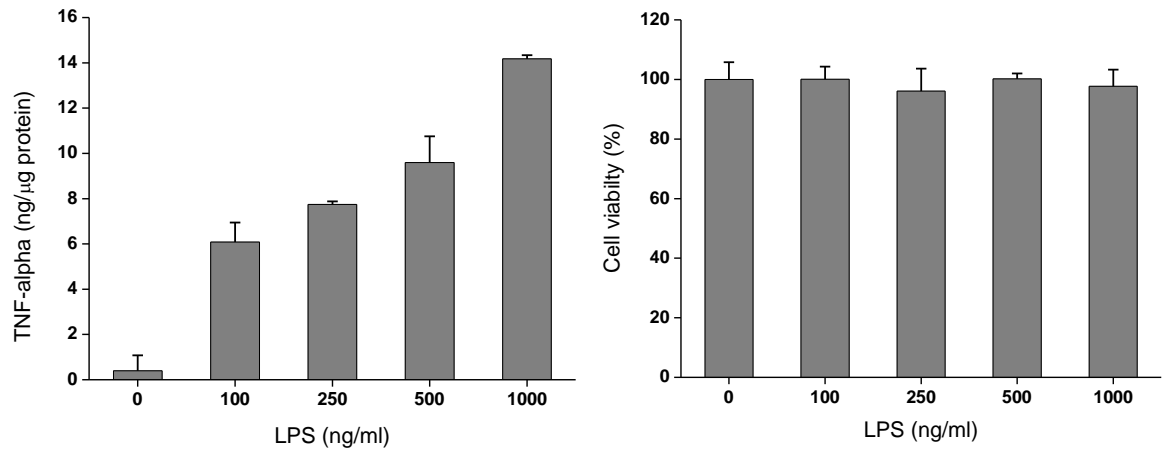
4.6 Supplementary Information

Figure 4-SI 1 Activation of RAW 264.7 macrophages with LPS. **Left**: production of TNF-α as a function of LPS concentration upon 24 h exposure. **Right:** viability of macrophages under the same conditions

Chapter Five

Conclusions and outlook

The aim of this thesis was to synthesise and characterise nanoparticles based on the electrostatic interactions of chitosan, TPP and HA as a non-viral gene delivery vector. A particular interest was taken on rationalising some of the chitosan molecular weight-dependent effects on the morphology, cellular fate and gene transfection efficiency of these nanoparticles.

In Chapter Two, we have illustrated the effect of chitosan molecular weight on the physico-chemical characteristics and morphology/structure of chitosan-TPP nanoparticles and their functional behaviour. The main findings are that

a) low molecular weight chitosan provides more compact nanoparticles, which have a lower swelling/shrinkage capacity and a higher cross-link density;

b) the bulk structure determines different modes of adsorption of HA, when the cationic nanoparticles are coated to provide a more protein-resistant and potentially CD44-binding surface. In particular, lower chitosan molecular weight, and thus higher nanoparticle bulk compactness, corresponded to the formation of an HA corona around the nanoparticles, while higher chitosan molecular weight and larger particle porosity appeared to allow HA infiltration in the nanoparticle bulk.

c) The morphological differences had significant effects on the overall nanoparticle behaviour. For example, lower molecular weight chitosan nanoparticles 1) were much less prone to aggregation due to the presence of excess HA, a phenomenon likely caused by depletion interactions; 2) showed a significantly lower protein adsorption both before and after decoration with HA. Using chitosanase as a tool to probe the facility of unpacking of the nanoparticle bulk, the enzymatic degradation of chitosan caused a significant DNA release only for higher chitosan molecular weight nanoparticles, which could be ascribed to the higher accessibility of chitosan.

In Chapter Three, we have investigated whether the above described different surface presentation of HA also influenced its presentation to cell surface receptors and thus also the phenomenon of receptor-mediated internalisation. HA-coated

Chitosan-TPP nanoparticles were prepared with different internal structures due to the use of different chitosan molecular weight or to different preparative protocols, and analogous Alginate-coated ones were used as controls.

First, the toxicity of the HA-coated nanoparticles (in RAW 264.7 macrophages) appeared to bear little sensitivity to chitosan molecular weight or the nature of the coating material (HA or alginate), but was strongly influence by the method of preparation, suggesting the major determinant of a toxic behaviour to be the possible exposure of chitosan. We have also proved that the morphological differences did not affect the mechanism of nanoparticle uptake, which appeared always to be a CD44-mediated phenomenon leading to acidified late endosomes. CD44 is an easily saturated receptor due to its slow representation (24-48 hr). Under such conditions, the internalisation kinetics of HA-coated nanoparticle would be governed by the amount of available receptors and indeed a clear saturation behaviour was recognisable. This also implies that a higher number of interaction sites, for example due to better presentation of HA, would allow the internalisation of a lower amount of more strongly bound nanoparticles. Emphasising how ligand surface presentation can affect the efficacy of delivery in a counter-intuitive fashion (lower affinity – larger amount of nanoparticles internalised) may be a way to enhance the efficacy of CD44-targeted nanoparticles.

In Chapter Four, the feasibility of CD44-dependent therapeutic approaches was investigated using HA-coated nanoparticles with or without a nucleic acid payload (pDNA and siRNA).

High nucleic acid entrapment efficiency was confirmed, although it was slightly dependent on the size of both chitosan and nucleic acid. HA-coated nanoparticles showed negligible cellular toxicity and did not cause significant inflammatory activation also in an inflammation-sensitive model such as RAW macrophages, which is a prerequisite for any delivery system and in particular for one targeting inflammatory diseases. Thereafter, HA-coated nanoparticles loaded with a reporter gene (pGL3) showed the possibility of CD44-mediated targeted nucleic acid therapy by differentiating heavily from poorly CD44-expressing cells. siRNA-loaded nanoparticles were also successfully used to mediate silencing of the reporter gene expression. In both cases, nanoparticles based on low molecular weight chitosan

showed better results than those based on high molecular weight chitosan, which was possibly the result of a more efficient intracellular liberation of the payload; a similar argument could be used to explain the higher efficiency recorded for siRNA than for pDNA, since a smaller payload is probably less tightly bound by chitosan and hence easier to deliver after endosomal disruption.

Last, we have investigated whether the different organisation and possibly different crowding and mobility of HA chains may give rise to significant effects on macrophage inflammatory activation. We have confirmed soluble HA increasing anti-inflammatory character with increasing molecular weight. However, HA concentrated on the nanoparticles surface, at an analogous concentration to soluble HA, seems to increase the anti-inflammatory effect. loading the nanoparticles with TNF-α silencing siRNA for potential synergic anti-inflammatory action revealed no additive effect on inflammatory mediators production which conclude that the anti-inflammatory character of the nanoparticles themselves, possibly arising from clustered binding to HA receptors such as CD44, overwhelmed any further action due to RNA interference to TNF-α expression.

Outlook and next steps. HA-coated chitosan-TPP nanoparticles show great promise as structures that may use their interactions with HA receptors (mainly CD44) to provide an inherent anti-inflammatory character and the possibility to deliver nucleic acid payloads in a CD44-targeted fashion. This potentiality seems to be largely influenced by the nanoparticle bulk structure and ultimately by chitosan molecular weight, indicating that the appropriate selection of the starting polymer is of paramount importance to enhance stability, targetability and gene transfection efficiency.

The last part of the present study should be (and currently is) complemented by a number of additional experiments to better understand the nucleic acid loading/release profile of nanoparticles, the mechanism of intracellular delivery and the anti-inflammatory nature of the nanoparticles - specifically, as follows.

A) For loading/release analysis, it would be interesting to develop a methodology to obtain a full recovery of the payload (i.e 100% DNA/RNA release) possibly through biodegradation of the polymeric network using an enzymatic cocktail.

B) For the nucleic acid delivery, it would be necessary to show whether CD44 clustering around nanoparticles could influence the nature of the endosomal environment (e.g. acidity) and to confirm in a quantitative fashion the influence of the nanoparticle bulk (e.g. chitosan molecular weight) on the kinetics of endosomal disruption.

C) For the anti-inflammatory character, we currently speculate the nanoparticle effect to be due to the signalling arising from CD44 clustering. However, we cannot completely rule out an effect of ROS scavenging, therefore it would be necessary to qualify the free radical scavenging efficiency of the nanoparticles, either in contact or in a paracrine fashion. Additionally, the extent of CD44 clustering should be quantified, and the specific related signalling should be at least qualitatively understood.

Further, these nanoparticles should be tested *in vivo*, in models of (tumoural or inflammatory pathologies) known to be associated to an overexpression of CD44 or other HA receptors.